EXPERIMENTAL INVESTIGATION OF VISCOSITY RATIO EFFECT ON DISPLACEMENT PERFORMANCE OF POLYMER SYSTEMS DURING HEAVY OIL RECOVERY

A Thesis

Submitted to the Faculty of Graduate Studies and Research

In Partial Fulfillment of the Requirements

For the Degree of

Master of Applied Science

In

Petroleum Systems Engineering

University of Regina

By

Pavlo Volodymyrovych Pantus

Regina, Saskatchewan

September 7, 2012

UNIVERSITY OF REGINA

FACULTY OF GRADUATE STUDIES AND RESEARCH

SUPERVISORY AND EXAMINING COMMITTEE

Pavlo Volodymyrovych Pantus, candidate for the degree of Master of Applied Science in Petroleum Systems Engineering**,** has presented a thesis titled, ***Experimental investigation of Viscosity Ratio Effect on Displacement Performance of Polymer Systems During Heavy Oil Recovery,*** in an oral examination held on August 20, 2012. The following committee members have found the thesis acceptable in form and content, and that the candidate demonstrated satisfactory knowledge of the subject material.

External Examiner:	Dr. David deMontigny, Process Systems Engineering
Supervisor:	Dr. Farshid Torabi, Petroleum Systems Engineering
Committee Member:	Dr. Fanhua Zeng, Petroleum Systems Engineering
Committee Member:	*Dr. Ezeddin Shirif, Petroleum Systems Engineering
Chair of Defense:	Dr. Saqib Khan, Faculty of Business Administration

*Not present at defense

ABSTRACT

Heavy oil production during secondary recovery is often plagued by high producing water/oil ratios; this is a direct result of the unfavourable viscosity ratio that leads to viscous instability at the displacement front between the injected water and the more viscous oil.

Polymer flooding has proven to be an exceptionally efficient enhanced oil recovery (EOR) technique that increases the stability of the displacing front, accelerating the pore displacement efficiency and improving the vertical and areal macroscale sweep efficiencies. This is especially important in heavy oil reservoirs, where recovery factors tend to be less than 10 % of original-oil-in-place (OOIP)

The instability behaviour (viscous fingering) results from the difference in fluid mobilities between the displacing and displaced phases. The impact of viscosity ratio on the polymer EOR process was determined through a set of experiments using an oil-saturated, synthetic glass bead sand-pack in a thin-fracture visual cell. The range of viscosity ratios of 20-, 40- and 80:1 was also evaluated for pressure, oil recovery, and dynamic adsorption response by conducting a series of coreflood tests in synthetic glass beads using conventional hydrolyzed polyacrylamide (HPAM) and hydrophobically associating (HAP) polymer solutions.

This thesis provides a new insight regarding oil displacement efficiency from water and polymer solutions using oil viscosities ranging from 22 to 2039 mPa·s. The fracture-model tests provided visual representations of viscous fingering behaviour. It was found that the polymer solutions exhibited much more stable fronts and improved sweep efficiency with far less occurrence of complex shielding, spreading and splitting

behaviour in the porous environment. In general, the coreflood tests using the HAP polymer showed faster recovery response with significantly higher resistance factors than HPAM at the same viscosity ratios; however, converse to what is observed with conventional polymer flooding, there was no significant difference in ultimate oil recoveries with either polymer type when flooded with different viscosity ratios. This result suggests that higher concentrations (and higher bulk viscosities) alone may not be as influential a parameter when considering polymer flooding for heavy oil EOR applications.

ACKNOWLEDGEMENTS

I would like to gratefully extend acknowledgements to my supervisor, Dr. Farshid Torabi, for his generous financial support, useful suggestions, and continuous assistance all the way from preparation and experimental practice to final project execution. His outstanding project management, understanding, and courteous support are also appreciated.

I say thank you to all committee members for their useful suggestions and comments while reviewing my thesis.

I also would like to acknowledge the Petroleum Technology Research Centre (PTRC) and Sustainable Technologies for Energy Production Systems (STEPS) program for financial support of the project and numerous progress meetings.

Additional funding received from the Faculty of Graduate Studies and Research (FGSR) is also gratefully acknowledged.

Special thanks are dedicated to Dr. Malcolm Wilson (PTRC) as well as to Mrs. Heather Quale Goranson and Nataliya Dvorak from Mera Development Corp. ("Mera") for encouragement, guidance, and persuasion to move forward, gain experience, and reach success.

The outstanding moral and academic support that were provided by Mr. Ryan Wilton, and also his remarkable willingness to get things done right and find the solutions to various scientific puzzles, are greatly appreciated and will never be forgotten.

I also would like to say thank you to all other fellow colleagues from Dr. Torabi's research group who assisted me during laboratory and academic courses sessions.

POST DEFENSE ACKNOWLEDGEMENT

I would like to acknowledge the External Examiner of the Defense Examination Committee – Dr. David deMontigny for his professionally-done suggestions and comments during thesis defense. I also thankful for our numerous meetings and discussions while doing all necessary revisions and corrections prior to submission of the final copy of the thesis to Faculty of Graduate Studies and Research (FGSR) for approval.

DEDICATION

Last but not least acknowledgement is given with gratitude to my parents – the biggest inspirations of my life – for their years of love, support, and worry. Therefore, I especially want to dedicate this thesis to the members of my family, who kept us united in a time of great challenges while staying away from each other and from home for a long time. The drive to move forward and be the best no matter what that I have received from my father Volodymyr Pantus helped me to fulfill all the requirements of my graduate program on time. Being an engineer for more than three decades and spending most of his life figuring out how to unlock the stored energy potential of Western Siberia, I also received a strong motivation to apply all my knowledge and efforts to study and develop a hypothesis on how this potential can be improved here in Canada – at the last frontier of unconventional resource exploration. The strong love and caring that I got from my mother Nataliya Pantus even while staying in far away land, always kept me in good spirits and helped me to overcome the constant challenges that I was facing while delivering final results of this project. I always will be thankful to my elder brother Andrii Pantus, who basically introduced me to the world of engineering and science when I was still little, and our numerous discussions that one day helped me to gain good personality and determination to succeed in future endeavors.

TABLE OF CONTENTS

LIST OF TABLES

LIST OF FIGURES

LIST OF APPENDICES

NOMENCLATURE

EOR	Enhanced oil recovery
OOIP	Original-oil-in-place
HPAM	Hydrolyzed polyacrylamide
HAP	Hydrophobically associating polymer
PTRC	Petroleum Technology Research Center
STEPS	Sustainable Technologies for Energy Production Systems
FGSR	Faculty of Graduate Studies and Research
M	Mobility ratio
F_{μ}	Viscosity ratio
k	Permeability (darcy)
I_{sc}	Peters and Flock's dimensionless number
R_{bt}	Bentsen's dimensionless number
PV	Pore volume (cm^3)
PAM	Polyacrylamide
N_c	Capillary number
F_R	Resistance factor
q	Injection rate (cm^3/min, cm^3/s)
A	Cross-sectional area of the porous media face (cm^2)
F_{Rr}	Residual resistance factor
IPV	Inaccessible pore volume
NaCl	Sodium chloride (brine)
DPR	Disproportionate permeability reduction

CPAM	Cationic polyacrylamide polymer
$CONH_2$	Amide groups
COO^-	Carboxyl groups
CO_2	Carbon dioxide
WHMIS	Workplace Hazardous Materials Information System
dP (ΔP)	Differential pressure (kPa, atm)
L	Length of the core (cm)
RF	Recovery factor (%OOIP)
IWF	Initial waterflood
PF	Polymer flood
EWF	Extended waterflood
RRF	Residual resistance factor
OF	Initial oil re-saturation
OFP	Oil flood after polymer
m_{pinj}	Mass of injected polymer solution (g)
m_{ieff}	Mass of the effluent polymer solution (g)
C_{Pinj}	Concentration of injected polymer solution (wt%)
C_{Pieff}	Concentration of the effluent polymer solution (wt%)
m_{sand}	Mass of sand (g)
C/Co	Fraction of final to initial polymer concentration
S	Saturation
H_2O	Water

Subscripts

w	Water phase
o	Oil phase
p	Polymer phase
or	Residual oil
oi	Initial oil

Greek symbols

λ	Mobility (darcy/mPa·s)
μ	Viscosity (mPa·s, cp)
Γ	Shear rate (SR) (s^{-1})
ϑ	Linear advance rate (q/φ·A)
φ	Porosity (fraction)

SI metric conversion factors

in.	x	2.540 000	E+00	=	cm
sq in.	x	6.451 600	E+00	=	cm^2
cu in.	x	1.638706	E+01	=	cm^3
°F	x	(°F-32)/1.8		=	°C
cp	x	1.000 000	E+00	=	mPa·s
darcy	x	9.869 000	E–07	=	m^2
psi	x	6.894 757	E+00	=	kPa
lbm/cu ft	x	1.601 846	E+01	=	kg/m^3
lbm	x	4.535 924	E–01	=	kg

1. INTRODUCTION

1.1 General introduction

Polymer flooding has proven a highly beneficial enhanced oil recovery technique in terms of reducing the tendency of injected fluid to channel through reservoir matrix. Therefore, typical heavy oil secondary recovery (waterflooding) process results in poor sweep efficiency and early breakthrough of the water at the producer, leaving substantial volumes of unswept oil behind. Polymer flooding as one of the chemical EOR methods is highly recommended to maximize reservoir recovery performance with over 40 successful years in commercial applications. It is proven as a low risk EOR method and applicable for a variety of reservoir conditions (http://www.snf-oil.com/). It is also considered to be an economically very attractive conventional enhanced oil recovery technique since it uses similar infrastructure as waterflooding process.

Polymer flooding is implemented typically in reservoirs that have been previously exposed to waterflooding and utilizes water-soluble polymers that are dissolved in injected water thereby potentially increasing the viscosity of the displacing aqueous phase. The process of polymer injection is typically prolonged until 30 % of reservoir pore volume is injected. This volume of polymer solution is then chased by extended waterflooding to move the mobilized by polymer oil bank and follow polymer slug towards the producer (**Figure 1.1**). As a result, improved sweep efficiency and far less occurrence of complex instabilities and channeling along the reservoir matrix is evident than with waterflooding.

Figure 1.1 A schematic representation of polymer flooding EOR process (low resolution reproduction from http://www.snf-oil.com/, courtesy of SNF FLOERGER®)

This effect is normally provided through the multiphase relative permeability effect and other important parameters that can quantitatively describe polymer flooding performance such as, for instance, mobility ratio (M) or viscosity ratio (F_μ):

$$\boldsymbol{M = \frac{\lambda_w}{\lambda_o} = \frac{k_w/\mu_w}{k_o/\mu_o} = \frac{k_w \cdot \mu_o}{k_o \cdot \mu_w}} \quad \textbf{(1.1)}$$

$$\boldsymbol{F_\mu = \frac{\mu_o}{\mu_w}} \quad \textbf{(1.2)}$$

where λ is the mobility (darcy/mPa·s) and μ – viscosity (mPa·s) of either water or oil phase, k – relative permeability to either water or oil phase (darcy).

Since polymers can increase the viscosities of water, they, at the same time, tend to decrease the mobility ratio (viscosity ratio), and, thus, they provide improved displacement performance. Therefore, the closer the mobility ratio to one, the more stable and efficient the oil displacement can be achieved. Highly viscous polymer solutions can be obtained through a wide range of concentrations, typically ranging from 0.05 wt% to 0.20 wt% in reported polymer flood applications.

All the above mentioned features and mechanisms of polymer flooding have already proven effective in light oil reservoirs. However, since little has been discovered in the field of heavy oil polymer flooding, it has been recommended to investigate its performance through the parameters described in further section.

1.2 Problem statement

As the subsequently presented comprehensive literature review proved, polymer flooding may be a highly beneficial EOR technique for heavy oil recovery. It is considered to be advantageous than conventional waterflooding for dealing with heavy oil displacement due to reduction of channeling through reservoir matrix that might

contribute to much of the residual oil being bypassed due to viscous instability behaviour. As the literature review also showed, viscous instabilities can be essentially characterized by such parameter as viscosity ratio between displaced and displacing phase. Therefore, one of the objectives of this thesis was to visually investigate and characterize the viscous instability behaviour in porous media during heavy oil displacement by water and polymer. The resistance factor, which is measured as a pressure differential during polymer flow to brine flow, essentially serves as a representation of polymer solution in-situ viscosity at applied shear rate in porous media. The residual resistance factor, on the other hand, represents the ability of the polymer solution to reduce the permeability to the subsequently injected water. All these important parameters, and also the effect of dynamic polymer adsorption, have been investigated and discussed in this thesis.

Since this work was funded by the Petroleum Technology Research Centre (PTRC), a report similar to this thesis was also submitted to PTRC (Torabi and Wilton, 2012). It is the goal of this thesis to evaluate the parameters discussed above in order to predict the potential technical feasibility of polymer injection in heavy oil reservoirs by improved conformance control and sweep efficiency. There are two ways to determine this:

- The effect of viscosity ratio on viscous fingering behaviour during the displacement of various heavy oils through visual representations in two-dimensional visual acrylic cell and accurately assessing each particular phenomenon and feature that occurs during visual observations.

- The effect of viscosity ratio on heavy oil recovery and pressure response as well as corresponding resistance and residual resistance parameters together with dynamic polymer adsorption during linear coreflood displacements.

The above-mentioned demonstrations will provide understanding of non-Newtonian fluid performance and further bases for possible applicability of polymer flooding as an EOR technique during heavy oil recovery.

1.3 Thesis organization

Chapter 2 illustrates comprehensive literature review pertaining to selected topic of the thesis and covers basic concepts and numerous experimental studies conducted earlier as well as the most recent ones. The subsequent section of the thesis (Chapter 3) describes the main fluid materials used in this study as well as procedures for their preparation. A detailed description of experimental equipment and experimental procedures are shown in Chapter 4. Chapter 5 showcases final results and corresponding discussion from the conducted experimental tests, while Chapter 6 highlights main conclusions derived from them together with recommendations pertaining to future studies.

2. BACKGROUND AND LITERATURE REVIEW

The primary focus of subsequent sections is two-dimensional and one-dimensional linear flows, since a little work has been done on three-dimensional problems. The given literature review aimed to provide a comprehensive analysis of the viscous fingering phenomenon occurring during only liquid-liquid immiscible displacement and also recovery performance corefloods. The review covers basic concepts of instability theory and focuses only on linear or rectilinear two-dimensional fluid displacement in transparent models. The review also presents a substantial portion of studies conducted on cylindrical 1D models with reference to viscosity ratio where possible. In addition, the review summarizes the research work conducted on dynamic polymer flow at pore-scale level in various visual models, sandpacks, and cores and its adsorption as well as resistance and residual resistance behaviour.

2.1 Viscous fingering during two-dimensional immiscible liquid-liquid displacement

2.1.1 Instability theory

The first detailed study about "viscous fingering" as a representative of instability of the transition zone during immiscible displacement process was presented by Engelberts and Klinkenberg (1950). As the study was carried out, a range of viscosity ratios (μ_o/μ_w) at different increments was applied to the model. Thus, higher viscosity ratios led to a decrease in the breakthrough recovery. This was associated with a phenomenon called "viscous fingering," which was eventually proved by study of the mechanism of the displacement. As a part of the study's observations, there was no significant instability recorded at $\mu_o/\mu_w = 1$. However, certain concerns were identified

for the other two values of the viscosity ratio where the transition zone between oil and water proved to be unstable.

Later, Hill (1952) carried out experiments that led to a theory of channelling, which can be described as one liquid penetrating another, creating channels in porous media. The viscosities and densities of both fluids have been taken into consideration while deriving a so-called critical velocity factor, which serves as an indicator of the onset of instabilities when the value is above critical. During the displacement of a less mobile fluid by a more mobile one, the viscosities of both have been defined as predominant parameters that lead to instabilities of the displacing interface.

Perhaps one of the first qualitative experiments that visually showed the viscous displacement of oil by water was conducted by van Meurs (1956). The study investigated displacement efficiency at viscosity ratios of 1:1 and 80:1 in a linear water drive. The displacement regime was then scaled to real reservoir conditions by applying principles described by Croes, Geertsma, and Schwarz (as cited in Richardson et al., 1957). The viscosity ratio of 1:1 demonstrated excellent displacement efficiency in uniform sandpacks (See **Figure 1, p. 296, paper SPE 678-G**). The viscous fingering phenomenon appeared to have a predominant effect during oil displacement at higher viscosity ratios (80:1) (See **Figure 2, p. 296, paper SPE 678-G**), however.

A follow up study by van Meurs and van der Poel (1958) aimed to provide detailed theoretical description of viscous fingering behaviour observed earlier in other studies. They introduced the concept of protrusions and oil pocket generation along the predominant finger.

Therefore, three distinct areas of instabilities have been identified: the area outside the viscous finger where oil flows freely; the sum of the center areas of the fingers where water flows freely; and areas with immobile oil and water at the edges of the viscous fingers.

A subsequent study by Chuoke et al. (1958) aimed to reduce the boundaries between experimental and theoretical viscous fingering analysis. It was the first attempt to provide a theoretical analysis of the onset of fingering. As Kueper and Frind (1988) describe, the authors extended the work of Hill (1952) by conducting a study on immiscible instabilities of two immiscible fluids' dynamics in homogeneous porous media on a planar interface. The critical velocity factor was derived similarly to that of Hill (1952) but then modified by introducing interfacial tension between fluids and a certain wavelength value greater than critical wavelength. In addition, the wavelength at which maximum instability occurs has been introduced; thus, for natural perturbations, this wavelength will dominate and characterize the onset of instability or viscous fingering. This study was the first to suggest that by applying instabilities into model scaling, a certain dimensionless group is required to be introduced.

The dimensionless numbers were, therefore, tested by Saffman and Taylor (1958). The instabilities generated by air injection displacing glycerin solution tended to be less evident at early stages of displacement but then tended to transform into at least a couple of "predominant fingers," leaving others behind and, thus, demonstrating complex "shielding" behaviour. Shielding behaviour typically happens when fingers of more mobile and less viscous fluid grow in the direction of the pressure gradient, penetrating

more viscous fluid. This results in the established predominant fingers outrunning and "shielding" others from further propagation.

A follow-up study by Saffman (1959) extended the theory of the motion of the interface between two viscous fluids in porous media or Hele-Shaw cells provided initially by Saffman and Taylor (1958). The exact solution for the fingers' propagation was provided by employing certain mathematical algorithms to finger front motion. In this case, interfacial stress effects are negligible and the viscosity of the driving fluid can be neglected as well. The finger propagation was also considered as equal for all equally spaced fingers. This led to the assumption that a predominant, long viscous finger advances through a parallel-sided channel filled with more viscous fluid.

Varnon and Greenkorn (1968) modified Saffman and Taylor's (1958) concept of instability behaviour by introducing three potentially important regimes of flow: a gravity-dominated unstable regime, a gravity-viscous balanced stable regime, and a viscous-dominated regime. Their results suggest that viscous fingers "are not always half as wide as their spacing; however their width depends on fluid and media properties and is dependent of velocity and spacing" (Varnon and Greenkorn, 1968). The asymptotic relative finger widths varied from 0.43 to 0.81 during experimental observations.

The prediction that viscous fingering is independent of microscopic irregularity and that the displacement is independent of wavelength was made by Gupta et al. (1973). The study also verified the Chuoke et al. (1958) theory; therefore, Chuoke's velocity and the number of Chuoke fingers have been introduced into later analyses. The experimental analysis revealed that the number of incipient fingers appeared to be the same as that obtained from Chuoke's theoretical model. The fingers' wavelengths were overridden by

some local heterogeneity, which was predicted to some extent. The generated predominant fingers tended to coalesce with others, creating one major finger, which advanced directly through the center of the model.

A great qualitative representation of immiscible displacement in linear models was performed by Perkins and Johnston (1969). As it turned out, the displacement front appeared to be relatively stable at the beginning of injection; however, as the displacement continued, instability formed. At this stage formation of multiple fingers was detected. Consequently, this led the fingers to coalesce into a couple of predominant fingers to propagate further to the fracture channel (See **Figure 2, p. 40, Paper SPE 2230**). As expected stable and uniform piston-like front was indicated during high rates of injection, while at low rates, when the capillary forces appeared to be predominant, the "island" effect took place, while for saturated cases the "entrance effect" (See **Figure 4, p. 43, Paper SPE 2230**) with further graded saturation dominated. The most significant differences of two-phase immiscible behaviour of initially saturated and non-saturated bead-packed models were observed during the displacement at very unfavourable mobility ratios. Thus, while under unsaturated conditions, the water-filled fingers were invaded by the bypassed oil (See **Figure 2, p. 41, Paper SPE 2230**), the behaviour of the initially water saturated model, a near irreducible minimum case, was represented by a high number of small fingers that occurred at the entrance of the flow channel. This kind of behaviour soon transformed into a fine dendritic network of channels, forming a so called "graded saturation zone" at later stages of displacement (See **Figure 4, p. 43, Paper SPE 2230**).

Peters and Flock (1981) were the first authors who arrived at a stability criterion for onset of instability prediction. While previously Engelberts and Klinkenberg (1950) mentioned the particular value of viscosity ratio at which sharp decrease of stability occurs, referring to further investigations, Peters and Flock (1981) used dimensionless number I_{sc} to identify the onset of instability, which caused a significant decrease in the breakthrough oil recovery for both cylindrical and rectangular types of systems. Both analytical and laboratory studies on stability theory proved that instability occurs in both oil- and water-wet media, and the optimal critical value for the onset of instability is I_{sc} = 13.56, beyond which a displacement would become unstable.

The impact of instabilities on Dow Corning oil, mineral oil, and kerosene displacement was investigated by Bentsen and Saeedi (1981). The experimental study was conducted also utilizing a range of viscosity ratios of 9-, 12:1, and one that is considered as favourable. The study often refers to the Buckley-Leverett theory of stable displacement. Therefore, the results of this study suggest that determined saturation profiles coincided with results predicted by linear immiscible displacement theory. Therefore, the displacements were stable for Dow Corning light oil displacement, and no entrance or outlet end effects were evident. The displacement of light mineral oil, on the other hand, demonstrated some fingering. A much more favourable viscosity ratio during kerosene displacement resulted in much lower occurrence of instabilities.

Bentsen (1985) described a comprehensive, new approach for instability theory in rectangular systems from a force potential point of view instead of velocity potential viewpoint. The force potential has been described as a form of perturbation potential of interface between displaced and displacing phases. Therefore, it has been suggested that

account should be taken of perturbation potentials for the water on the oil side of the interface and vice-versa. As it turned out, the perturbation velocity identification for both steady-state and unstable scenarios has been an important variable for continuity to take place as continuity represents an important variable of this study, together with symmetry. As for the stability criterion, it is proportional to one obtained by Peters and Flock (1981).

An attempt was made to describe viscous fingering behaviour, both qualitatively and quantitatively, by Sarma (1986). The impact of viscosity ratio on viscous fingering behaviour and recovery efficiency in both drainage and imbibition conditions and during different displacement regimes have been investigated. The analysis of viscous fingering displacement of mineral oil by distilled water and other miscible fluids at varying viscosity ratios 2.25-, 36-, 40-, and 16.4:1 formed the basis for qualitative analysis of the presented phenomenon. The quantitative analysis was performed by employing a concept originally derived by Chuoke et al. (1958). As it was initially expected, the wavelengths of fingers appeared to be functions of the displacement rate. Higher displacement rates contributed to smaller fingers' wavelengths, thereby providing a larger number of grown fingers. In addition, the imbibition regime appeared to be a more efficient displacement process since the fingers in the imbibition direction have greater wavelengths than in the drainage condition.

A great deal of research on the new approach described previously was conducted by Sarma and Bentsen later in 1987. The main goal was to determine how the linear time function would work with the theory developed earlier by Bentsen (1985). According to the authors, the breakthrough recovery as a function of instability number showed good

resemblance to predicted values and experimentally obtained results for each of the chosen mobility ratios. Thus, obviously, the highest possible breakthrough recovery factors were obtained from low mobility ratios, corresponding to stable regions of displacement. The transition region can be described by the significant decrease in recovery factor corresponding to a more than twice larger mobility ratio. One final prediction could be made in that stability was not as dependent on instability dimensionless number as it was on mobility ratio.

Homsy (1987) aimed to provide a comprehensive summary of work that was done on viscous fingering analysis in homogeneous porous materials. The qualitative analysis of viscous fingering behaviour was carried out through detailed discussion of complex shielding, spreading, and splitting behaviour that are typical for this kind of liquid-liquid instability. The saturation differences that occurred behind the displacement front can provide a mobility reduction to all phases. Therefore, typical "spreading" behaviour can be described as a direct result of capillary imbibition as one fluid is being displaced by another, and this numerically can be described as diffusive effect.

Coskuner and Bentsen (1988) developed an assumption that the immiscible displacement of one fluid by another can be described as a moving boundary problem. The model earlier developed by Bentsen (1985) was taken as the basis of this new model. The results suggested that no significant difference in shape of propagating finger was observed in either water-wet or oil-wet systems conversely to Chouke et al. (1958), whose work suggested that displacing fluid should be non-wetting. Therefore, for water-wet systems, the thickness difference can potentially alter the fingers' structure.

A comparative analysis of viscous fingering patterns was conducted for comparison of both homogeneous and heterogeneous porous media by Brock and Orr (1991). The results from the homogenous model suggest that dynamic finger propagation can be described by spreading, splitting, shielding, and coalescence complex behaviour. Thus, fingers that move ahead of others more often "shield" the others from further propagation; meanwhile, others unite during coalescence into faster moving fingers. The examined fingering patterns led to the conclusion that fingering behaviour was more sensitive to mobility ratio differences than to flow rate. In the heterogeneous model, on the other hand, the flow followed the path of high permeability at mobility ratio = 1 and the viscous perturbations were not as evident as for homogeneous scenarios.

A similar study to Peters and Flock (1981), but later, in 1992, was carried out by Chakrabarty and Bentsen (1992). The dimensionless instability number and its critical value were obtained through the application of boundary and compatibility conditions to water-oil perturbation velocities in cylindrical systems. Although the instability number can be clearly predicted or estimated, especially during the initial stages of the displacement process, the importance of mobility ratio should be considered, as well. Thus, several considerations should be taken into account as the unfavourable mobility ratio slows down the displacement front.

The impact of injection flow rates and viscosity ratio on two-phase immiscible displacement under drainage conditions was studied by Pavone (1992). The following conclusions were made from visual representations of moldings obtained during the tests at different flow rates and viscosity ratios. According to the results, viscous fingering can be characterized as having two areas: a stable area, which is common in all of the

obtained patterns, is characterized by the length of the finger, and is stable enough in terms of displacement efficiency. The next area is where instability occurs. It is caused by the viscosity difference between two phases and can be characterized by the volume of fingering zone.

In order to describe the instabilities on a megascopic level, Sarma et al. (1994) deployed a series of tests that considered the effect of viscosity ratio. Its effect on relative permeability at four different flow rates has been also considered. Bentsen's (1985) instability number was used for instability behaviour prediction. As a result, however, some inconsistencies with the basic concepts of instability theory developed initially by Peters and Flock (1981) and Bentsen (1985) took place during breakthrough recovery estimation. Thus, while the Bentsen's number aligns well with stability concepts during stable displacement, during unstable regimes, the R_{bt} values increase with increasing instabilities in medium-heavy oil. More viscous oil displacement, however, demonstrated no changes in R_{bt} with varying instabilities.

2.1.2 Polymer flooding viscous fingering analysis

Bonn et al. (1995) reported a study of polymer instabilities in thin linear flow compared with Newtonian fluids using finger width as a function of finger velocity. The authors used Saffman and Taylor's (1958) work as a reference to classical instability theory. The first scenario utilized an aqueous surfactant solution representing more viscous fluid displaced by less viscous oil (0.407 mPa·s). The results were compared to those obtained by injection of 0.002 wt% and 0.05 wt% polymer solution. While the surfactant displacement aligned well with the classical behaviour of instability theory, the

classical instability theory basic concepts were significantly altered when dealing with non-Newtonian complex fluid flow.

A comparative viscous fingering analysis of HPAM polymer systems and newly developed so-called hydrophobically associative polymers (HAP) displacing 200-mPa·s oil was conducted recently by Aktas et al. (2008). The HAPs are believed to have greater in-situ viscosities at the same concentration as HPAM, providing better sweep efficiency and much more stable displacement. Comparative viscous fingering patterns were obtained for both Flopaam 3630S and Superpusher S255 and for brine versus pore volume throughput (See **Figures 9 and 7, pages 10 and 9, Paper SPE 113264**) in both cases after brine flooding and polymer flooding alone. The obtained experimental results suggest that low associative polymer substantially improved the microscopic displacement efficiency of viscous oils, positively affecting recovery when compared to polyacrylamide solution.

Another micromodel viscous fingering study was conducted later by Jamaloei et al. (2010) but this time using low-tension polymer flooding for displacement of 80.61-mPa·s crude. The authors employed a series of dimensionless parameters to quantify the unstable behaviour. The follow-up study by Jamaloei et al. (2011) resulted in a more detailed qualitative analysis of visual interpretation of the viscous fingering behaviour of low-tension polymer flooding from the previous study. The fingers tended to establish diagonal connections between injector and producer in an etched model. Typical splitting and spreading mechanisms of viscous fingers were indicated, which was responsible for the growth of the viscous fingers and development of the fingering patterns during polymer injection. The mechanism of sideways expansion of the fingering patterns is an

intermediate phase of the fingered pattern development. Contrary to the onset of fingering, where the pressure drop increases sharply, sideways finger propagation results in a relatively uniform pressure differential decline. Such mechanistic behaviour as finger coalescence (Brock and Orr, 1991) is mainly a result of larger fingers consuming major volumes of the injected fluid while at the same time holding back smaller fingers from further propagation.

A subsequent study by Buchgraber et al. (2011) in etched micromodel extended the knowledge of viscous fingering comparison between HPAM and HAP polymers by conducting a mechanistic study to observe the stability of advancing fronts of injected aqueous solutions. The same polymer systems were used as in Aktas et al. (2008) but with varying concentrations from 0.05 wt% to 0.25 wt% displacing crude oil with 210-mPa·s viscosity. The results of the study indicate that sweep efficiency and recovery were substantially improved by polymer concentration in a range of 0.125-0.150 wt%. Interestingly, the highest concentration of 0.25 wt% led to poor recoveries and sweep efficiencies. While in case of brine flooding, severe fingering took place, polymer flooding demonstrated substantial improvement in recovery with far less occurrence of viscous instabilities. As expected, associative polymer systems improved displacement front stability with only minor fingers present (See **Figure 17, p. 16, Paper SPE 122400**). The HPAM system, on the other hand, exhibited severe viscous fingering for all ranges of studied concentrations (See **Figure 13, p. 13, Paper SPE 122400**). Generally, even though the associative polymer system showed an improved displacing front, the ultimate recovery did not significantly differ from recovery with HPAM polymer flooding at all concentrations.

An excellent follow-up study was conducted later by Clemens et al. (2012). The results of viscous fingering propagation in the micromodel study conducted by Buchgraber et al. (2011) were taken as input parameters for the study of the viscous instability phenomenon at the pore scale (See **Figure 14, p. 14, Paper SPE 154169**). The results suggest that the shear rates are higher in the pore throats than in the pores with corresponding lower shear-thinning polymer solution viscosities. This demonstrates that the displacement efficiency of the polymer system exhibits shear-thinning behaviour in porous media. Concentrations, however, appeared to be independent of the abovementioned factors, as well as of pressure. It was also concluded that polymer shear-thinning behaviour can contribute to microscopic displacement efficiency.

A recent study conducted by Doorwar and Mohanty (2011) focused on viscous fingering behaviour during heavy oil displacement in a micromodel by water and 0.30 wt% 3630S HPAM injection. The displacement efficiency was investigated with corresponding viscosity ratios of 1-, 10,000-, and 100:1. As expected, the viscosity ratio of 1:1 gave the most stable displacement while 10,000:1 demonstrated severe fingering behaviour. After brine flooding, one predominant tree-like finger appeared in the front, leaving substantial volumes of intact oil behind (See **Figure 4, p. 6, Paper SPE 146841**). Even though the sideways branches of the fingering also contained a significant amount of water, they negatively affected further displacement. Therefore, the oil next to them is considered as immobile. This could indicate lower oil relative permeability than for lighter oil displacement at the same saturation conditions (Wang et al., 2006). The final picture of brine flooding showcases some sort of complex spreading and dispersion (See **Figure 5, p. 7, Paper SPE 146841**). Comparatively different behaviour was observed

during polymer injection. A predominant finger appeared with side branches growing simultaneously (See **Figure 6, p. 8, Paper SPE 146841**). After both fingers reached breakthrough, other fingers in the displacement front started to grow and sweep more oil out, thereby forming an interconnected, dendritic network of channels along the model (See **Figure 7, p. 8, Paper SPE 146841**). It was concluded that viscosity ratio can control viscous finger propagation, so, therefore, before breakthrough; an increase of viscosity ratio contributes to a decrease in the number of viscous fingers.

A recent study by Skauge et al. (2012) investigated 2000-7000-mPa·s heavy oil displacement performance by water and polymer injection. The results from all heavy oil floods demonstrated strong viscous fingering during waterflooding. Typical for viscous fingering, multiple finger tip splitting, reinforcement, and thickening took place during finger propagation. In addition, finger coalescence, originally described by Brock and Orr (1991), appeared to dominate during brine injection. Polymer injection, on the other hand, led to faster recovery response for less viscous oil and provided better sweep efficiency for all oil viscosities. However, it left the ultimate oil recovery at almost the same level for both oils, leading to the conclusion that oil viscosity was not the major parameter influencing the displacement process. However, at higher oil viscosities, sharper fingers were evident in both waterflood and polymer flood scenarios, and they became more evident at more unfavourable mobility ratios. This suggests that finger shape is mainly controlled by mobility ratio. The results from this study were also compared to those obtained with 1D corefloods conducted earlier by Bondino et al. (2011).

2.2 1D corefloods literature review

2.2.1 Main mechanisms behind profile modification by polymer flow in porous media

The generally held belief that polymer flooding does not contribute to increase of recovery at micro-scale level was contradicted by Wang et al. (2000). This concept was previously accepted because it is known that capillary number (N_c) had to be increased significantly in order to get large increase in recovery; however, polymer flooding can give only small increases. Viscoelasticity of polymer solution, on the other hand, can contribute to residual oil being "pulled" out. The viscous-elastic effect on residual oil of non-Newtonian fluid (polyacrylamide) versus Newtonian was investigated at a micro-scale level. Four different types of residual oil were identified: an accumulated oil film on the rock surface, "dead end" residual oil, oil in pore throats held by capillary forces, and unswept oil in micro-scale heterogeneous core spaces. All these types of residual oil can be reduced by viscous-elastic polymers. However, one should take into consideration that different types of elastic non-Newtonian fluids have different rheological parameters. Numerous coreflood tests from this study showed that polymer solutions can significantly increase oil recovery (5~8 %OOIP); thus, the displacement efficiency can be increased. However, the mechanism behind this behaviour was not fully studied. A series of coreflood tests was conducted to analyze performance of HPAM in two scenarios: after water and glycerin flooding and after water but before glycerin flooding. The results indicated that, in first case both glycerin and HPAM contribute to increased recovery while the second case does not show recovery improvement after glycerin. This reveals some additional properties, besides viscosity, of polymers that contribute to improved

recovery performance. Since polymer solution is more viscous than water, it can displace the residual oil that was initially trapped by capillary forces. In addition, due to much more favourable mobility between polymer and oil, more trapped oil can be driven out (See **Figure 16, p. 9, Paper SPE 63227**). However, it was found that, after more detailed visual analysis, the residual oil is "dragged" and "stripped" rather than "pushed" out (See **Figure 18, p. 9, Paper SPE 63227**). This suggests that elasticity of polymer solution possibly contributes to displacement efficiency. Generally speaking, the difference between visco-elastic fluids and fluids with no elasticity is visually noticeable. Visco-elastic behaviour of HPAM for example, can demonstrate superior microscale displacement efficiency, comparing to water in porous media environment.

A subsequent study by Wang et al. (2007) illustrates the influence of elasticity as the main driving parameter for polymer solutions on displacement efficiency. The comparison of microforces interacting between driving fluids in both fluids with and without elastic properties was analyzed by means of a micromodel, 1D coreflooding, and numerical simulations. The results from both laboratory conditions and at field-scale indicate that displacement efficiency of polymer flooding is much higher than waterflooding. The main postulates of polymer rheological properties state that different viscosities of Newtonian fluids cannot change the displacement efficiency. However, they can contribute to mobility ratio change and sweep efficiency. Non-Newtonian (e.g., HPAM) fluids at different concentrations, on the other hand, can influence displacement efficiency with viscosity change, as was found from experimental studies (See **Figure 9, p. 6, Paper SPE 109016**)

The above-described study was extended in a subsequent paper by Wang and Wang (2012). A residual after waterflooding oil blob was considered for study of the effect of polymer elastic properties specifically on displacement efficiency. The results showed that microforces during polymer flooding are usually 20 times higher than those during waterflooding. The displacement efficiency in this case can be increased due to deformation and further mobilization of the residual oil blob. This deformation and mobilization can be observed in both oil-wet and water-wet micropores (See **Figures 4 and 8, p. 6-7, Paper SPE 153070**). Generally, the results show that viscosity has an impact on mobility ratio (M) and, therefore, on macro-scale sweep efficiency, and, at the same time, on volumetric sweep efficiency. The elasticity of non-Newtonian fluids themselves contributes to interaction at micro-scale level, thereby generally contributing to change in displacement efficiency.

An excellent study conducted by Jennings et al. (1971) provides a unique insight into factors that affect mobility control of polymer solutions. The wide variety of polymer solutions with different properties have been investigated (e.g., Xanthomonas, Polyisobutylene, HPAM, etc.) in cores. The paper provides some of the fundamental knowledge of polymer flow in porous media. The paper suggests that during low flow rate polymer flooding and with no change in permeability, a so called "resistance factor" transforms into the relation of polymer viscosity to water viscosity μ_p/μ_w. The resistance factor (F_R) itself represents the reduction of polymer solution mobility compared to the flow of either aqueous solution and serves as indicator for in-situ polymer viscosity:

$$\boldsymbol{F_R = \frac{\lambda_w}{\lambda_p}} \qquad \textbf{(2.2.1)}$$

where λ is the mobility of either polymer or water phase (darcy/mPa·s).

Therefore, the shear rate (Γ) at the wall of capillary in simple porous medium model can be calculated from:

$$\boldsymbol{\Gamma} = \frac{\boldsymbol{\vartheta}}{\left[\mathbf{0.5}\left(\frac{\boldsymbol{k}}{\boldsymbol{\varphi}}\right)\right]^{\mathbf{0.5}}} \quad (s^{-1}) \qquad \textbf{(2.2.2)}$$

where ϑ is the linear advance rate ($q/\varphi A$), k – absolute permeability of porous media (darcy), φ – porosity, A – cross-sectional area of porous media (cm^2), and q – injection flowrate (cm^3/min).

The residual resistance factor (F_{Rr}), on the other hand, indicates the reduction of water post-polymer injection mobility compared to water injection before polymer flooding:

$$\boldsymbol{F_{Rr}} = \frac{\boldsymbol{\lambda_w(initial)}}{\boldsymbol{\lambda_w(after\ polymer)}} \qquad \textbf{(2.2.3)}$$

where λ is the mobility of water phase (darcy/mPa·s).

Generally, the residual resistance factor also provides evidence of permeability change initiated by polymer flow. F_{Rr} can be also easily considered from a practical or economical point of view. Since polymer injection is considered only for a portion of a waterflood secondary recovery process, the residual resistance controls viscous instabilities caused by mobility difference between polymer and water that is injected after polymer. The polymer adsorption in this case does not have a substantial effect on resistance produced by the polymer.

2.2.2 Heavy oil polymer flooding studies

A good comparative analysis of four different concentrations of polymer solutions with three different molecular weights during the displacement of two low API gravity crudes, 220- and 1140 mPa·s, was conducted by Knight and Rhudy (1977). The results from waterflooding and subsequent polymer injection suggest that 220-mPa·s oil displacement by HPAM solution of the highest molecular weight demonstrated much better performance than HPAM with lower molecular weights at the same concentrations. While waterflooding efficiency of higher viscosity oil displacement decreased, polymer injection recovered more additional oil. It is critical to note that oil recovery was a function of injection volume for all cases. All in all, higher concentrations of polymer solution improved oil recoveries.

Wang et al. (2006) investigated the effect of viscosity on relative permeability behaviour during heavy oil displacement. They tested a range of 430-13550-mPa·s heavy oils. The results indicate that viscosity can change oil-water relative permeability curves. It has been concluded that with an increase in oil viscosity, residual oil saturation tends to increase while irreducible water saturation decreases. This perfectly aligns with the viscous instability studies of heavy oil displacement by Doorwar and Mohanty (2011). This is explained as since in strongly water-wet systems (sandpacks), the water tends to invade the small pores or narrow channels, especially during heavy oil waterflooding, so much of the oil is left behind in large pores due to severe viscous fingering.

The effects of oil viscosity, polymer solution concentration, and displacement velocity and rock permeability have been studied by Asghari and Nakutnyy (2008). A broad range of HPAM polymer solution concentrations from 0.1 to 1 wt% was used to

displace heavy oils with viscosities from 1000 to 8400 mPa·s in sandpacks with varying flow rates. Better oil recovery was indicated for less viscous oil and at higher concentrations of polymer solution at both injection rates tested in this study. The effect of polymer concentration basically confirmed the results of Wang and Dong (2007). Permeability variation did have an effect on oil recovery; more permeable sandpacks demonstrated higher recovery factors under similar conditions and the same polymer concentrations, while higher injection rates led to poorer recovery probably due to severe viscous fingering that tends to occur often at high injection rates. All in all, the threshold value for polymer solution concentration to be effective appeared to be 0.5 wt%.

In Wang and Dong (2007), HPAM was used to displace 1450-mPa·s heavy oil in the same sandpack as described earlier in Wang et al. (2006). The main conclusion from all experimental tests was that increased polymer effective viscosity contributed to an increase in tertiary oil recovery. Wang and Dong (2009) extended their studies on HPAM solutions displacing viscous heavy oils by defining the "optimum effective viscosity value" of polymer solution for heavy oil displacement. The study, conducted on sandpacks similar to Wang and Dong (2007), involved heavy oil displacement but with a broader range viscosity oil systems from 430 to 5500 mPa·s. The results of this study revealed that tertiary oil recovery increases with increased volumes injected. The increased effective viscosity of the polymer solution also contributed to increased oil recovery (See **Figure 2, p. 157, Wang and Dong, 2009**). As was noted in the previous study by Wang and Dong (2007), the tertiary recovery versus effective viscosity of polymer solution plots show an S-shape, where a specific viscosity range of polymer solution for each oil sample exists in which the recovery increases significantly with

increased effective viscosity of polymer solution only at a certain optimum range of viscosities (See **Figure 3, p. 157, Wang and Dong, 2009**). One may note that even though the polymer concentration for each oil sample was increased accordingly, the ultimate oil recovery after tertiary polymer flooding appeared to be relatively the same for each individual oil viscosity. However, this conclusion could be attributed to the same waterflood performance and similar residual oil saturation; therefore, oil recovery response would be different if the same pore volumes for waterflood or polymer flood were injected for each oil viscosity case. As the authors suggested, this scenario needs to be investigated in future studies.

The results of Levitt et al. (2011) appeared to contradict the conclusions of Wang and Dong (2009). Insensitivity of oil recovery to a wide range of polymer viscosities was demonstrated. Displacement of 1900-2300-mPa·s oil was conducted by Flopaam 3630S (HPAM) at two different viscosities of polymer solution (6 and 60 mPa·s). As the results of the study indicate, two viscosities yielded high incremental oil recovery with the same injected volume of tertiary polymer injection. However, tertiary injection did not make a substantial difference in terms of ultimate recovery for two different polymer viscosities; the experiment reached ~60 %OOIP recovered in total (See **Figures 1 and 2, p. 14, Paper SPE 150566**). The differential pressure, however, increased with increasing polymer solution concentration. In addition, the same amount (~2 PV) of 3-mPa·s polymer solution was tertiary injected after continued waterflooding. The incremental oil recovery from polymer injection was, again, quite significant; however, the ultimate oil recovery appeared to be similar to the 6- and 60-mPa·s polymer injection cases. Therefore, several dimensionless groups, as in Peters and Flock (1981), Sarma and

Bentsen (1987) and Pavone (1992), were introduced into the final data analysis to identify the onset of instability, since it was believed that some instability on the displacement front can have an effect on otherwise identical recovery performance.

The effect of the variation in rock geometry on displacement efficiency was investigated by Bondino et al. (2011). They earlier presented a part of the work of Skauge et al. (2012) on HPAM displacement of extra heavy crude 7000-9000-mPa·s oil by matching results of 2D visual displacement tests with 1D corefloods. The desired polymer solution viscosity for both types of tests was 60 and 25 mPa·s at 10-70 s^{-1} of shear rate, respectively, yielding ~0.165 wt% of Flopaam concentration. The results of this study revealed that very early waterflood breakthrough took place at approximately 0.1 PV of injection due to very unfavourable viscosity ratio. Therefore, an impressive additional recovery of 29.8 % was obtained from polymer injection with corresponding waterflood response of 30.7 %. Similar results were obtained from the 2D experiments, suggesting that the model geometry is not a very important parameter when considering only incremental oil recovery after polymer injection.

An excellent study on heavy oil displacement by polymer solutions was conducted by Wassmuth et al. (2007). The study utilized three flood tests with 280, 1600-mPa·s heavy oil displacing by 0.15 wt% polymers with 18, 25 mPa·s of in-situ viscosity. Breakthrough was indicated at ~0.18 PV due to poor mobility and generally unfavourable viscosity ratio. The subsequent polymer slug injection resulted in differential pressure buildup due to higher viscous phase penetrating porous media. Superior recovery after waterflood was indicated at 52 %OOIP, while polymer injection, however, gave only 16 %OOIP of incremental recovery. The simulated polymer and tracer components in the

effluent indicated that polymer slug breaks through much faster than tracer due to inaccessible pore volume (IPV) (Pancharoen et al., 2010) (See **Figure 3, p. 8, Paper 2007-182**). Comparatively lower recovery after water injection was obtained during heavier (1600 mPa·s) oil displacement, which is expected, since more unfavourable mobility ratio is present and more inaccessible pore volume was evident. Subsequent polymer injection accelerated sweep efficiency to ~22 %OOIP of incremental recovery. It is critical to note that during polymer injection for heavy oil displacement, substantially accelerated displacement efficiency occurred with more favourable mobility ratio (M) (See **Figure 5, p. 9, Paper 2007-182**).

2.2.3 Inaccessible pore volume

Dawson and Lantz (1972) first coined the expression "inaccessible pore volume" (IPV). They proved that all of the pores may not be accessible and this phenomenon can affect polymer propagation significantly. Comparative analysis of injected polyacrylamide versus salt tracer suggested that even though both fluids were injected simultaneously, one passed the core with different velocity and broke through earlier than the other. Therefore, the polymer slug broke through sooner than the salt. Generally, total pore volume of the core was much larger than what the polymer could access. The presence of adsorption does have an effect on IPV. Therefore, with certain amounts of polymer, adsorption delays polymer slug breakthrough, while a stronger IPV effect contributes to faster breakthrough response.

An experimental and theoretical study by Sorbie et al. (1987) aimed to provide a physical understanding of xanthan biopolymer transport in porous media. The results obtained from effluent concentration profiles of Pfizer Flocon 48000™ polymer solution

suggested that velocities of higher concentrated polymer molecules appeared to be larger than those of solvent and tracers. Since there was slight evidence of polymer retention, the IPV effect can also be described through the polymer adsorption or retention. By combining these two physical mechanisms, macromolecules in smaller spaces can significantly reduce the pore throats' cross-sectional areas, thereby leaving some pore spaces inaccessible.

A study on inaccessible pore volume of associative polymer was conducted by Pancharoen et al. (2010). The experimental approach for measuring IPV in a sandpacked core utilized injection of 0.2 wt% of three types of Superpusher S255, D118, and B192 (HAP) and Flopaam 3630S (HPAM) versus 0.02 wt% of solution mixed with 1 wt% of NaCl. The results from the superposition model and conventional reservoir simulation model revealed that molecular weight of associative polymers is the main parameter that can contribute IPV behaviour changes. The conventional polymer solution, on the other hand, demonstrated IPV to be less than from the experimental data, suggesting the dependency of IPV on molecular weight.

2.2.4 Dynamic polymer adsorption studies

Mezzomo et al. (2002) presented an ultimate method for polymer dynamic adsorption measurement. A so-called isotorque method utilized injection of different concentrations of HPAM solutions in a water-saturated sandstone core containing no oil. As with all other methods for dynamic adsorption measurements, different phenomena, such as the IPV effect, must be considered. In order to validate the effectiveness of the newly developed isotorque method, the results were matched to those obtained from a conventional spectrophotometric method. The decision was also made to flush the core

after polymer injection in order to obtain stable values of RRF (residual resistance factor), which appeared to be low (< 2.0), confirming no plugging or significant restrictions at the sandface. On the other hand, as expected, the F_R tended to increase during higher concentrated polymer injection. A comparison of the results indicated that the isotorque method is much more precise in terms of adsorption profile interpretation. Therefore, it has been suggested to use this method particularly for dynamic adsorption measurements.

A qualitative analysis of Ali and Barrufet (1994) investigated dynamic adsorption by analyzing resistance and residual resistance data, since it best represents a degree of permeability reduction due to adsorption in porous media. As expected polymer adsorption contributed to the increase in irreducible water saturation in the core. With increasing polymer concentration, irreducible water saturation tended to increase. Therefore, increased polymer concentration can contribute to increase in permeability reduction. The final experimental results suggested that polymer adsorption numbers for starch polymers in a given porous system are lower than those for polysaccharides or polyacrylamides.

A study by Broseta et al. (1995) aimed to provide a mechanistic interpretation of polymer adsorption of two types of polymer systems: conventional polyacrylamide and several types of anionic HPAMs. The results from 100 % brine saturated (oil-free) porous media indicate that adsorption of water-soluble polymer systems on hydrophobic rock surfaces is larger than that of hydrophilic materials. The comparison of oil-wet and water-wet porous media revealed that the presence of oil in oil-wet systems at residual oil saturation (S_{or} = 0.19) significantly affected adsorption, decreasing it from 56 to 10-11

µg/g. The completely opposite effect was evident in water-wet systems at residual oil saturation. The presence of oil contributed to a slight increase of dynamic adsorption in all sand systems with all polymer types. Thus, for PAM, this effect was strongest – 33 to 43 µg/g at S_{or} = 0.19, while for HPAM, it was 7.5 to 10 µg/g at S_{or} = 0.2.

Experiments utilizing both two-phase flow and single phase flow were performed in both water-wet and oil-wet sandpacks and sandstone cores by Zaitoun and Kohler (1988). Permeability reduction to water was identified via comparison of xanthan and PAM adsorption on sand surface. The effect of permeability reduction is usually described by the RRF, which is equal to the ratio of initial permeability to its final value. The results of the study indicate that residual oil in water-wet porous media is trapped in front of the pore throats by capillary forces. In addition, these residual oil droplets are not in contact with water layers on water-wet rock surface; therefore, additional resistance might apply when dealing with oil droplets being trapped in front of the pore throats and simultaneously reducing the cross-sectional area accessible for water to flow (See **Figure 2, p. 10, Paper SPE 18085**).

A subsequent study by Zaitoun et al. (1998) revealed that adsorption enhances water saturation by means of hydration. In addition, the inaccessible pore volume of oil is possibly increased by plugging of fine pore channels by an adsorbed polymer layer. The possible end-point situations for water-wet scenarios are depicted on (See **Figure 8, p. 8, Paper SPE 39631**)**.** Converse to the observation where residual oil droplets can potentially reduces the accessible pore throat cross-sectional area, at irreducible water saturation, the size of the pore throat accessible for oil is not significantly reduced by the adsorbed polymer layer. In addition, the adsorbed polymer layer can be compressed by

oil flow in most narrow throats, and oil susceptibility to flow through the center of the pore channels can be also substantially improved.

Al-Sharji et al. (2001) investigated disproportionate permeability reduction (DPR). The effect of DPR was examined using commercial kerosene as oil phase and cationic polyacrylamide polymer (CPAM) of 2.7 mPa·s as the displacing phase. The results from one-phase flow (water-wet model, no oil) indicated the presence of piled-up polymer layers in areas of low flow velocity (See **Figure 4, p. 7, Paper SPE 68972**). The polymer material build-up occurred mostly along the grain-grain contacts. The polymer build-up was also indicated by pressure increase, and it, thus, contributed to reduction of cross sectional area to flow, thereby increasing the resistance of flow (Zaitoun and Kohler, 1988). The oil-wet scenario did not reveal any significant changes in flow characteristics and pressure response and also had small RRFs; thus, no DPR effect was present. A water-wet case of two-phase flow suggested that "water flow at S_{or} represents a larger effect than oil flow at residual water saturation" (Al-Sharji et al., 2001). Therefore, RRF_w for water-wet cases is much greater than RRF_o, showcasing the existence of the DPR effect. The polymer layer that was dynamically formed significantly decreased the effective permeability to water but did not change the oil flow, potentially due to fluid distribution and adsorbed polymer layer location.

A great comparative analysis of PAM and Xanthan dynamic adsorption was performed by Amro (2008). At constant permeability, the increased polymer concentration resulted in higher values of F_R and RRF. The increase of the brine concentration in polymer solution, on the other hand, decreased the F_R and RRF factors.

2.3 Summary of literature survey

The given literature review provided a comprehensive analysis of the viscous fingering phenomenon occurring during liquid-liquid immiscible displacement. The analysis indicated that viscous fingering or instability behaviour can be characterized by one major parameter – viscosity ratio. This parameter may control both displacement front advancement behaviour and also shape of viscous instabilities.

It has been found not enough sufficient information on heavy oil viscous fingering behaviour during polymer injection. Therefore, subsequent chapters of the thesis provided qualitative analysis of viscous fingering behaviour by comparing performance of waterflood sweep efficiency with polymer injection.

The review covered basic concepts of instability theory and also presented a substantial portion of studies conducted during coreflood displacement tests. Some of major mechanisms pertaining to polymer unique (viscoelastic) properties have been explained. It has been summarized that during 1D oil displacement by polymers not only instability behaviour is predominant mechanism but also resistance and residual resistance behaviour as well as adsorption. All these parameters can affect the recovery efficiency and injectivity of polymers, therefore series of coreflood tests were conducted to investigate their performance with respect to viscosity ratio.

The provided review demonstrated that the area of heavy oil polymer flooding is not completely investigated and some mechanisms pertaining to heavy oil recovery are not well understood as oppose to the light oil recovery field. Therefore it is reasonable to recommend additional tests in this area since it is believed that the benefit can be higher than from conventional oil recovery.

3. EXPERIMENTAL MATERIALS AND PROCEDURES

A general description of fluids used for the research and their basic physical and chemical properties are presented in this chapter. A generally approved description of various chemical solution preparation practices to satisfy the requirements of the thesis project is also given in this chapter. These procedures are supported by detailed formulations of various desired chemical compounds in the appendices of the thesis. This section also describes the equipment and detailed procedures applied for both 2D viscous fingering qualitative studies and 1D linear coreflood experiments.

Two-dimensional acrylic fracture model tests utilized only visual analysis of viscous instability dynamic behaviour during displacement of medium and heavy oil in porous media by means of both waterflooding and polymer flooding and their sensitivity to viscosity ratio.

The major part of the research was conducted in a Swagelok® steel sandpack holder utilizing the same type of porous media and heavy oil as was used for viscous fingering tests to quantitatively validate the displacement efficiency of heavy oil by various polymer systems.

3.1 Brine system

The brine system was prepared using sodium chloride SX0420-3 powder obtained from EMD Chemicals Inc. The required weight of NaCl was added to de-ionized water such that the final concentration of NaCl yielded 1 wt%. The solution was then stirred for over one hour to let the powder dissolve in water.

Table 3.2.1 List of used polymers and their properties (SNF FLOPAAM™, 2004)

Fluids	Type	Hydrolysis (mol%)	Approximate molecular weight (g/mol)
Flopaam 3630S	Anionic HPAM	25-30	$20 \cdot 10^6$
Flopaam 3530S	Anionic HPAM	25-30	$16 \cdot 10^6$
Superpusher C319	HAP	Medium density	$12\text{-}16 \cdot 10^6$

3.2 Polymer systems

For the purposes of this research, partially hydrolyzed polyacrylamide (Flopaam 3630S, Flopaam 3530S) and hydrophobically-associating (Superpusher C319) polymer solutions were used. Both polymer types were obtained from SNF FLOERGER®. The list of polymer fluids and their properties is given in **Table 3.2.1**. Both polymer types were mixed in 1 wt% NaCl solution at various desirable concentrations. As numerous studies showed, HPAM solution usually represents a solution of higher viscoelasticity than conventional xanthan gum biopolymer solutions (Wang et al., 2006). In partially hydrolyzed polyacrylamide solutions, polyacrylamide groups tend to react with sodium or potassium hydroxide or sodium carbonate. As a result, hydrolysis transforms amide groups ($CONH_2$) into carboxyl groups (COO^-), leading to reduced adsorption on mineral surfaces. Negative charges on the backbones of the polymer chains are then introduced by hydrolysis, which consequently impacts the rheological properties of the polymer solutions (Sheng, 2011) (**Figure 3.2.1**).

HPAM also acts as a copolymer of acrylamide and acrylic acid. The negative charges of the polymer chain backbones cause them to repel each other at low salinity or in fresh water, causing the polymer chains to stretch. This results in higher polymer viscosity. The chain stretching can be reduced if more electrolytes (NaCl) are added to polymer solution. Therefore, repulsive forces are neutralized or shielded by a double-layer electrolyte. As a consequence, this will lead to HPAM flexible chain compression, resulting in decrease in polymer solution viscosity.

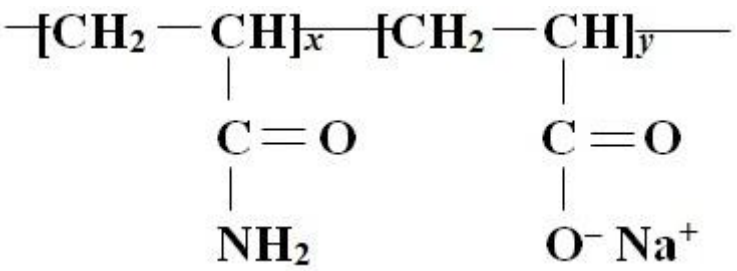

Figure 3.2.1 Hydrolyzed polyacrylamide chemical structure (adapted from Sheng, 2011)

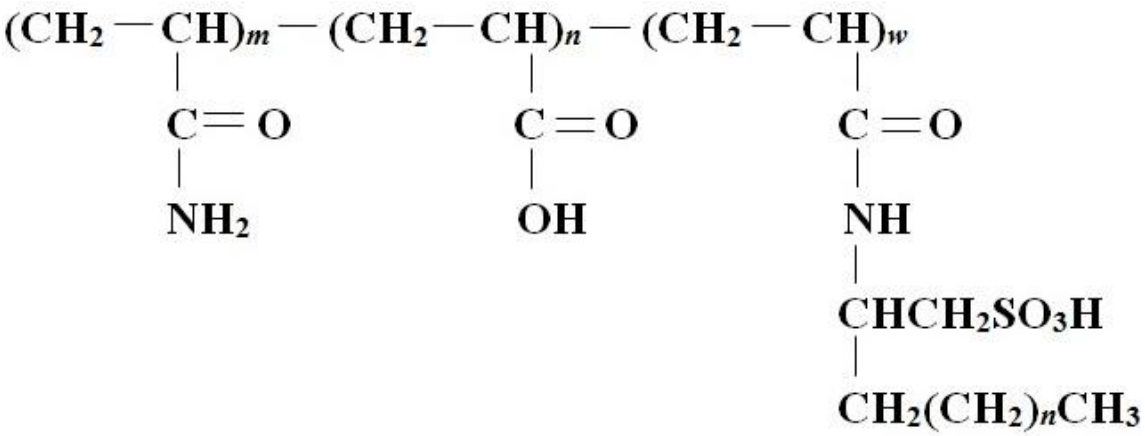

Figure 3.2.2 Hydrophobically associating polymer chemical structure (adapted from Sheng, 2011)

At higher hydrolysis, COO^- increases, resulting in reduced adsorption, increased viscosity, and reduction in chemical stability due to less $CONH_2$. On the other hand, lower hydrolysis leads to increased chemical stability and increased adsorption.

The hydrophobically associating (HAP) type of water-soluble polymer contains both water-soluble (acrylamides) and water-insoluble (hydrophobic) monomers (**Figure 3.2.2**).

The polymer hydrophobicity provides both intermolecular and intramolecular types of associations. Intermolecular association leads to increased hydrodynamic size of polymers and increased solution viscosity, while intramolecular association leads to a decrease in viscosity of the solution. The change in viscosity usually depends on factors that influence each association.

3.2.1 Polymer solution preparation

HPAM and HAP polymers are presented in the form of dry powder. Both polymer types can be prepared by either making the initial dilution using a mechanical stirrer or diluting the mother (initial) solution into a series of desired concentrations using a laboratory magnetic stirrer. Each experiment utilizes only freshly prepared polymer solution, since polymers tend to degrade over time and lose their unique properties.

Before conducting each experiment, an accurate process of polymer solution preparation should be applied. This process is not the same as for brine or other Newtonian aqueous fluids preparation. The process used followed that generally applied by SNF FLOERGER® (SNF FLOPAAM™ Brochure, 2004), which is a sophisticated methodology of preparation since the polymers are non-Newtonian fluids and their viscosities are shear dependant. This methodology was also discussed in Shriwal and

Lane (2012). The degassed 1 wt% brine is stirred using a high shear, mechanical stirrer at a speed high enough to make a strong vortex. The polymer powder is then slowly introduced into the side of the vortex as shown on **Figure 3.2.3**. This was applied in order to avoid formation of "fisheyes" which can be formed if the powder is not wetted evenly.

The solution is stirred for a certain time at a high rotation speed until the solution becomes viscous enough so the vortex transforms into a flat surface. The rotation speed is then decreased, and the solution is left stirring for 24 hours. It is critical to ensure no air bubbles get trapped in the solution. Once the desired concentration polymer solution is prepared, filtering should be applied. Since all the experiments utilized flow through porous media, superficial plugging effects might be evident. Therefore, by using 5.0 μm microfiltration flat hydrophilic membrane filters (e.g., Whatman®, Millipore™) and a sintered glass funnel with sand media, the polymer solution is properly filtered.

3.2.2 Polymer solution viscosity measurement

After the polymer solution with desired concentration was prepared, sample viscosities were measured using a Brookfield LV-DV II+ viscometer utilizing the S-40 cone and plate spindle normally used for viscosities less than 3000 mPa·s with the maximum used viscosity fluids in this research being 2039 mPa·s. The experimental temperature was controlled at the same specified set-point (23 °C) as during the main experimental procedures. Therefore, more accurate measurements and results were achieved. The desired temperature was applied to the tested sample in a sampling cup and kept constant using a Brookfield Circulating thermo-regulated waterbath. Temperature reading was performed from an RTD temperature sensor.

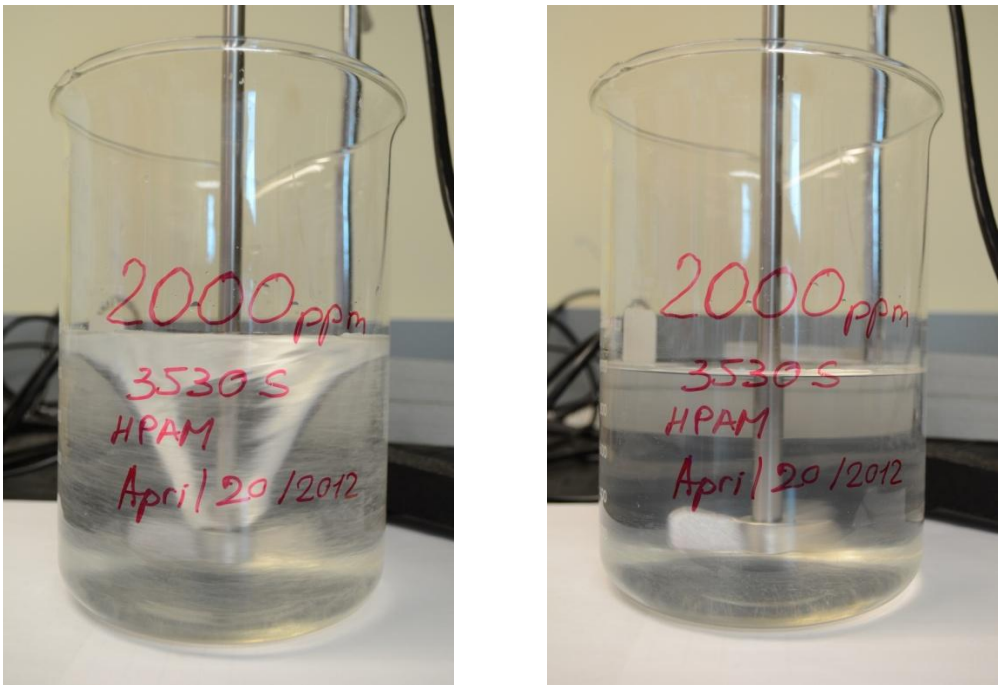

A **B**

Figure 3.2.3 An example of shear polymer vortex: A – start of stirring; B – end of stirring at the same applied shear rate (original in colour)

The Electronic Gap Adjustment™ allowed calibration of the viscometer for each particular type of fluid and its viscosity. Continuous and automatic viscosity, shear rate/stress, spindle speed, %torque data gathering process, and further historical comparison was provided by Brookfield's Wingather™ software (Brookfield catalog, 2001). Unlike testing light, light-medium, and heavy oil samples or brine solutions, polymer solutions exhibit non-Newtonian behaviour, or, simply, their viscosities are shear dependant. Therefore, the allowable speed range of 18 different speeds provided a good capacity for measuring polymer viscosity at all possible (for this type of viscometer) shear rates. The collected data were then exported into Microsoft® Excel for further analysis of measured samples and determination of desired viscosity ratio.

3.3 Oil systems

Two types of oil systems were used in this project. The clear, light-medium, and medium oils were obtained from EM® Science (MX 1561/2 and MX 1560/2 mineral oil), and each had a measured viscosity of 22 and 153 mPa·s at 23 °C. The heavy oil was a golden-coloured Esso Spartan 680 Industrial Gear oil, and the viscosity was measured as ~2039 mPa·s at 23 °C. It was diluted with ~5 wt% kerosene to obtain a ~960-mPa·s viscosity. Hydrocarbon fluid properties, as well as some of the aqueous fluids used in this project, are summarized in **Table 3.3.1**.

Table 3.3.1 List of used fluids and their properties

Fluids	Viscosity at 23 °C (mPa·s)	Density (kg/m^3)
MX 1561/2 mineral oil	22	832
MX 1560/2 mineral oil	153	844
Spartan 680 industrial gear oil	2039	878
Spartan 680 industrial gear oil with 5 wt% kerosene	960	928
SX0420-3 NaCl	1.03	877
Green food colouring	1.03	877

3.4 2D viscous fingering test procedure

An acrylic fracture visual cell was used to accommodate the narrow grain-size (80-100 mesh) glass beads as a porous media. The beads, obtained from Opta Minerals Inc. and were the B10-type having original grain size of 80-190 μm. In order to obtain required narrow grain size distribution glass beads were previously sieved. This particular mesh size of beads was chosen as it best allows to fit the dimensions of the 2D acrylic model fracture channel while packing.

The use of glass beads also provided an advantage over modern micromodels, since for some extend it better represents real reservoir conditions. On the other hand, for each new experiment a new sandpack was prepared which can be a disadvantage during comparative analysis. It was believed that this type of porous material better simulates real reservoir material (e.g. Pelican Lake field). The properties of the beads sandpack were determined only during 1D coreflood tests since the design of 2D visual model did not allow the pressure differential readings collection and operation at different injection rates. It is critical to note that these parameters are important during permeability calculations. As a result from coreflood tests, the determined porosity and absolute permeability of the sandpack demonstrated good match with reported formation properties of the field. This particular type of porous material was also chosen due to initial availability in research facility therefore all delays due to ordering or shipping of the different materials were avoided. The oils used for these experiments either synthetic or mineral oils were chosen for their transparency in the visual model.

3.4.1 Acrylic fracture visual model

This model was used to study the viscous instability process during two-phase immiscible displacement. The impact of altering the viscosity ratio (oil:displacing phase – 40:1 and various unfavourable viscosity ratios) was qualitatively examined during water and polymer flooding. The model consisted of two polished acrylic plates, each side lined with an o-ring and reinforced with 0.63-cm bolts to prevent fluid leakage. The fracture dimensions were 4-cm wide by 20-cm long with a 0.06-cm aperture. The two sandwiched plates were sealed with two end-caps and reinforced with long, threaded rods. A mesh material between end-caps was used to secure the beads in place and to prevent them from dislodging during displacement. Transfer vessels were used for oil, coloured water, and polymer samples. All three were connected to the set-up via 0.15-cm Swagelok® tubing and displaced using a Teledyne Isco 250D series syringe pump.

It is critical to indicate that due to design specifications of this model it allowed only qualitative analysis of viscous fingering patterns. Therefore a more detailed description of what should be done for qualitative analysis is provided in **Section 5.2**. The schematic of the experimental set-up, as well as photos of the actual set-up, are shown in **Figures 3.4.1** and **3.4.2**, respectively.

3.4.2 2D viscous fingering experimental procedure

Each experiment was conducted utilizing freshly packed fracture channels of the model in order to clearly demonstrate the viscous instabilities caused by viscosity difference as well as to exclude the effect of adsorbed polymer on the mineral surface. Three viscosity ratios of water and HPAM polymer solutions were investigated.

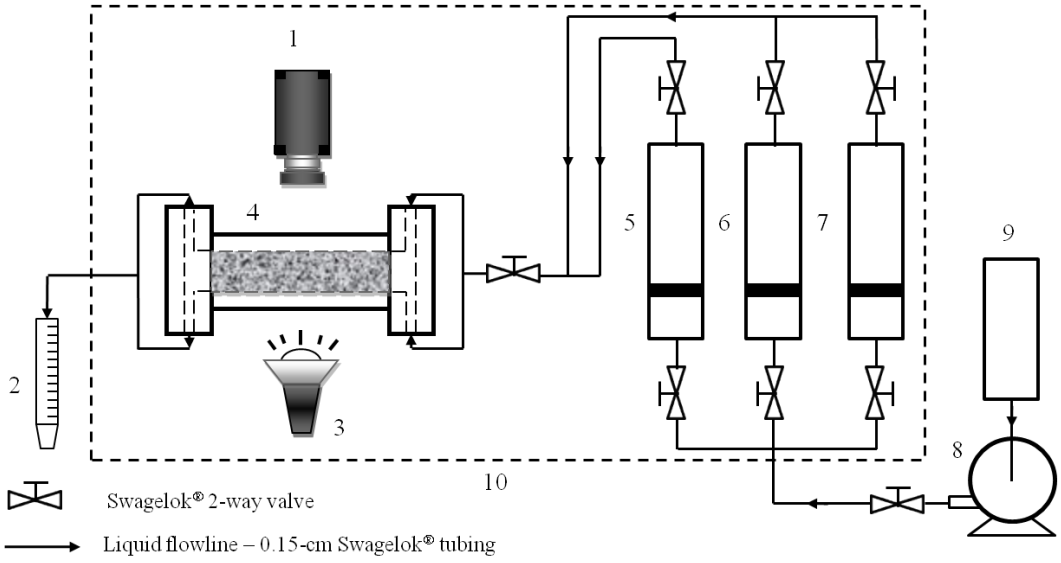

1 – digital camcorder; 2 – production vessel; 3 – light source; 4 – horizontally-mounted acrylic fracture visual cell (top view); 5 – oil transfer vessel; 6 – polymer solution transfer vessel; 7 – brine transfer vessel; 8 – Teledyne Isco 250D Series pump; 9 – water reservoir; 10 – airbath thermoregulated at 23 °C

Figure 3.4.1 Schematic of 2D viscous fingering experimental set-up

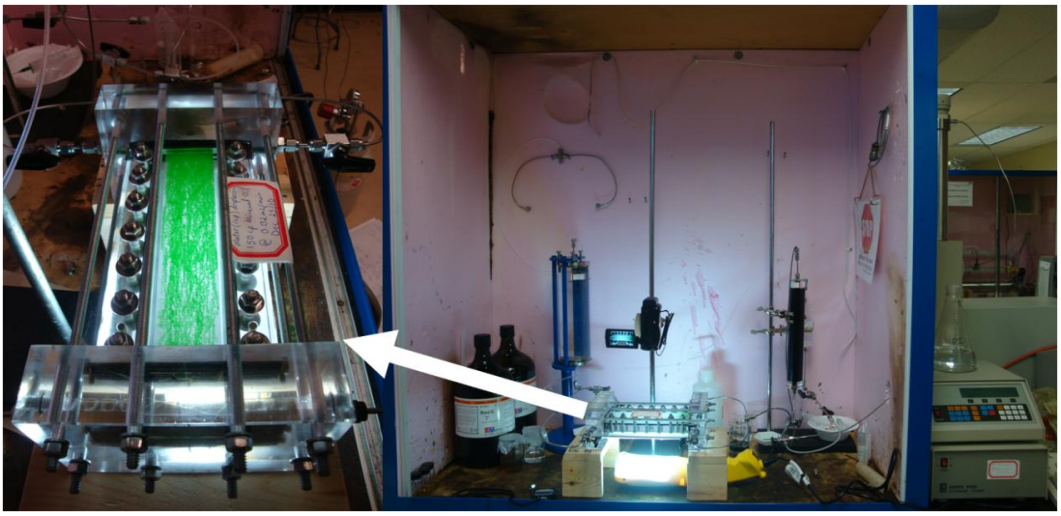

Figure 3.4.2 Photos of 2D viscous fingering experimental set-up (original in colour)

The following experimental procedure has been applied in the 2D viscous fingering tests:

1) The glass beads were slowly introduced into the fracture channel and packed as such that one uniform pack is obtained with no air trapped between sand grains, and no "layers of sand" were evident.
2) Air was blown through the model from the top down to securely pack the beads. This was followed by CO_2 injection under a 103.4 kPa differential to displace the air prior to saturation.
3) Water saturation of the model was chosen to be top-down while the model was in the vertical position to further enhance the strength of the pack and to prevent any beads from dislodging and providing a sufficiently uniform front. Water saturation was conducted at 0.2-0.5 cm^3/min.
4) Oil saturation was completed in a similar manner at a rate of 0.2 cm^3/min. Checks for leaks and pack consistency were completed throughout the saturation process.
5) After saturation of the model, it was placed horizontally over a light source. All lines were purged of air and connected to the model. Green-coloured water or polymer solution was injected at 0.02 cm^3/min; based on the pack dimensions, this yielded a Darcy velocity of ~1 m/day. The injection took place until breakthrough occurred.
6) When the experimental run was considered to be finished, the fracture acrylic model was disassembled and rigorously cleaned to remove any residual sand and fluids.

The immiscible viscous fingering displacements usually took approximately one hour to complete and were filmed with a Sony HDR-CX350V camcorder. Time-lapse videos of the displacement processes were made, representing 5000% compressed speed such that the complete viscous fingering process could be viewed within several minutes. This was done in order to analyze the viscous instability behaviour and derive certain conclusions based on the viscous instabilities' dynamics. Still-frame images were also extracted for the purposes of this research, as will be discussed in **Chapter 4** of the thesis.

The produced fluids from all experiments were disposed in Workplace Hazardous Materials Information System (WHMIS) certified disposal vessels for further utilization.

3.5 1D two-phase coreflood test procedure

1D corefloods were conducted using the same 80-100 mesh fraction of glass beads obtained from Opta Minerals Inc. and the same heavy oil system. This approach was done in order to combine 2D viscous fingering tests with 1D coreflood displacement tests with the best approximation. The B10-type of beads for the best extend represents real reservoir properties. For this particular research Pelican Lake oil pool was chosen having average permeability of 1-3 darcy of homogeneous unconsolidated sand, which in fact was well-simulated by the sandpack of B10 beads. A schematic and photo of the experimental set-up are shown in **Figures 3.5.1**and **3.5.2**, respectively.

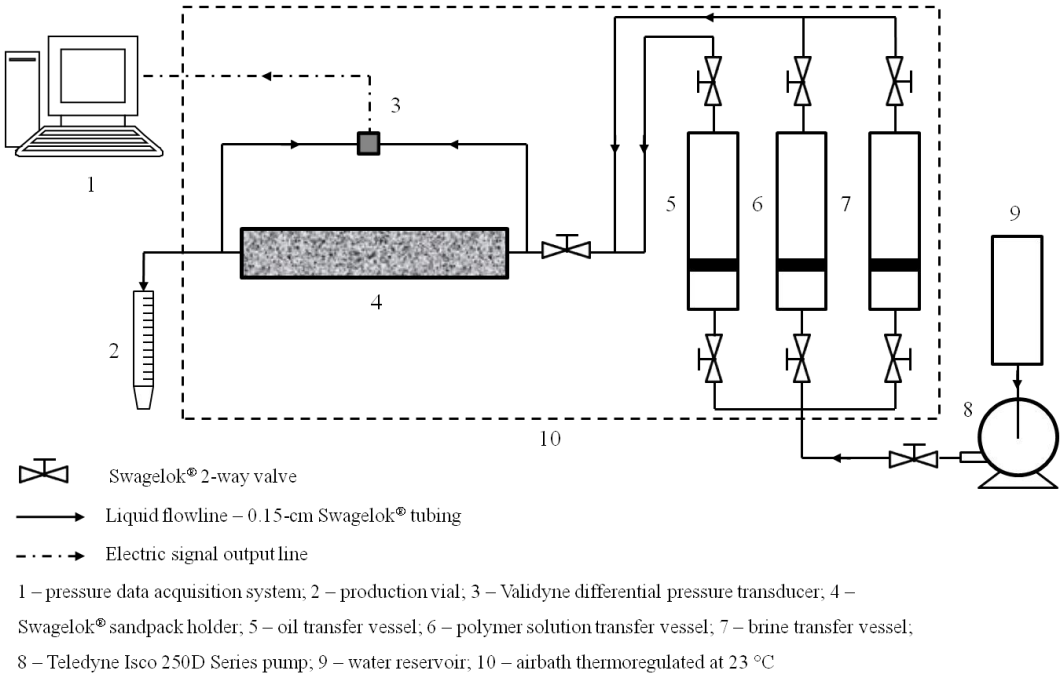

Figure 3.5.1 Schematic of 1D corefloods experimental set-up

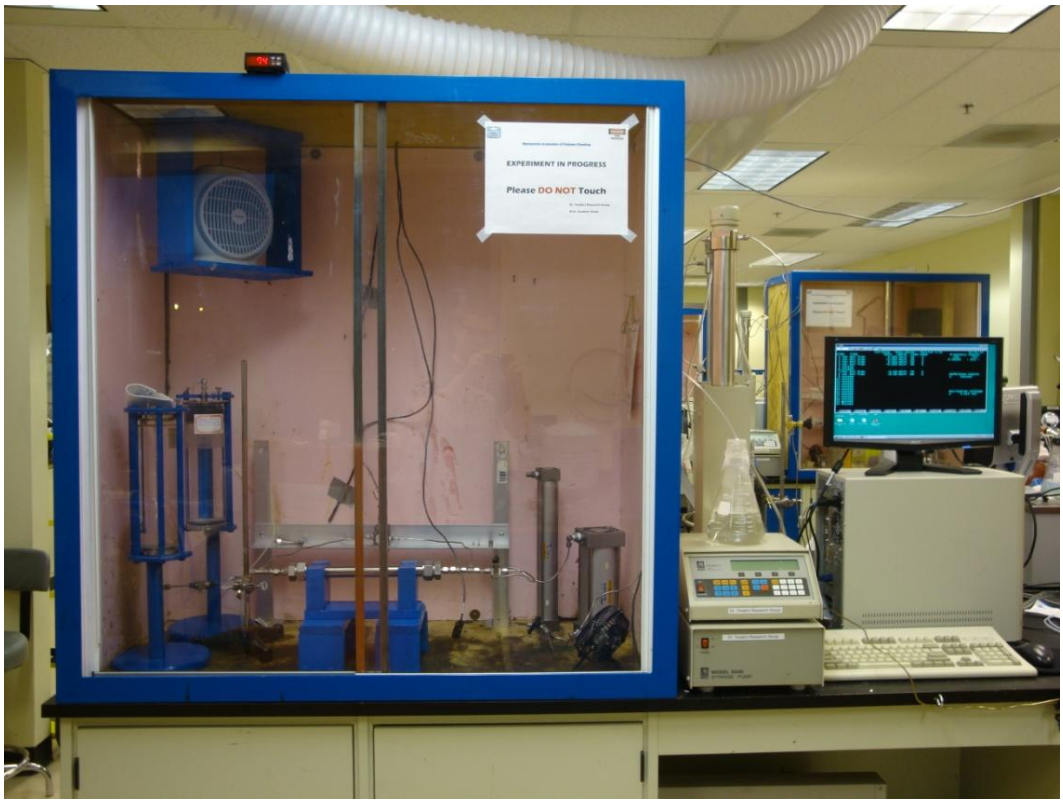

Figure 3.5.2 Photo of 1D coreflood experimental set-up (original in colour)

3.5.1 Swagelok® sandpack holder

For these experiments, a modified Swagelok® sandpack holder (30.48-cm length) was internally machined to accommodate distribution inserts that were secured by lockers and end-caps from both the inlet and outlet sides of the holder (**Figure 3.5.3**).

During the experimental type of displacement described in this section, the fluid that has to be injected might enter the porous face at one single point and be non-uniformly distributed. The finger-like instabilities in this case can propagate independently for a short distance, after which they transform into a "graded saturation zone" (Perkins and Johnston, 1969; Bentsen and Saeedi, 1981). This behaviour could lead to a large amount of oil left behind near the inlet of the core, which can interfere with obtaining good final results in the experiment. On the other hand, outlet-end effects can also contribute to unfavourable "large saturation gradients" at the outlet end of the sandpack, delaying breakthrough, and, as a result, breakthrough recoveries can be higher than the Buckley-Leverett theory predicts. In order to overcome these problems, specially-designed high-permeability distributors with a 200-mesh stainless steel screen were manufactured to fit the inlet and outlet ends of the Swagelok® sandpack holder.

The simple design of the sandpack holder provided good reliability, flexibility, and versatility, especially while dealing with the polymer flood experiments when each time a new experiment was conducted, a freshly packed sandpack was used.

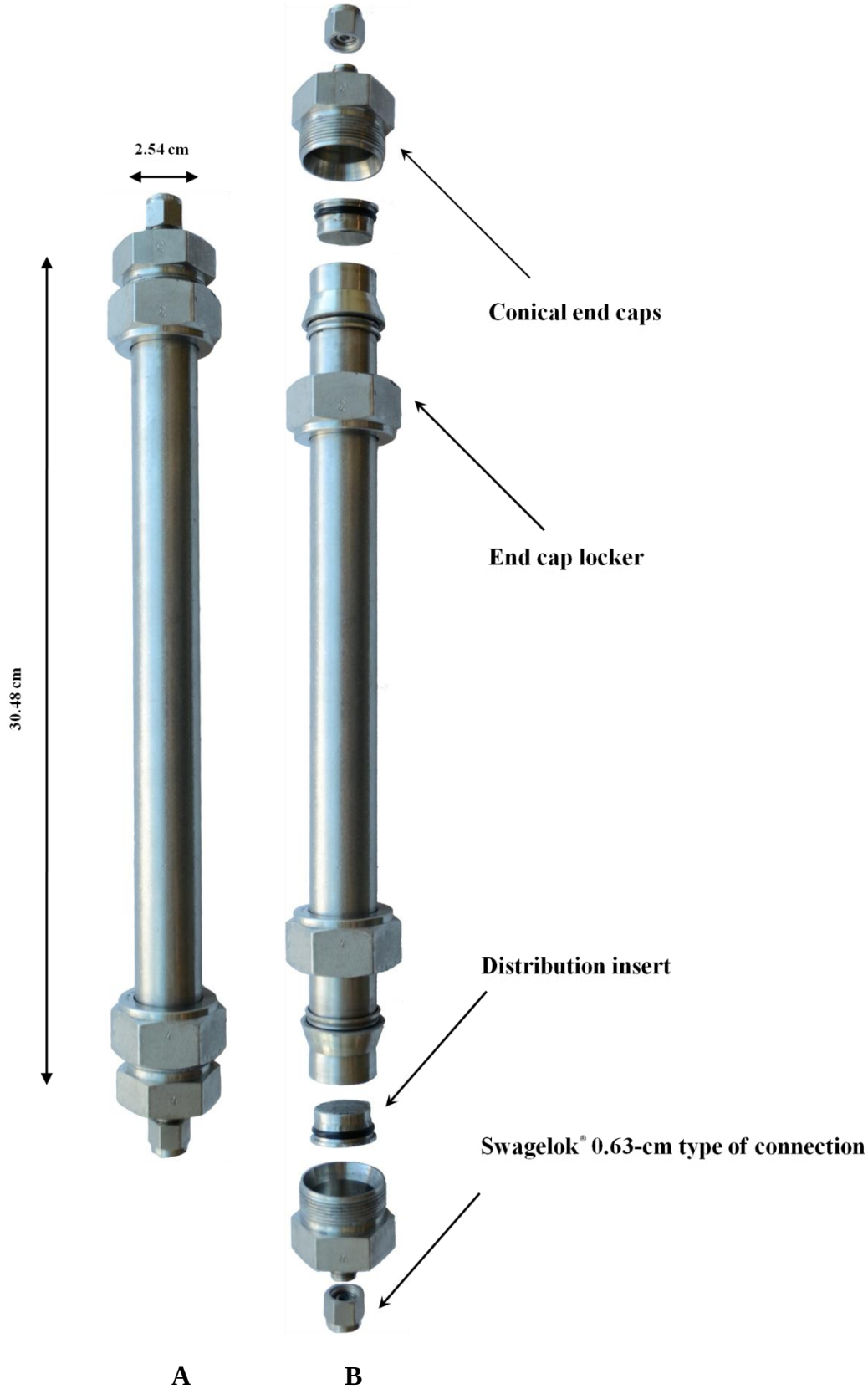

Figure 3.5.3 Swagelok® sandpack holder: A – assembled; B – disassembled

3.5.2 1D two-phase coreflood experimental procedure

Each experiment was conducted utilizing a newly-coated inside surface of the holder and freshly packed sandpack. A new sandpack should be used for each experiment in order to exclude the effect of adsorbed polymer on the mineral surface from previous runs, as well as reduce the potential for fluid to follow the channels and paths in the sand left after previous experiments. Three viscosity ratios of each type of polymer (HPAM and HAP) were investigated.

The following experimental procedure has been applied in the 1D coreflood tests:

1) The inside surface of 30.48-cm Swagelok® sandpack holder was coated with liquid Blue Magic waterproof electrical tape and subsequently covered with Wabiskaw sand in order to obtain a dry thin layer of rough material adhered on the tube surface. This will minimize fines migration issues and subsequent water channelling along the tube walls and contribute to more accurate absolute permeability determination.
2) The coated Swagelok® sandpack holder was then placed vertically and wet-packed with 80-100 mesh glass beads utilizing fresh degassed 1 wt% brine solution while submerged into a sonicator filled with water in order let the beads settle uniformly.
3) The pore volume (PV) and porosity of the packed porous media were calculated using the mass of sand and brine during the packing process taking into account dead volumes in the system.
4) The sandpack holder was then placed into a horizontal position and connected to a pump and transfer cylinders. Absolute permeability (k) to fresh, degassed 1 wt%

NaCl was determined at 0.2, 0.4, 0.6, 0.8, 1, 1.2, 1.4, 2, and 5 cm^3/min using Darcy's law for piston-like displacement, allowing for stabilized dP at each flow rate.

$$\boldsymbol{k = \frac{q \cdot \mu \cdot L}{A \cdot \Delta P}} \text{ (darcy)} \qquad \textbf{(3.5.1)}$$

where q is injection flowrate (cm^3/s), μ – viscosity of injected fluid (cp), k – absolute permeability of the porous media (darcy), L – length of the porous media (cm), A – cross-sectional area of the porous media (cm^2) and ΔP – differential pressure across the porous media (atm).

Alternatively, the slope of the pressure drop vs. flow rate plot was used to deduce the permeability by extracting the fluid viscosity and core length parameters.

5) Oil saturation was commenced at 0.2 cm^3/min, and the produced brine was collected evenly in 15-cm^3 vials until the water cut in produced oil was < 3%. The initial oil saturation (S_{oi}) was then calculated by subtracting the dead volumes.
6) Initial waterflood (IWF) was commenced by injecting brine at 0.2 cm^3/min for up to 1 PV. The collected samples were centrifuged, and the corresponding recovery factors (RF) were determined. The brine injection was carried out until the differential pressure (dP) across the core stabilized and oil cut in produced fluid was < 3%.
7) The experimental system was then immediately switched to polymer flood (PF) injection at 0.2 cm^3/min. The produced emulsion containing oil, brine, and polymer solution was collected evenly in vials for recovery factor (RF) and dynamic adsorption calculations. Dead volumes of the system from tubing and model end caps were considered during calculation. The polymer solution

injection was carried out until the differential pressure (dP) across the core stabilized and oil cut in produced fluid was < 3%. Resistance factor (F_R), which represents the ratio of the mobility of water (λ_w) during initial waterflooding (IWF) to the mobility of a polymer solution (λ_p) during polymer flood (PF) and in-situ polymer solution viscosity, was calculated using the following equation:

$$\boldsymbol{F_R = \frac{\lambda_w}{\lambda_p} = \frac{\Delta P_{PF}}{\Delta P_{IWF}} \approx \mu_p} \qquad \textbf{(3.5.2)}$$

where λ is the mobility of either polymer or water phase (darcy/mPa·s), μ – viscosity of polymer phase (mPa·s) and ΔP – differential pressure across the porous media (kPa).

8) Subsequently, extended waterflood (EWF) was immediately initiated after polymer injection at 0.2 cm^3/min to displace any residual or unadsorbed polymer in the sandpack and to complete the material balance on the dynamic adsorption measurement. It was conducted to also observe any additional oil recovery. The brine injection was carried out until the differential pressure (dP) across the core stabilized and oil cut in produced fluid was < 3%. The stabilized pressure drop served as an indicator of the reduction in permeability due to polymer adsorption and also was used to calculate residual resistance factor to water (RRF_w) – the ratio of water mobility before the polymer injection (IWF) to mobility of water after polymer injection (EWF):

$$\boldsymbol{RRF_w = \frac{\lambda_{w(before\ polymer\ injection)}}{\lambda_{w(after\ polymer\ injection)}} = \frac{k_{w(before\ polymer\ injection)}}{k_{w(after\ polymer\ injection)}} = \frac{\Delta P_{EWF}}{\Delta P_{IWF}}} \qquad \textbf{(3.5.3)}$$

where λ is the mobility of water phase (darcy/mPa·s), k – permeability to water phase and ΔP – differential pressure across the porous media (kPa).

9) A post-polymer oil injection (OFP) was conducted at 0.2 cm^3/min until the differential pressure (dP) across the core stabilized and water cut in produced fluid was < 3%. A residual resistance factor to oil (RRF_o), the ratio of mobility of oil during initial core oil re-saturation (OF) to mobility of post-polymer oil injection (OFP), was calculated using the following equation:

$$\boldsymbol{RRF_o = \frac{\lambda_{o\,(during\ initial\ saturation)}}{\lambda_{o(during\ post-polymer\ saturation)}} = \frac{\Delta P_{OFP}}{\Delta P_{OF}}} \qquad \textbf{(3.5.4)}$$

where λ is the mobility of oil phase (darcy/mPa·s) and ΔP – differential pressure across the porous media (kPa).

10) After the experiment was finished, the sandpack holder was disassembled and the glass beads disposed of. The coating was then removed and the holder prepared for the next experiment.

An assumption was made to apply a pressure differential value during absolute permeability measurements into the equation for F_R calculation, completely stabilized differential pressure across the core was not reached in all cases and the dP of post-polymer brine injection was higher than for brine injection itself. An effort, described in **Section 4.3.2**, was made to reach this point of fully stabilized pressure drop; however, ~2.6 PV of brine injection was not enough. Therefore, in practical terms, it would take approximately 20 pore volumes of water injection at a flow rate of 0.2 cm^3/min to reach the true waterflood endpoint for the 960 or 2039-mPa·s oil. Even on a coreflood-scale, obtaining the endpoint for given oil was not practical.

The produced fluids from all experiments were disposed in Workplace Hazardous Materials Information System (WHMIS) certified disposal vessels for further utilization.

3.5.3 Differential pressure response measurement

Differential pressure drop was continuously monitored as a function of flow rate and PV injected via a Valydine pressure transducer connected to a personal computer. Valydine UPC Easy Sense 2100 pressure data gathering software was used to record and save the data in Microsoft® Excel format for further sorting and analysis. Pressure transducer diaphragms of 344 kPa (for 960 mPa·s oil displacement) and 861.8 kPa and 1378.95 kPa (for heavier 2039-mPa·s oil displacement) were calibrated before each test. The calibration was necessary in order to ensure that the pressure transducer diaphragms responded accurately to changes in pressure and also to obtain conversion factors for the desired units of measure (psi or kPa) since readings are initially delivered as mV/V. Pressure drop data was interpreted for resistance and residual resistance factor information pertaining to the polymer flood.

3.5.4 Dynamic adsorption measurement experimental procedure

The method used to deduce the adsorption of polymer on sand/rock systems was adapted from the technique published by Mezzomo et al. (2002). The isotorque method was shown to have greater reliability and lower variation than spectroscopic methods for adsorption determination. Since the complete details of the method were not disclosed, the method was interpreted to the best of the author's knowledge, and it was used to determine the effluent concentrations of polymer. While conducting polymer flooding (PF), the effluent polymer solution must be in a steady state condition. Therefore, the produced polymer samples must contain equal concentrations. The effluent samples from extended waterflood (EWF) phase should also be run through a viscometer. The procedures described next were used.

Figure 3.5.4 Photo of Brookfield LV-DV II+ experimental set-up (original in colour)

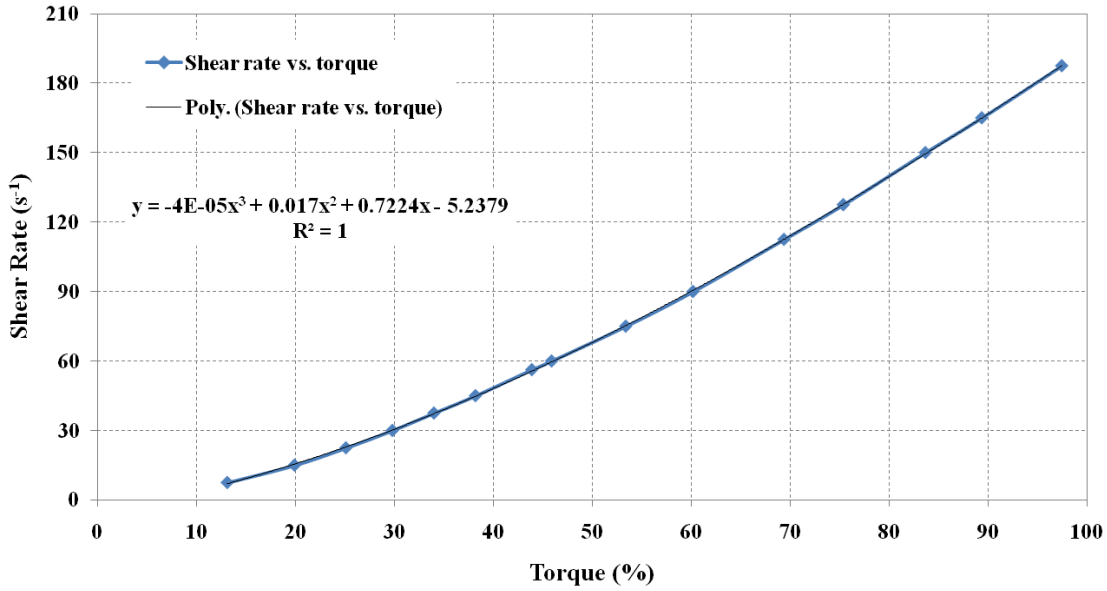

Figure 3.5.5 Example of sear rate vs. torque plot used to determine shear rate at 70 % torque for each effluent sample

1) All samples were centrifuged for ~30 minutes at the highest possible speed, and the mass of each sample was determined.
2) To confirm the steady state conditions, effluent samples from both PF and EWF must be extracted from sampling vials and tested with the viscometer such that corresponding values of shear rate at 70 % torque can be obtained. Therefore, a Brookfield LV-DV II+ viscometer using an S-40 spindle sensor together with Wingather™ software were used for the purpose of collecting the percentage of torque (~15-100 %) and corresponding shear rate data from each sample. The temperature was kept constantly thermoregulated at 23 °C by a temperature-controlled waterbath (**Figure 3.5.4**). The plot of shear rate versus torque was then built (**Figure 3.5.5**). A polynomial function was then applied, and an equation obtained from the trendline function. By substituting a value of 70 into the equation, the value of the shear rate specifically at 70 % torque was thus obtained for each measured effluent.
3) Once the effluent samples containing the same shear rate values (or values in one range) were determined, they were considered as being in steady state (i.e., the effluent polymer concentration was assumed to be equal to the injected concentration, and the core was at complete equilibrium with polymer solution).
4) The effluent samples with equal concentration were then accurately extracted from the sampling vials and mixed to one bulk solution (preferably 50 cm^3). It is critical to note that since sampling vials also contain oil, extractables should be only aqueous phase.

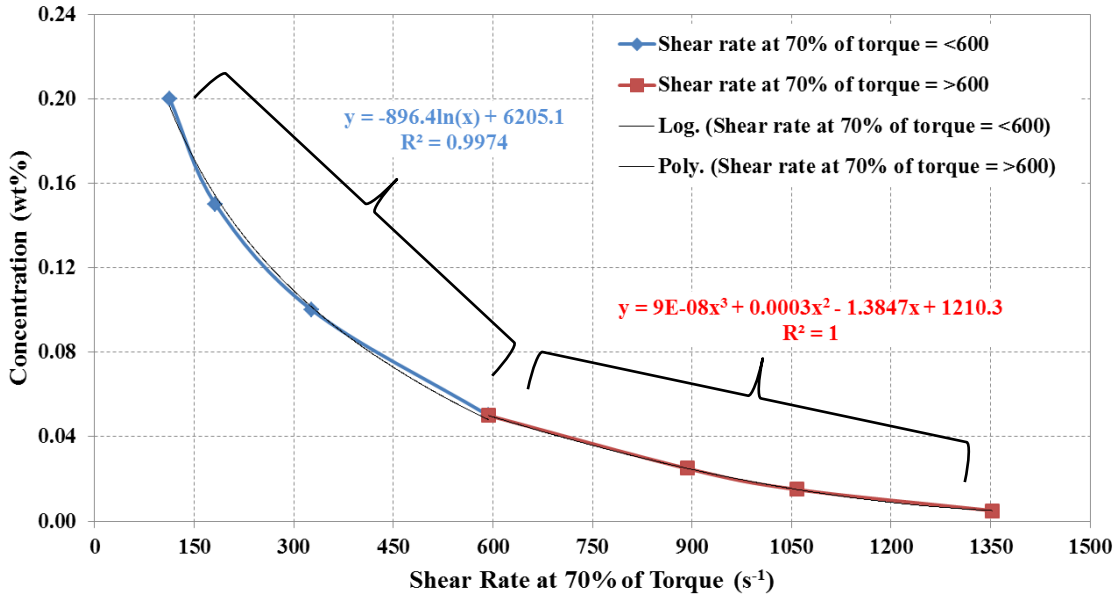

Figure 3.5.6 Example of isotorque calibration curve used to determine effluent polymer concentrations (original in colour)

5) Mixed bulk polymer solution was then diluted to various concentrations used to build an isotorque calibration curve. The solution concentrations were not related to sample viscosity directly but to the shear rate necessary to cause a constant percentage of maximum torque of the rotational viscometer used. Each diluted sample was then measured for shear rate at 70 % torque and was then plotted versus concentration. The isotorque calibration curves can be best described by best fit two separate functional relationships (i.e., polynomial or logarithmic) for shear rates less than and greater than ~400-600 s^{-1}. Two separate functional relationships can better describe behaviour of polymer in first region where strong shear thinning is evident and then tendency of its behaviour towards a Newtonian fluid (much lower thinning behaviour) in the second region. **Figure 3.5.6** shows an example of an isotorque calibration curve used.
6) The exact concentration of each effluent sample can be determined by substituting shear rate values of each sample into the corresponding equation of functional relationships.
7) Once the concentrations from all the effluent samples were measured along with the masses of each sample, the mass of polymer in each sample could be determined.
8) Polymer mass adsorption was calculated from the difference of the total mass of polymer injected and the mass of polymer collected in the effluent:

$$\boldsymbol{m_{P.ads.} = \sum\left(m_{P_{inj}} \cdot C_{Pinj}\right) - \sum_{i=1}^{n}(m_{i_{eff}} \cdot C_{i_{eff}}) + \cdots + (m_n \cdot C_n)} \quad \textbf{(3.5.5)}$$

where m_{Pinj} – mass of injected polymer solution (g), m_{ieff} – mass of the effluent polymer solution (g), C_{Pinj} – concentration of injected polymer solution (wt%) and C_{ieff} – concentration of the effluent polymer solution (wt%).

9) Dynamic polymer adsorption number was then calculated using the following equation:

$$\boldsymbol{Dynamic\ Adsorption = \frac{m_{P.ads.}}{m_{sand}}}\ (\mu g/g) \quad \textbf{(3.5.6)}$$

where $m_{P.ads.}$ – mass of polymer adsorbed (µg) and m_{sand} – mass of sand in the sandpack (g).

4. RESULTS AND DISCUSSION

4.1 Rheological measurements of polymer solutions

This section illustrates the basic rheological parameters of polymer solutions used in this research. It is within the scope of the current work to evaluate the effect of viscosity ratio on various parameters during immiscible displacement of heavy oil by polymer solutions. Therefore, rheological measurements were applied in order to set the desired viscosity ratios to certain scenarios of displacement.

4.1.1 Basic rheological measurements for HPAM polymer solutions for the purposes of viscous fingering analysis

In order to obtain a 40:1 viscosity ratio with the 153-mPa·s medium oil, a concentration of 0.10 wt% Flopaam 3630S was required in the green colourant. This yielded a displacing phase viscosity of 3.8 mPa·s at 22.5 s^{-1} of shear rate (**Figure 4.1.1**).

Only two major dilutions were made from 0.40 wt% mother polymer solution and exponential functional relationship was then applied to the curve of viscosity versus concentration. It is important to note that more dilutions could have resulted in different shape of the trend however for this particular experiment only initial portion of the graph was considered for calculations.

The shear rates demonstrated here are taken from literature and are not to be considered as applicable for real reservoir oil displacements. Therefore, in real polymer flood piloting or full-scale projects a sophisticated methodology applies for determination of possible shear rate in the reservoir.

The general rheological behaviour of required 0.10 wt% Flopaam 3630S in green colourant polymer solution is depicted in **Figure 4.1.2**.

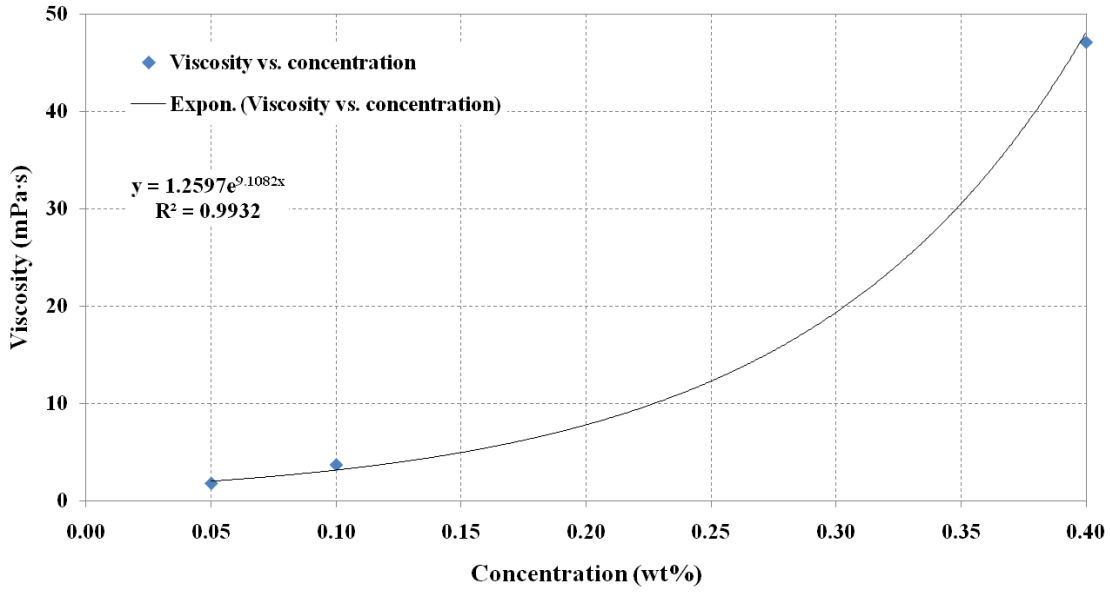

Figure 4.1.1 Viscosity vs. polymer concentration of 0.40 wt% Flopaam 3630S in 3 wt% NaCl green colourant

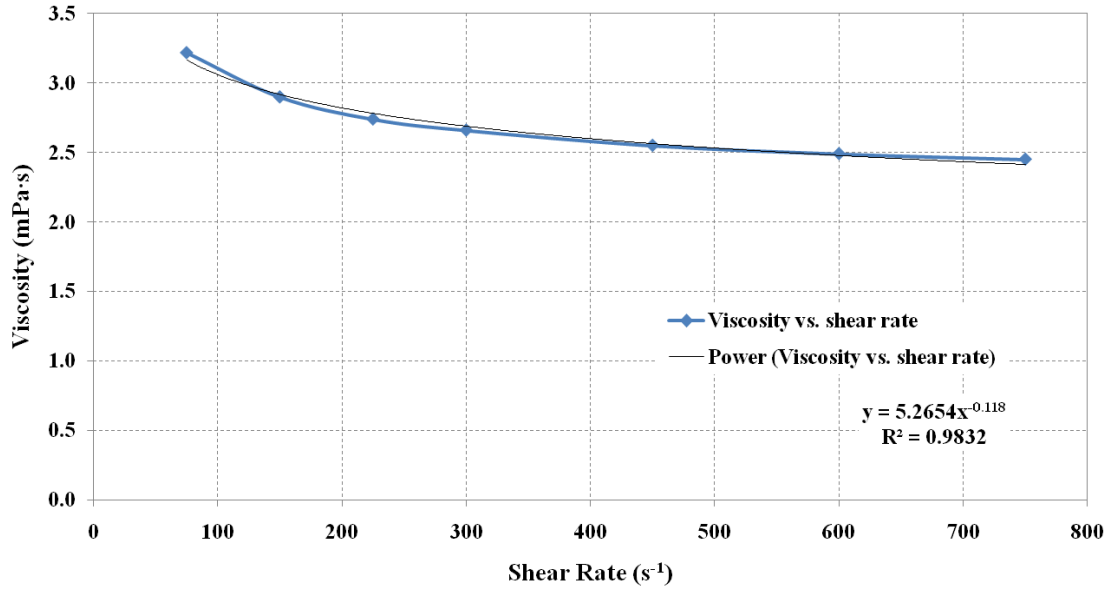

Figure 4.1.2 Viscosity vs. shear rate of 0.10 wt% Flopaam 3630S in 3 wt% NaCl green colourant

Since the green colourant contained some chemicals such as tartrazine, citric acid, and sodium benzoate, the overall effect on the polymer solution viscosity was similar to that of 3 wt% NaCl brine. A standard curve was produced with viscosity versus concentration such that the appropriate concentration would give a 40:1 viscosity ratio with the 153-mPa·s oil.

Similar to the previous experiment, a standard curve was created in order to determine a polymer concentration that yield a 40:1 viscosity ratio with the 960-mPa·s heavy oil. This was found to be a polymer concentration of 0.33 wt% Flopaam 3630S in the green colourant, which resulted in a polymer viscosity of 24 mPa·s at a shear rate of 25 s^{-1} (**Figure 4.1.3**).

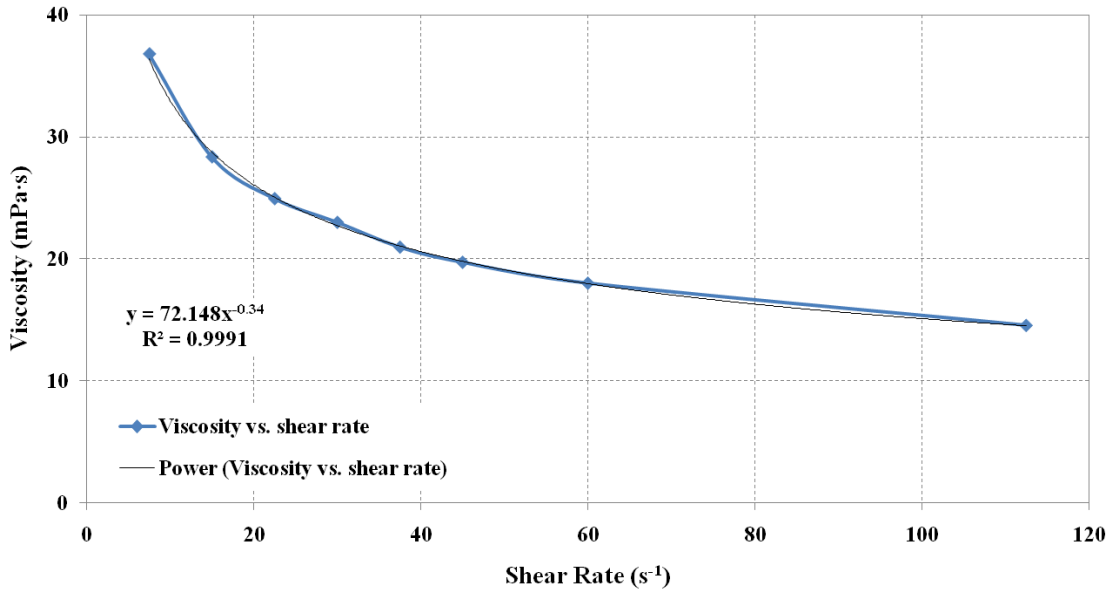

Figure 4.1.3 Viscosity vs. shear rate of 0.33 wt% Flopaam 3630S in 3 wt% NaCl green colourant

4.1.2 Basic rheological measurements of HPAM and HAP polymer solutions for the purposes of 1D coreflood tests

Since polymer solutions are non-Newtonian fluids, so their viscosities change with applied shear rate, a series of curves were developed to describe viscosity-polymer concentration behaviour of two tested types of polymer systems in 1 wt% NaCl (**Figure 4.1.4**). This was also done in order to specify the viscosity ratio for each particular test. All polymer solutions were mixed as a mother solution of 0.30 wt% in brine following standard operational procedures described previously in detail in **Section 3.2.1** of the thesis. The mother polymer solution was then diluted into a wide range of concentrations from 0.05 to 0.25 wt% and left for 1 hour to ensure proper mixing using a magnetic stirrer. A Brookfield LV-DV II+ viscometer using a S-40 spindle sensor together with Wingather™ software were used to collect the required data for graphical interpretation at a constant temperature of 23 °C.

The results observed from the trends revealed no significant difference in viscosity behaviour due to concentration changes between two different types of polymer systems at a specified shear rate of 75 s^{-1}. However, certain values appeared to be different, such as, for instance, starting from 0.15 wt%, particularly hydrolyzed polyacrylamide viscosity tended to rise and ended up with approximately 28 mPa·s for 0.3 wt% polymer versus hydrophobically-associating polymer solution 26 mPa·s at 0.3 wt% concentration in 1 wt% NaCl.

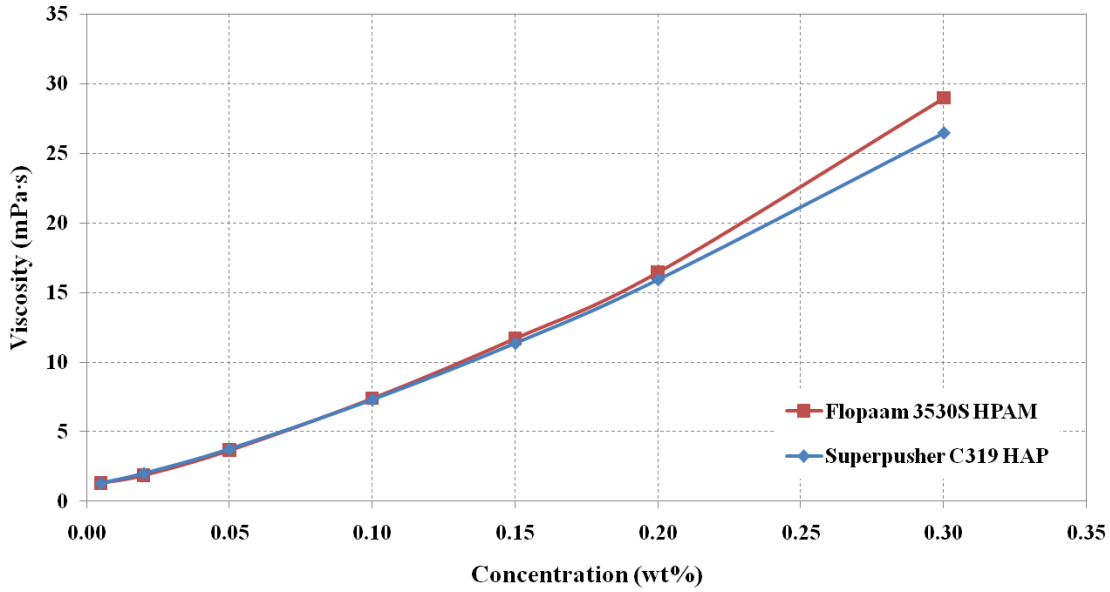

Figure 4.1.4 Viscosity vs. concentration of HPAM and HAP polymer solutions at shear rate 75 s^{-1}

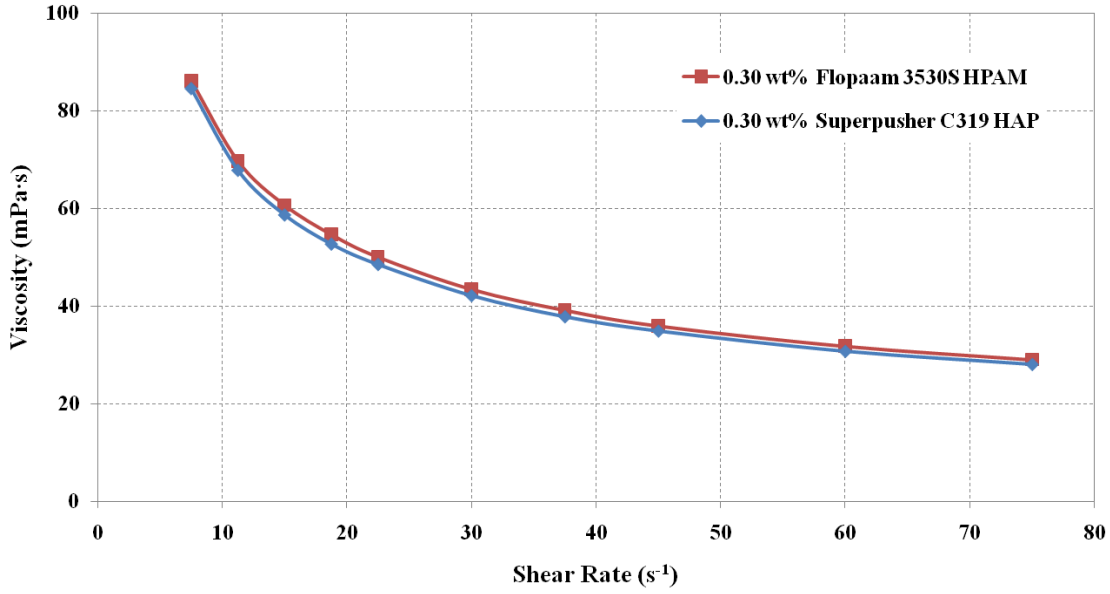

Figure 4.1.5 Viscosity vs. shear rate of 0.30 wt% HPAM and HAP polymer solutions

The shear rate effect on polymer solution viscosity (**Figure 4.1.5**) revealed no significant difference between the two tested polymer types at the same bulk concentrations of 0.30 wt%. Therefore, they exhibited the same classical polymer solution behaviour trend of viscosity declining with each applied shear rate. A significant drop in polymer viscosity was observed as the concentration yielded 0.18 and 0.20 wt%. Thus, for instance, at approximately 40 s^{-1} of applied shear rate for a 0.30 wt% polymer system, the viscosity was 37 mPa·s, while for 0.20 wt% of concentration at the same shear rate, the viscosity changed to ~20 mPa·s. A concentration of 0.18 wt%, as expected, showed a significantly lower concentration profile (**Figure 4.1.6**).

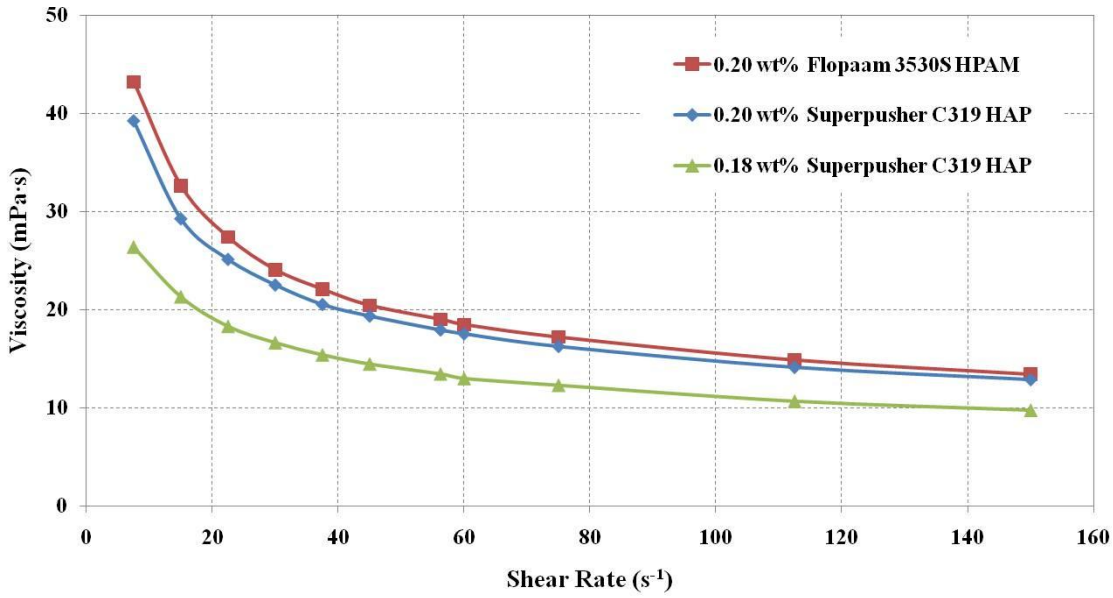

Figure 4.1.6 Viscosity vs. shear rate of 0.20 wt% HPAM and HAP polymer solutions

4.2 Viscous fingering visual experiments

The following sections discuss the displacement of the 22- and 153-mPa·s mineral oils and the 960-mPa·s heavy, gear oil by green-coloured brine (22-, 153- and 960:1 viscosity ratios) and polymer at a 40:1 viscosity ratio. Each test was documented and supported by still frame images from high definition video at various time intervals during the displacement process until breakthrough occurred. It is critical to note that particular time marks of the displacement process have been selected for illustration of corresponding onset and initiation of each particular phenomenon (e.g., complex shielding, spreading, etc.) (Jamaloei et al., 2011). All images are presented originally in colour. The displacement process was initiated from right to left direction in all cases.

4.2.1 Effect of unfavourable viscosity ratio (153:1) on displacement of medium oil (153 mPa·s) by water

The first viscous fingering test involved the displacement of a 153-mPa·s medium mineral oil by water. The injection rate was set to 0.02 cm^3/min and appeared to be relatively stable after the first three minutes of injection, as shown in **Figure 4.2.1**. At approximately the 10-minute-mark, multiple small fingers began to form near the injection end of the model, as shown in **Figure 4.2.2**. Therefore the displacement process could be identified by two distinct zones: a relatively stable zone and a fingering zone (Pavone, 1992).

As the injection process proceeded, additional perturbations occurred, and the growing fingers tended to coalesce and form predominant major fingers, as described by Perkins and Johnston (1969). The formation of these dominant fingers occurred at the 20-minute-mark for water displacing the 153-mPa·s oil, as shown in **Figure 4.2.3**.

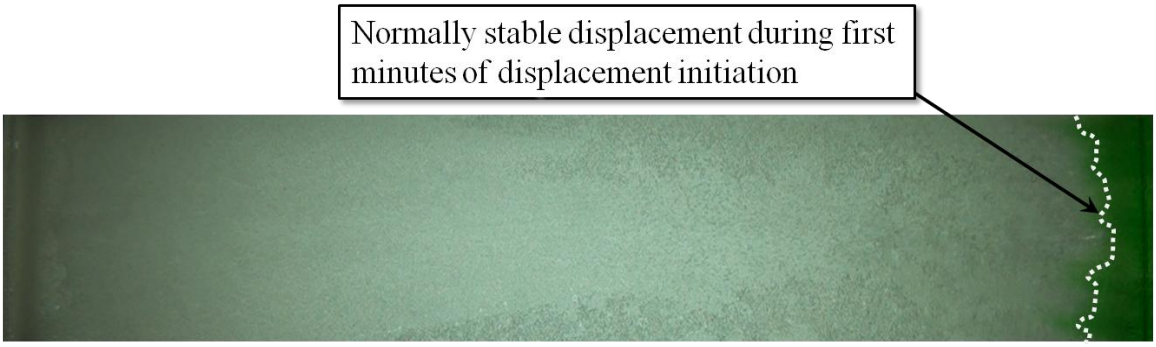

Figure 4.2.1 Water displacing medium oil at 3-minute-mark

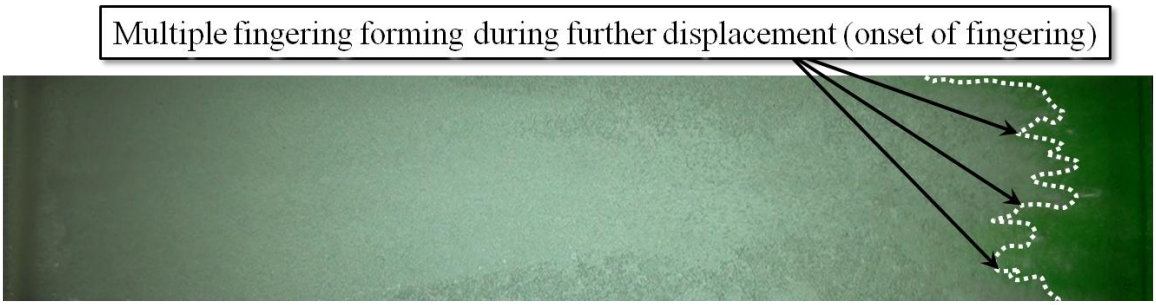

Figure 4.2.2 Water displacing medium oil at 10-minute-mark

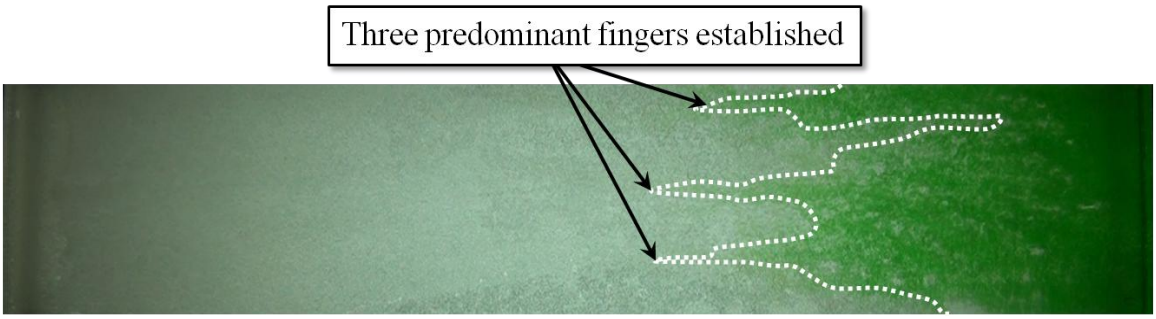

Figure 4.2.3 Water displacing medium oil at 20-minute-mark

At approximately half-way to breakthrough, the lagging or initial displacement front was represented by a fine, dendritic network of channels (Doorwar and Mohanty, 2011) that showed relatively poor displacement efficiency, while the major fingers continued to propagate toward the outlet, a phenomenon that can been described as the "shooting effect," where the dominant fingers exhibit poor sweep efficiency resulting in bypassed oil. Very little production occurs after breakthrough, as shown in **Figure 4.2.4**.

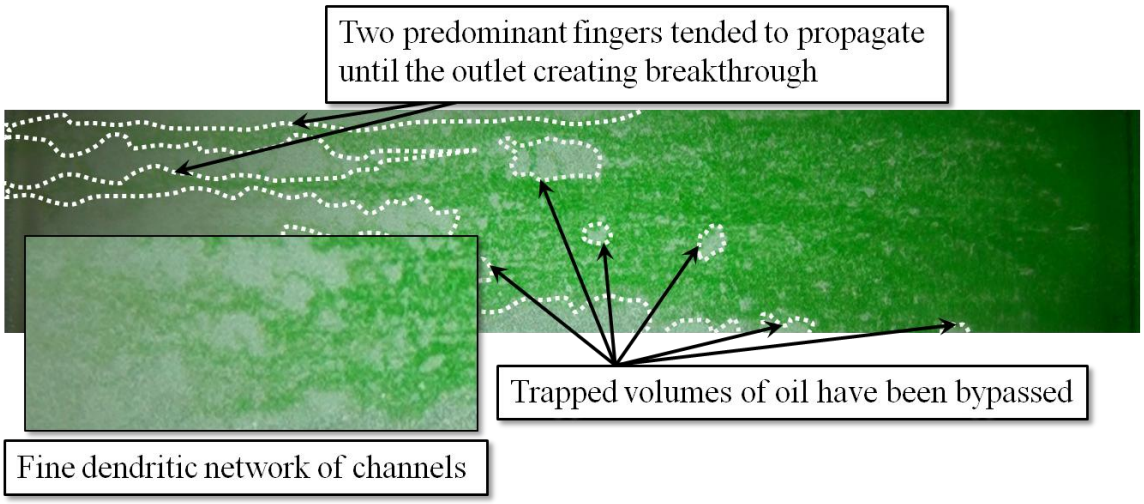

Figure 4.2.4 Water displacing medium oil at 30-minute-mark (breakthrough)

4.2.2 Effect of 40:1 viscosity ratio on displacement of medium oil (153 mPa·s) by Flopaam 3630S HPAM

The addition of polymer to the displacing phase resulted in a much more stable displacement front compared to water at the same flow rate of 0.02 cm^3/min. This is shown in the images in **Figures 4.2.5** and **4.2.6**, representing the 5- and 10-minute-mark of the experiment. In addition to this, throughout the early stages of the displacement, there was far less occurrence of multiple finger formation, and only one major macro-finger dominated the displacement process through the entire experiment until breakthrough; this is shown up to the 30-minute-mark in **Figures 4.2.7** and **4.2.8**.

The boundary of the polymer-invaded region can be characterized as a dispersed region of lower concentration forming a dendritic network of microscopic fingers that invade and displace the oil saturated regions, greatly improving the sweep efficiency. Multiple sideways spreading behaviour was observed within the "core" region of the predominant finger, and it is characterized by a highly concentrated region at the 40-minute-mark, as shown in **Figure 4.2.9**. This coincides with Pavone (1992) in that the finger width continued to grow proportionally to the finger length.

When comparing the images for water and polymer displacing oil at breakthrough, the water displacing resulted in no additional spreading (and, therefore, very little oil recovery) after breakthrough at the 50-minute-mark. This was not the case for the polymer displacement test. As shown above in **Figure 4.2.10**, additional sideways spreading continued even after breakthrough, greatly improving the sweep and displacement of additional oil from the model. The "shooting effect" described for water displacement was absent for the case of polymer displacement.

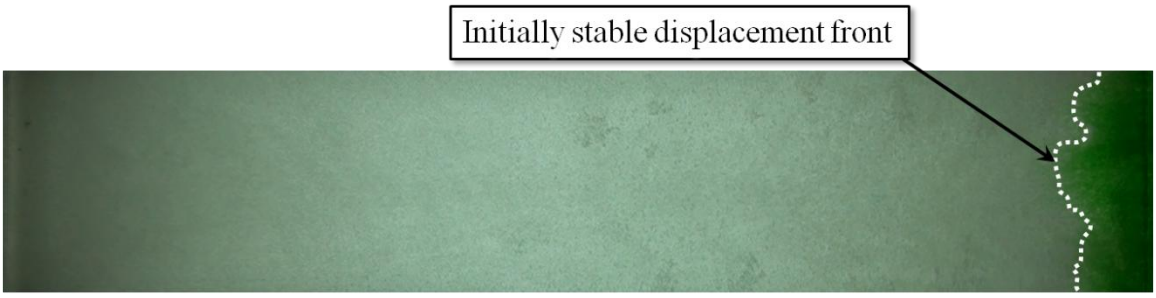

Figure 4.2.5 Polymer (3.8 mPa·s – 40:1) displacing medium oil at 5-minute-mark

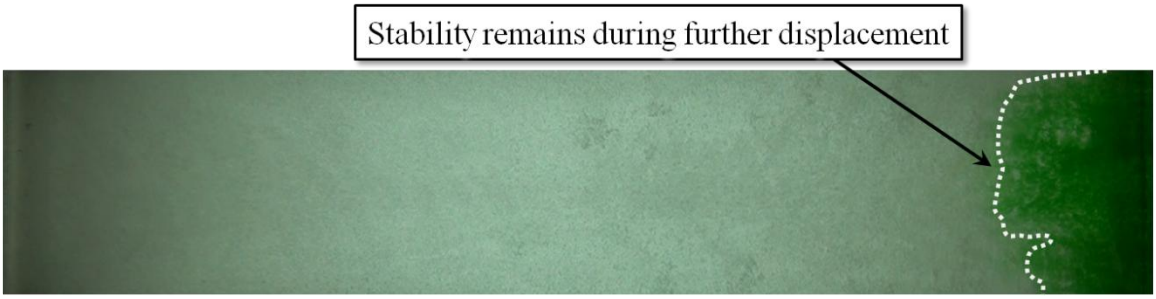

Figure 4.2.6 Polymer (3.8 mPa·s – 40:1) displacing medium oil at 10-minute-mark

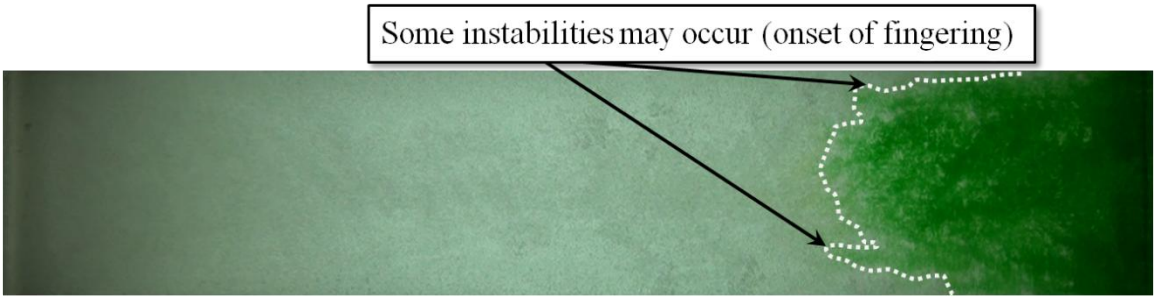

Figure 4.2.7 Polymer (3.8 mPa·s – 40:1) displacing medium oil at 20-minute-mark

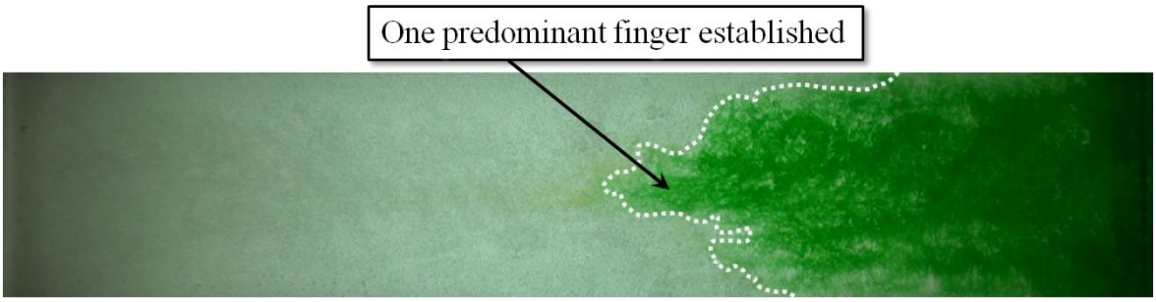

Figure 4.2.8 Polymer (3.8 mPa·s – 40:1) displacing medium oil at 30-minute-mark

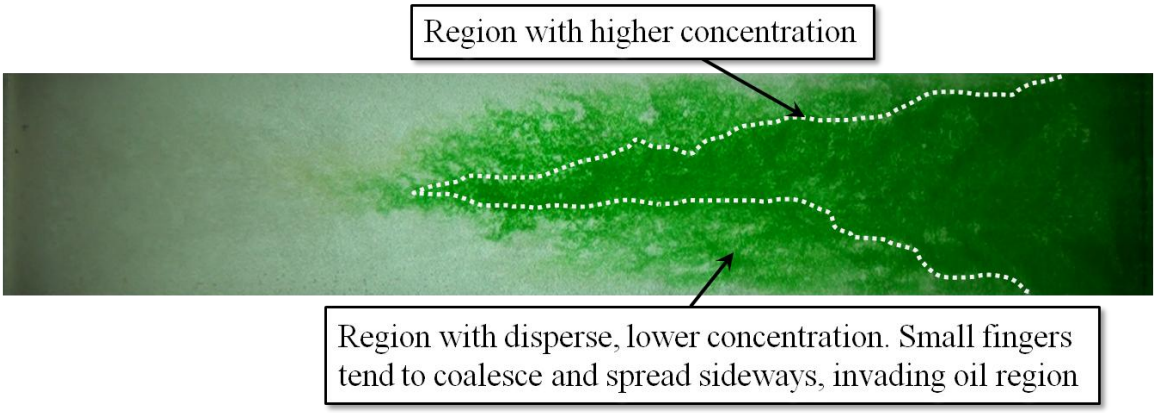

Figure 4.2.9 Polymer (3.8 mPa·s – 40:1) displacing medium oil at 40-minute-mark

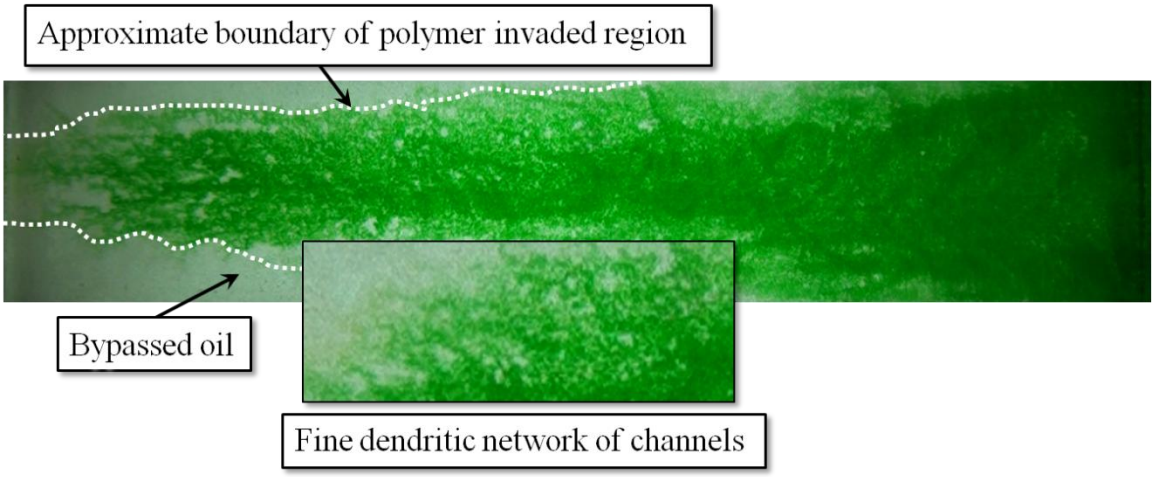

Figure 4.2.10 Polymer (3.8 mPa·s – 40:1) displacing medium oil at 50-minute-mark (breakthrough)

4.2.3 Effect of unfavourable viscosity ratio (960:1) on displacement of heavy oil (960 mPa·s) by water

As somewhat expected, for the viscous fingering experiments describing the displacement of heavy oil, the viscous fingering behaviour was significantly different. A delay in viscous fingering development was observed at a rate of 0.02 cm^3/min as a greater initial pressure was required to displace the initial volume of oil to initiate fingering. For this case, there was no stability region as observed in the water displacement of 153-mPa·s oil. After approximately 12-minutes of injection, a strong entrance effect was observed, as described by Perkins and Johnston (1969) and Doorwar & Mohanty (2011), whereby dominant fingers formed immediately without a stabilized region. For this heavy oil case, the displacement process can be characterized by three distinct regions. First, the creation of predominant, "tree-like" fingers occurred immediately; this growth continued through to the 24-minute-mark, as shown in **Figure 4.2.11**. No coalescence of fingers occurred, and significant volumes of oil remained bypassed. Second, as injection continued, no further propagation in the smaller finger occurred, and fluid injection contributed further to the major finger development; this greatly reduced the sweep efficiency (**Figure 4.2.12**).

Thirdly, as shown in **Figure 4.2.13**, throughout the propagation of the major finger, very complex splitting and spreading behaviour was observed whereby the dendritic shape of the finger created multiple branches that nearly spanned the width of the 2D model. This type of behaviour was also noted in the Jamaloei et al. (2010) study.

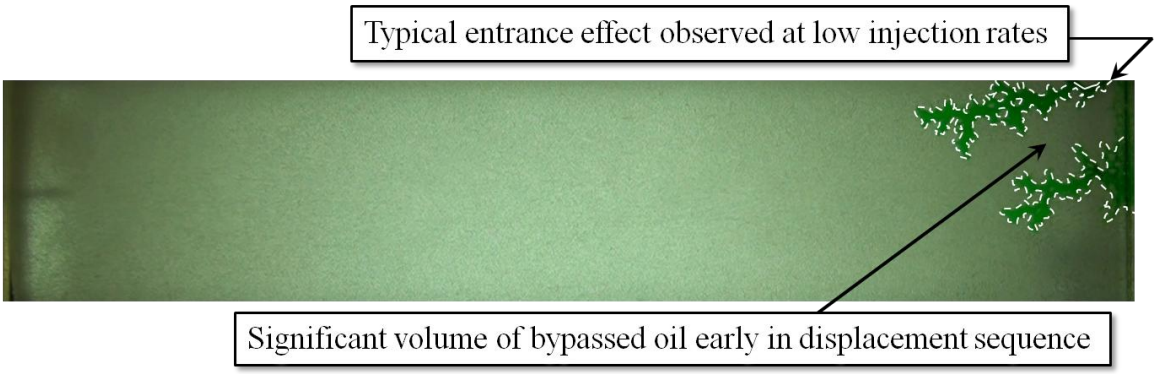

Figure 4.2.11 Water displacing heavy oil at 24-minute-mark

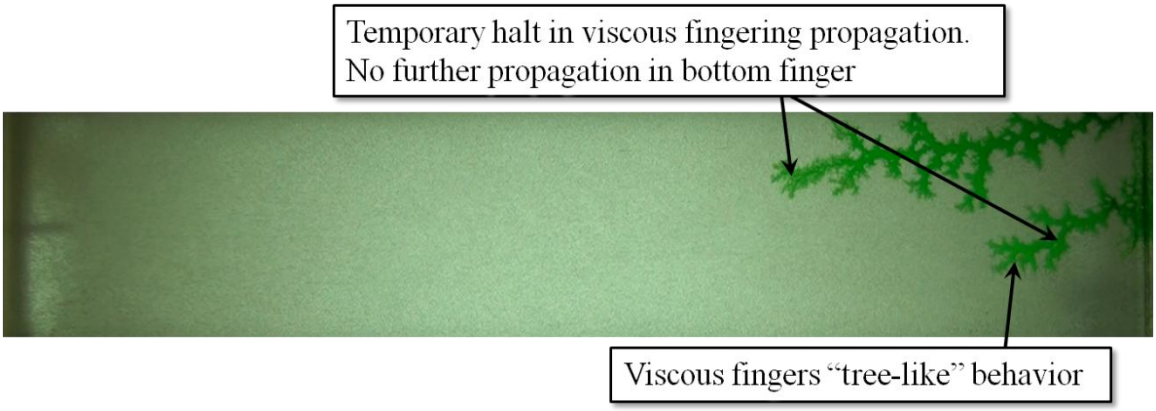

Figure 4.2.12 Water displacing heavy oil at 30-minute-mark

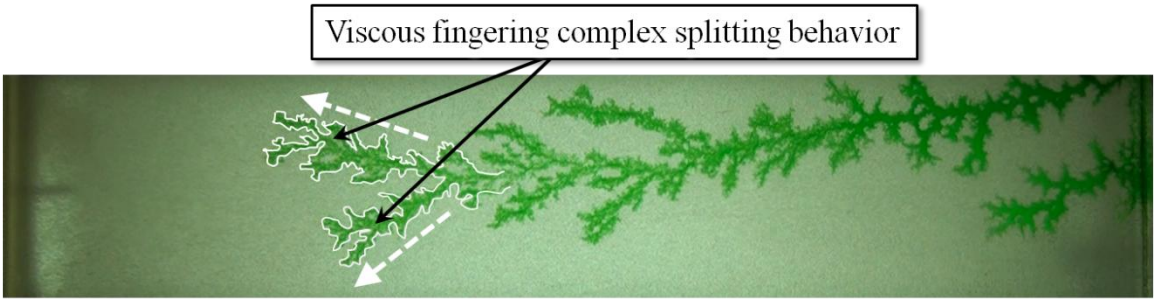

Figure 4.2.13 Water displacing heavy oil at 50-minute-mark

Eventually, the dominant finger channel broke through to the production end of the model, and no additional spreading or oil recovery was observed. Instead, mass transfer between the fingers' mixing zone was created ahead of the clearly defined finger front **Figure 4.2.14** (Sarma, 1986). This is likely typical of a heavy oil displacement by waterflooding, except in reality, the fingering behaviour can occur in three dimensions such that the sweep efficiency could be even worse in some regions of the reservoir. However, these tests confirm the change in behaviour from a medium to heavy oil displacement.

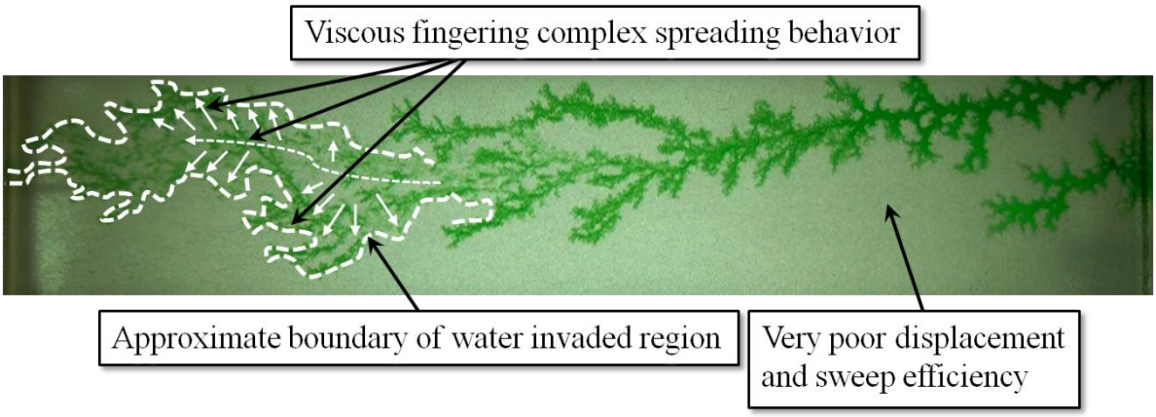

Figure 4.2.14 Water displacing heavy oil at 54-minute-mark (breakthrough)

4.2.4 Effect of 40:1 viscosity ratio on displacement of heavy oil (960 mPa·s) by Flopaam 3630S HPAM

The time delay was found to be much greater due to the additional pressure build-up required to commence viscous fluid injection and displacement of the heavy oil. The typical entrance effect that had been observed for water displacing the heavy oil was not initially observed in this case; in fact, it took nearly one hour for the polymer solution to enter the porous media at a flow rate of 0.02 cm^3/min. The actual and potential fluid invasion profiles are shown in **Figure 4.2.15**. However, after two hours of injection, severe fingering was observed along the side boundaries of the porous media visual cell as shown in **Figure 4.2.16**; the fingering at the side of the pack may have been due to a non-uniform distribution of the glass-bead sandpack. However, during this time, the initiation of a major finger in the middle of the porous media began to also form, which halted the progression of the side-finger channeling. No additional propagation of the front occurred over the next hour of injection, and it was decided to stop the experiment at this time (**Figure 4.2.17**). Injection continued the next day at the same rate of 0.02 cm^3/min for an additional four hours, but no significant propagation occurred.

At this time, it was decided to increase the injection rate with increments magnitude of 2. However, only 10-fold increase in injection rate up to 0.2 cm^3/min, allowed to observe if any further propagation. Immediately, several dominant fingers began to emerge from the polymer-contacted region. Three dominant fingers formed with similar “tree-like” splitting patterns, as shown in **Figure 4.2.18**; however, they were not as severe as in the water-displacing-heavy oil fingering patterns.

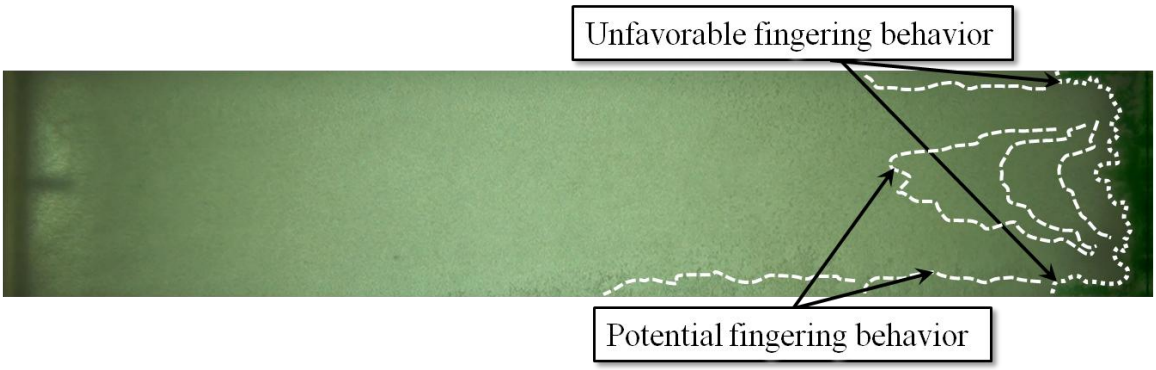

Figure 4.2.15 Polymer (24 mPa·s – 40:1) displacing heavy oil at 60-minute-mark

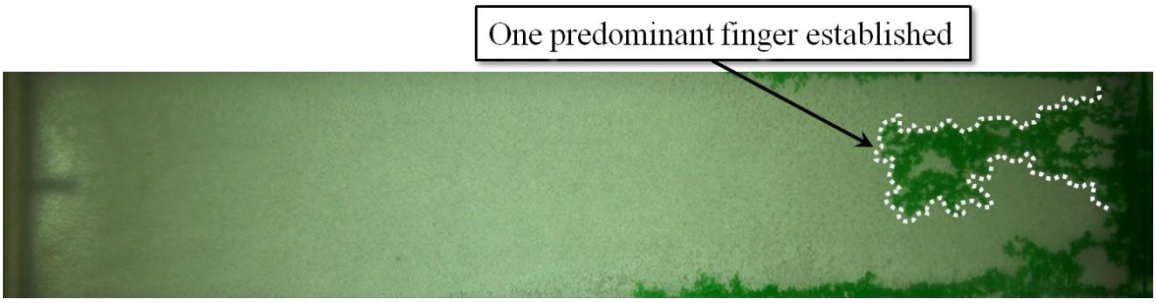

Figure 4.2.16 Polymer (24 mPa·s – 40:1) displacing heavy oil at 120-minute-mark

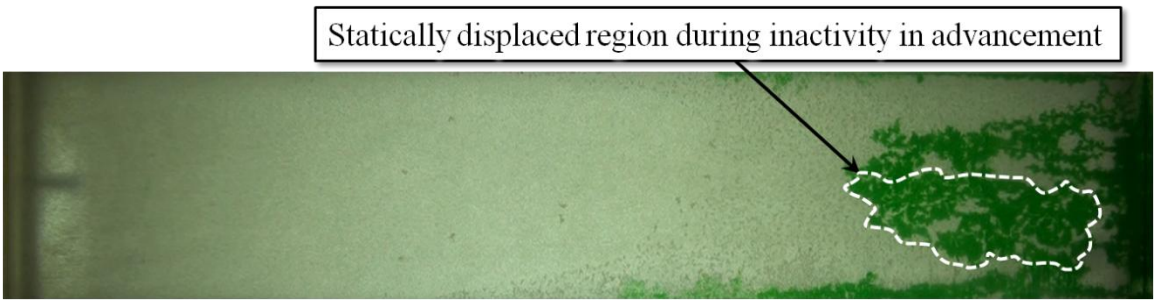

Figure 4.2.17 Polymer (24 mPa·s – 40:1) displacing heavy oil at 240-minute-mark

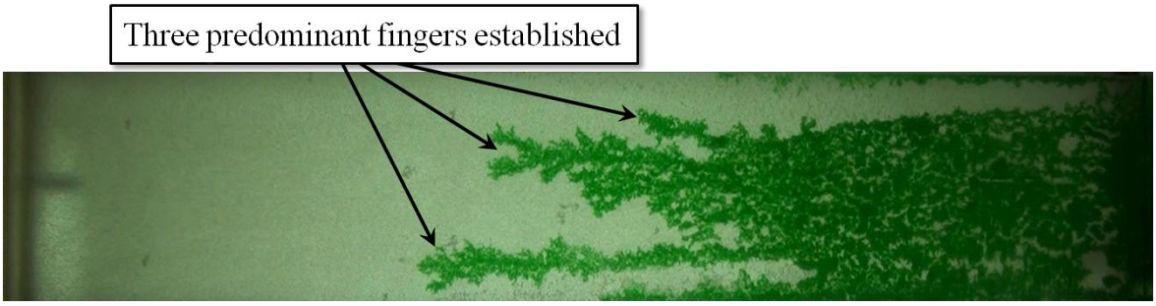

Figure 4.2.18 Polymer (24 mPa·s – 40:1) displacing heavy oil 30 minutes after rate increase

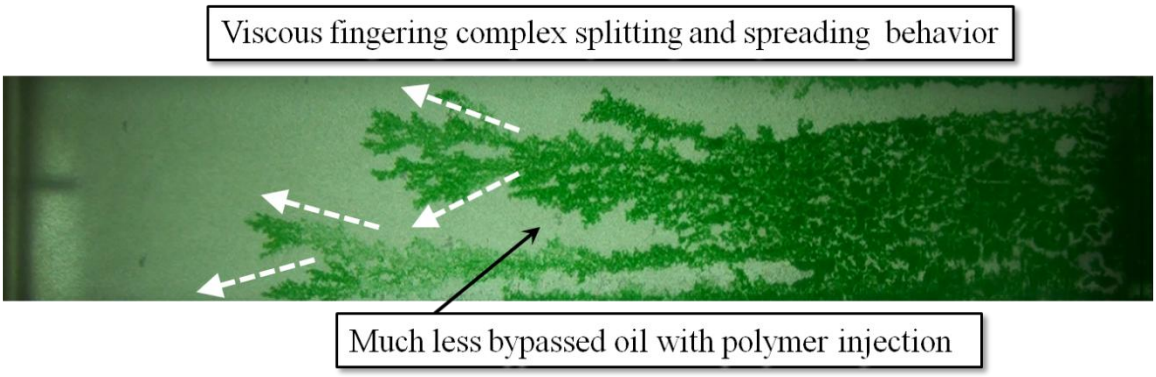

Figure 4.2.19 Polymer (24 mPa·s – 40:1) displacing heavy oil 45 minutes after rate increase

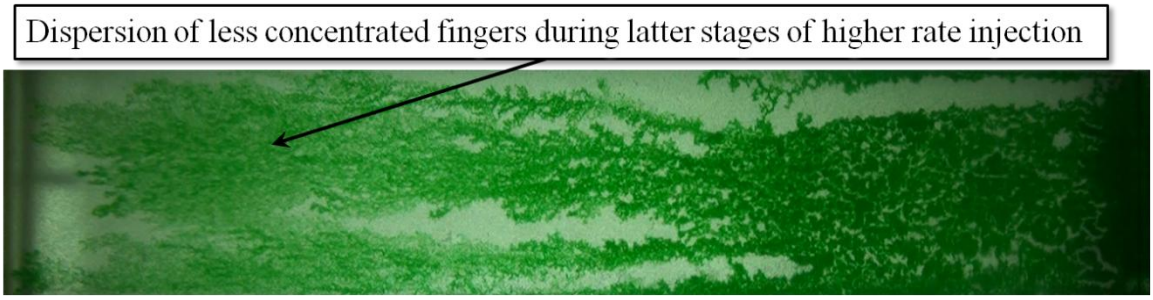

Figure 4.2.20 Polymer (24 mPa·s – 40:1) displacing heavy oil 60 minutes (breakthrough)

The addition of polymer significantly mitigated the multiple branch formation and "thickened" each of the propagating fingers, greatly improving the overall sweep efficiency and oil recovery of the flood, as shown in **Figure 4.2.19**. Upon breakthrough, the high flow rate caused significant dispersion of the lower-concentrated fingers (Doorwar and Mohanty, 2011). It is possible that the high flow rate also caused some dislodging of the pack near the outlet to occur. The final sweep efficiency is shown in **Figure 4.2.20**.

4.2.5 Effect of unfavourable viscosity ratio (22:1) on displacing medium-light oil (22 mPa·s) by water

A displacement of 22-mPa·s medium-light oil by water was initially conducted for a reference of 22:1 viscosity ratio. The injection of water resulted in initially unstable displacement of oil by formation of viscous instabilities shortly after two minutes of injection (**Figure 4.2.21**). Further propagation of the displacement front transformed into two predominant fingers that penetrated oil phase. The strong establishment of viscous instabilities was not completely evident until the displacement sequence reached the 5 minute mark of the displacement process (**Figure 4.2.22**). An additional five minutes of injection resulted in some pore spaces being left intact by displacing phase. Furthermore two initially established fingers tended to dominate the instability process (**Figure 4.2.23**). Severe fingering coalescence, described by Brock and Orr (1991) or Jamaloei et al. (2011) became evident soon after the additional five minutes of injection at a flow rate of 0.02 cm^3/min. This coalescence effect resulted in larger fingers taking up more volume of the injected fluid and simultaneously preventing growth of the smaller fingers and, also, shielding the rest of the displacement front from further propagation within the media (**Figure 4.2.24**). This resulted in substantial volumes of oil being left behind due to poor sweep efficiency. Interestingly, complex splitting behaviour (**Figure 4.2.25**) was transformed into rapid coalescence, thereby supporting just a single major finger towards the breakthrough (**Figure 4.2.26**) rather than multiple fingering behaviour. It is believed that the large water intake of larger fingers is attributed mainly to the pressure gradient, which is steeper for larger fingers than for smaller ones.

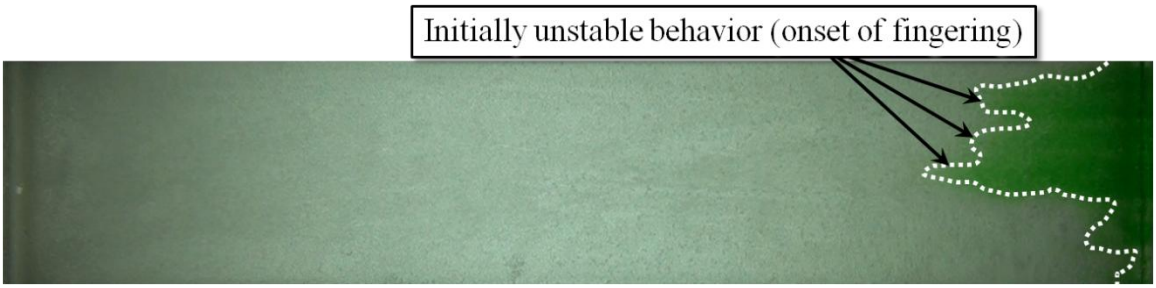

Figure 4.2.21 Water displacing medium-light oil at 2-minute-mark

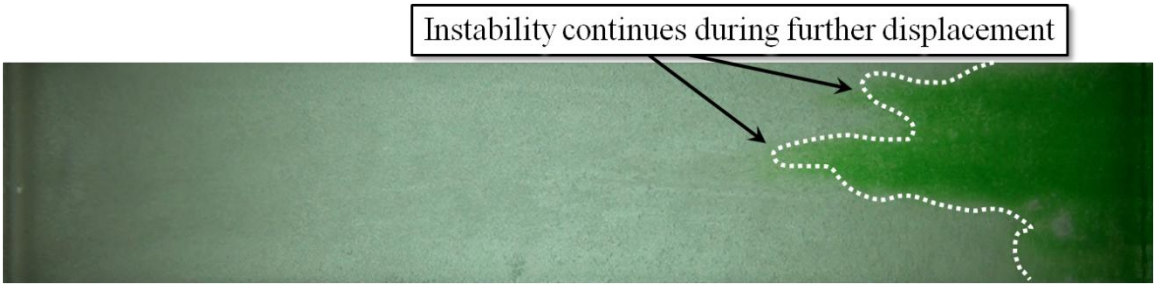

Figure 4.2.22 Water displacing medium-light oil at 5-minute-mark

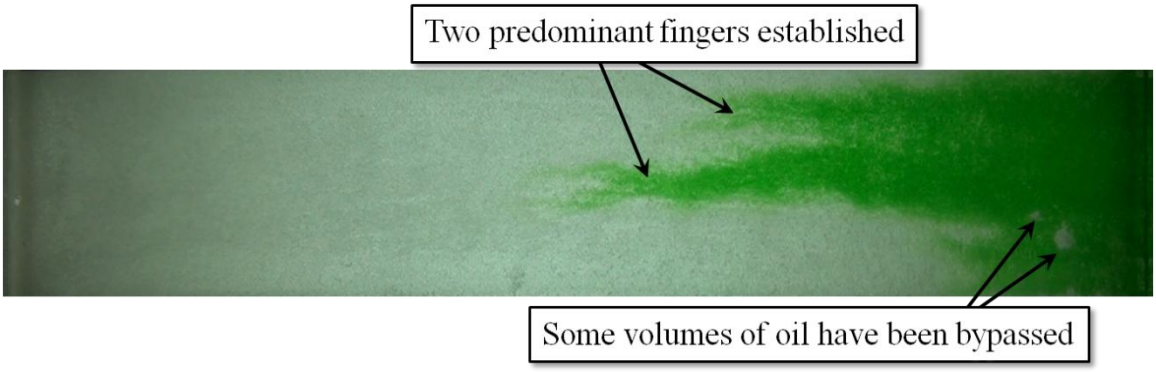

Figure 4.2.23 Water displacing medium-light oil at 10-minute-mark

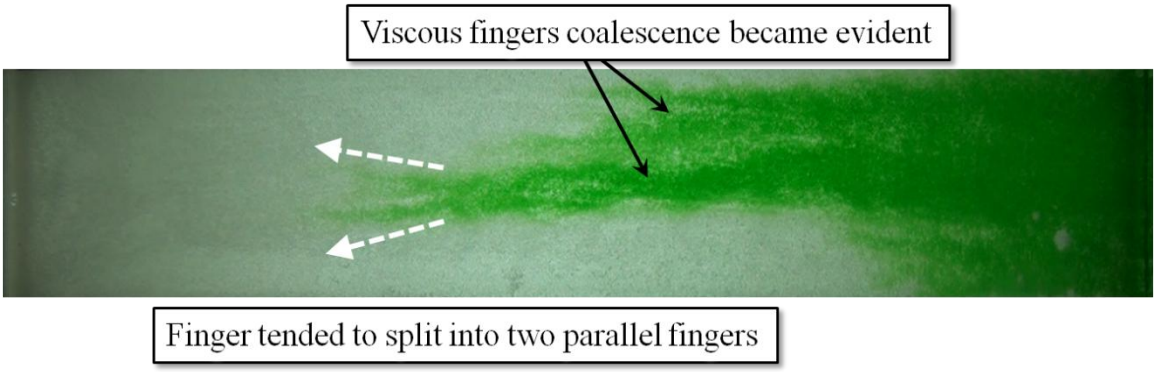

Figure 4.2.24 Water displacing medium-light oil at 15-minute-mark

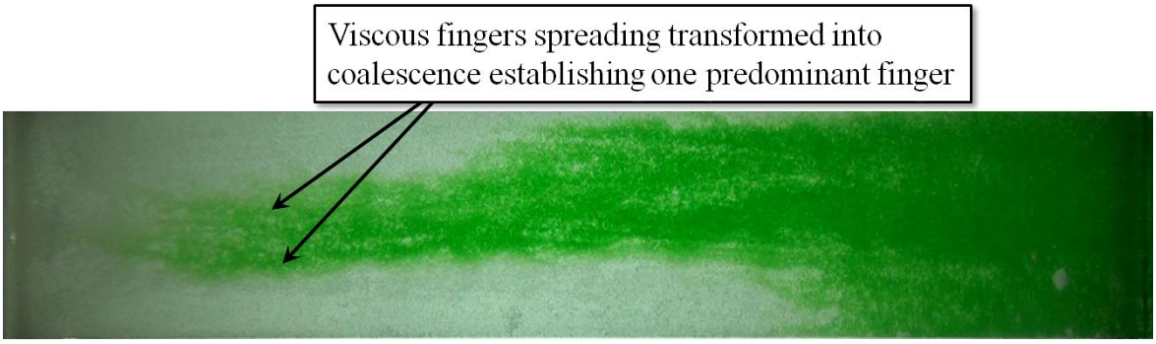

Figure 4.2.25 Water displacing medium-light oil at 20-minute-mark

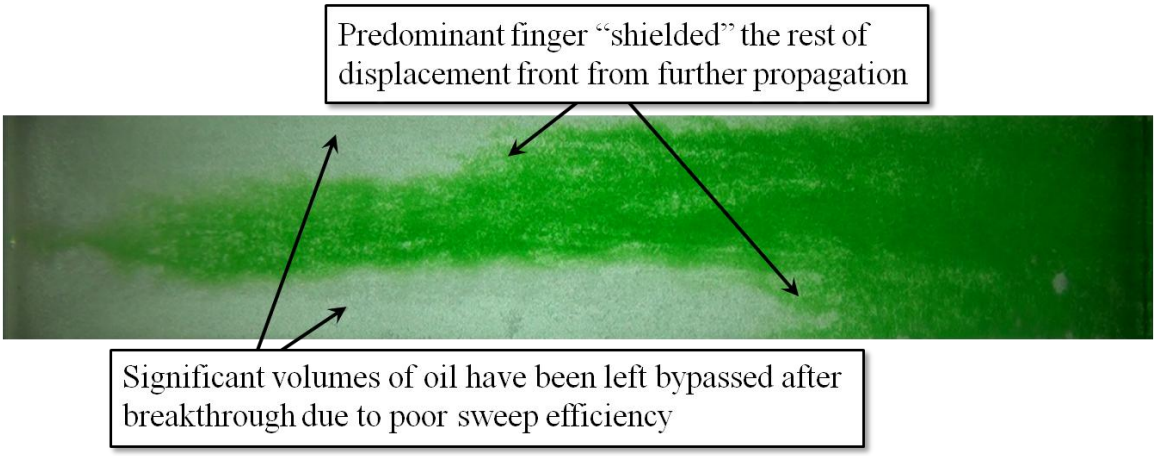

Figure 4.2.26 Water displacing medium-light oil at 21.07-minute-mark (breakthrough)

Therefore, certain recommendations can be made with respect to upgrading the model for the purposes of pressure readings (see **Section 5.2** of the thesis). Generally, the viscous instability behaviour during light oil displacement was similar to 153-mPa·s oil displacement but with far less occurrence of multiple branches and dendritic network of channels.

4.3 1D two-phase corefloods performance sensitivity to viscosity ratio

The following sections describe a series of coreflood tests that compare a 20-, 40-, and 80:1 viscosity ratio displacement of a 960 and 2039-mPa·s heavy oil. Generally, the main purpose of this part of the study was to observe the effect of viscosity ratio on heavy oil polymer flooding performance. The experiments utilized both HPAM and HAP at various concentrations of 0.18 to 0.30 wt% in 1 wt% NaCl. The comparative analysis includes the pressure differential and oil recovery data with respect to injection throughput, as well as tables of resistance and residual resistance data, saturation profiles, and dynamic adsorption profiles. The main sandpack properties are given in **Table 4.3.1.** The different absolute permeabilities and slightly different porosities for each sandpack were obtained since freshly-packed sandpack was used for each new test. All graphics from these sections are originally in colour.

The approach was partially taken from Wang and Dong (2009), who suggested that oil recovery response would be different if the same pore volumes for waterflood or polymer flood were injected for different oil viscosities since the residual oil saturations will be different.

Table 4.3.1 Sandpack physical properties for 1D corefloods

	Test#							
Parameter	1	2	3	4	5	6	7	8
Length (cm)	29.24	29.24	29.24	29.24	29.24	29.24	29.24	29.24
Area (cm^2)	3.63	3.63	3.63	3.63	3.63	3.63	3.63	3.63
PV (cm^3)	37.5	37.37	31.70	32.40	31.00	32.70	33.30	33.40
Porosity	0.29	0.35	0.29	0.30	0.29	0.30	0.31	0.31
Absolute permeability (darcy)	2.54	5.13	1.55	3.42	1.44	3.86	1.69	1.51
Sand mass (g)	123.2	169.0	131.2	126.9	120.4	118.6	121.8	120.7

4.3.1 Effect of 40:1 viscosity ratio on displacement of a heavy oil (960 mPa·s) by Flopaam 3530S HPAM

An initial waterflood was conducted to approximately 0.95 PV of injection, after which the subsequent polymer flood sequence was initiated. Incremental recovery from the initial waterflooding, demonstrated comparatively poor efficiency: almost 19 % of OOIP was recovered (**Figure 4.3.1**) with almost 10 % of initial water cut (**Figure 4.3.2**) produced. It is noticeable that water cut trend does not start from any specific point on the water cut versus volume injected plot. This could be a direct result of experimental error, since some water was evident in the system's dead volumes.

The core saturation profile changed from 0.76 of initial oil saturation (S_{oi}) to 0.61 (**Table 4.3.2**). The corresponding pressure differential from waterflood performance raised up to 240 kPa indicating for water bank propagating through the sandpack, displacing oil and at the breakthrough it reduced to 21.31 kPa (**Figure 4.3.1)**. The completely stabilized dP in this test was not obtained; therefore, a decision was made to input the pressure differential data from previously conducted absolute permeability readings.

This differential pressure behaviour is typical for each of the stages of displacement and was indicated in all tests provided in this chapter. The pressure build-up was an indication of either water or polymer bank advancing through the porous media displacing heavier fluid until it reached breakthrough. At this point of displacement the pressure starts dropping down until it should reach a stabilized value and the sandpack is in equilibrium with injected fluid.

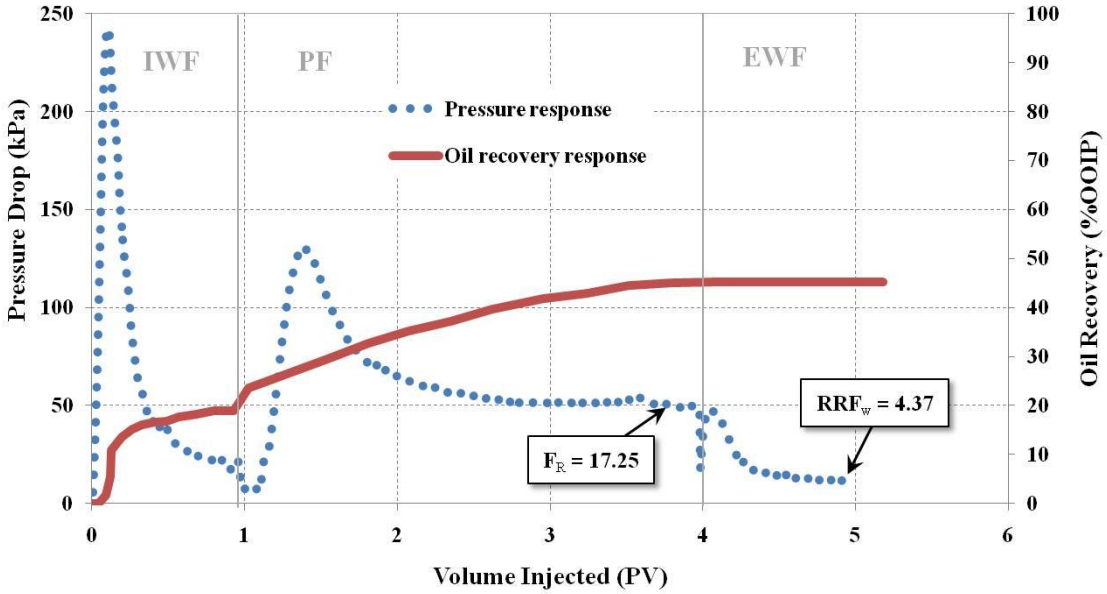

Figure 4.3.1 Oil recovery and pressure response during test #1

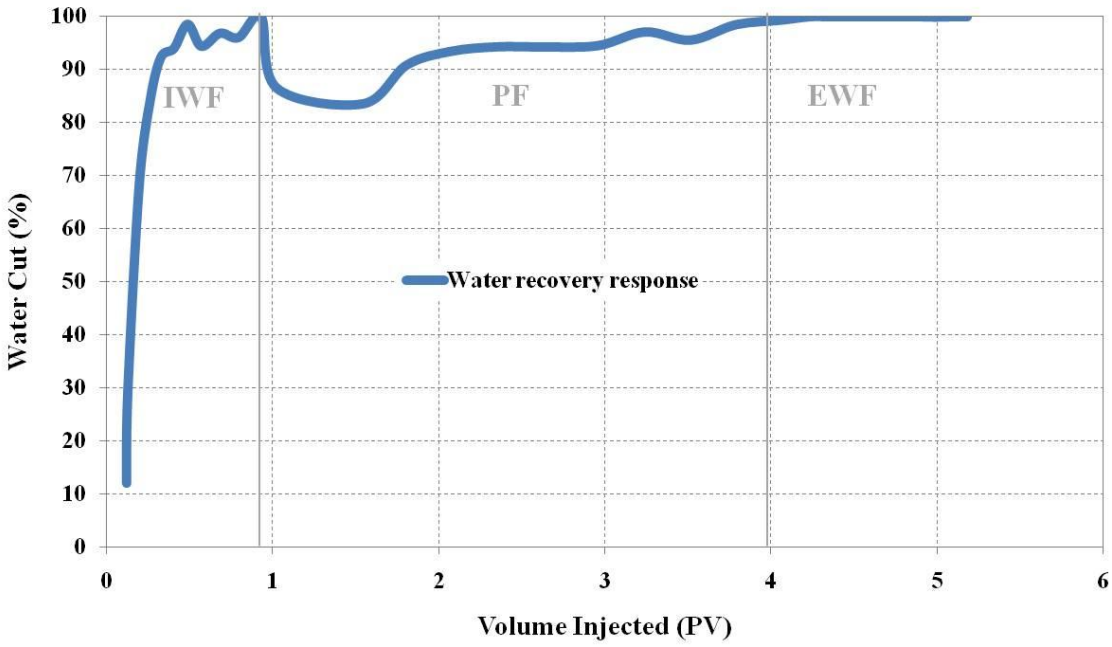

Figure 4.3.2 Water production response during test #1

Generally, it is noticeable from graph of oil recovery and pressure response, polymer flood initial pressure response demonstrated a slight delay. This could be attributed to specifications of experimental set-up. It is believed that transfer vessel's piston required some time for pressure to be build-up and move it towards outlet side. All these features and anomalies apply to all tested cases in this chapter.

The injected polymer viscosity of 0.20 wt% HPAM was determined to be 34.85 mPa·s at a theoretical shear rate of 14.72 s^{-1} based on the correlation between porosity, permeability, and Darcy advancement rate in Jennings et al. (1971). The subsequent injection of 2.82 pore volumes of polymer solution resulted in a well-stabilized pressure drop of 50.3 kPa with a corresponding resistance factor of 17.25, representing polymer solution in-situ viscosity. Therefore, viscosity decreased to almost two times that measured in the viscometer, demonstrating shear thinning behaviour. The ultimate recovery factor from HPAM injection increased to approximately 47 % of OOIP. Therefore, incremental recovery after polymer injection was almost 25 %OOIP with initially reduced water cut of 83 % (**Figure 4.3.2**). The polymer injection reduced the oil saturation and increased aqueous phase saturations to 0.38 and 0.62, respectively. The effluent viscosity at steady-state conditions was slightly reduced (31.82 mPa·s) compared to injected polymer at the calculated theoretical shear rate.

Extended waterflooding (EWF) was then carried out. The final residual oil saturation stayed the same since only a little fraction of a percent was recovered after EWF. The corresponding pressure differential was much lower than that for initial waterflood – 12.74 kPa. This resulted in a residual resistance factor of 4.37, meaning a permeability reduction of 4.37.

Post-polymer oil injection was then initiated until stabilized pressure drop was reached. Therefore, the RRF-to-oil (RRF_o) was slightly greater than one, at 1.03. The dynamic adsorption response demonstrated similar behaviour as for Wabiskaw sand (Wilton, 2008). Thus, the dynamic adsorption number for this test was 72.8 µg/g of sand. Plots of concentration and instantaneous mass of produced polymer with respect to injected volume are depicted in **Figure 4.3.3**.

It is noticeable that effluent concentration initial curve demonstrated immediate response; this in fact can be neglected firstly due to slightly different ways of samples collection therefore no normalization is possible due to unavailability of samples at this time therefore re-measurement of masses required. Secondly, only later stage of response is under main consideration (i.e. steady-state stage) in current research. All these assumptions apply to all tested cases.

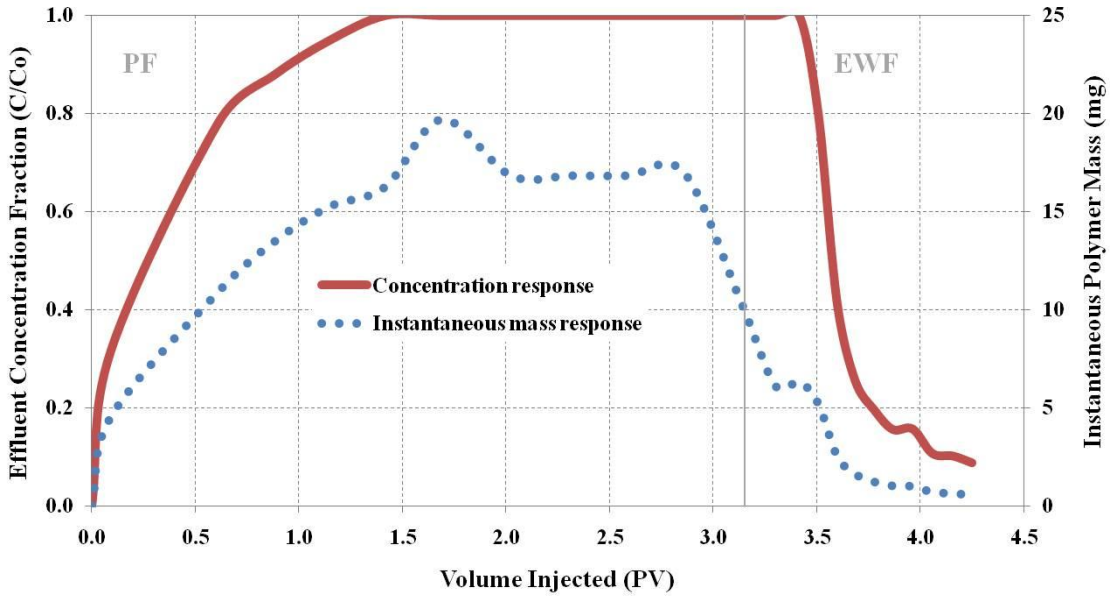

Figure 4.3.3 Concentration profile and instantaneous produced polymer mass response during test #1

4.3.2 Effect of 40:1 viscosity ratio on displacement of a heavy oil (960 mPa·s) by Superpusher C319 HAP

An initial waterflood of the sandpack was conducted to approximately 2.6 PV of injection at a rate of 0.2 cm^3/min. An oil recovery of 26.64 % of OOIP was obtained at a water cut of less than 1 %. As seen from the plot of the pressure differential response (**Figure 4.3.4**), 2.6 pore volumes of injected brine was not sufficient to reach completely stabilized dP for resistance and residual resistance data calculations. The differential pressure drop slightly exceeded 11 kPa. Therefore, an assumption was applied to take into consideration differential pressure response during sandpack absolute permeability measurement and use it for F_R calculation, as discussed previously in **Section 3.5.2**. A second oil flood was conducted to re-saturate the sandpack until stable differential pressure drop was established along the core, and the main water/polymer flood sequence was conducted thereafter.

A second waterflood was conducted to approximately 0.85 PV of injection when the experiment was changed to injection of Superpusher C319 HAP in 1 wt% NaCl polymer solution. Approximately 27 %OOIP was recovered from the waterflood until initial oil saturation (S_{oi}) 0.92 dropped to residual oil saturation (S_{or}) of 0.64. **Table 4.3.2** shows a summary of the saturation profiles for each injection phase during each coreflood. The pressure during the waterflood increased to nearly 21.83 kPa, higher than the previous flood.

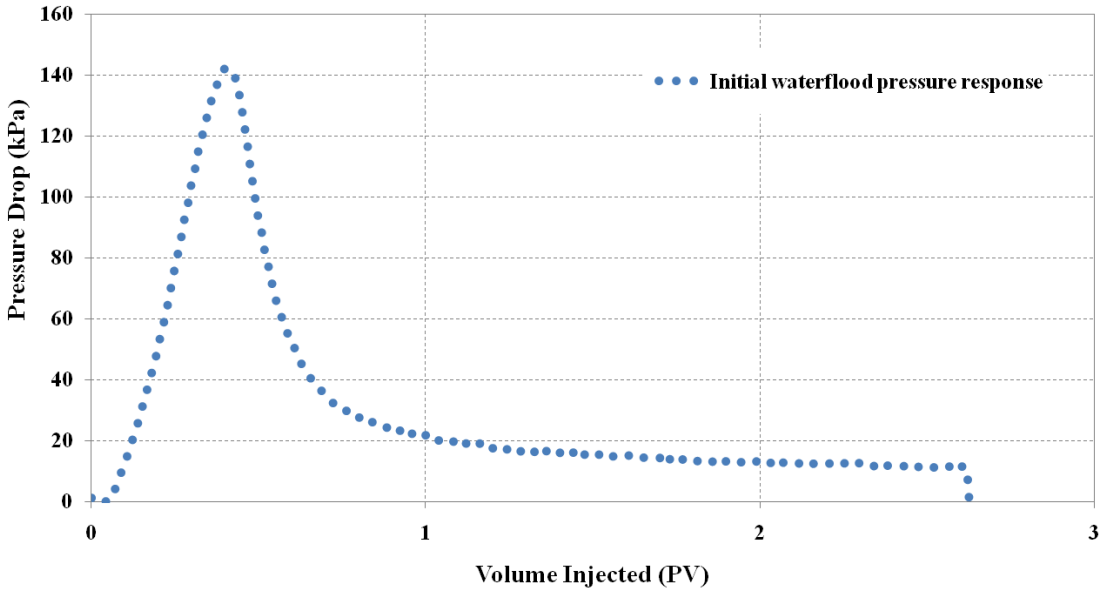

Figure 4.3.4 Pressure response during the effort to reach fully stabilized pressure drop for initial waterflood

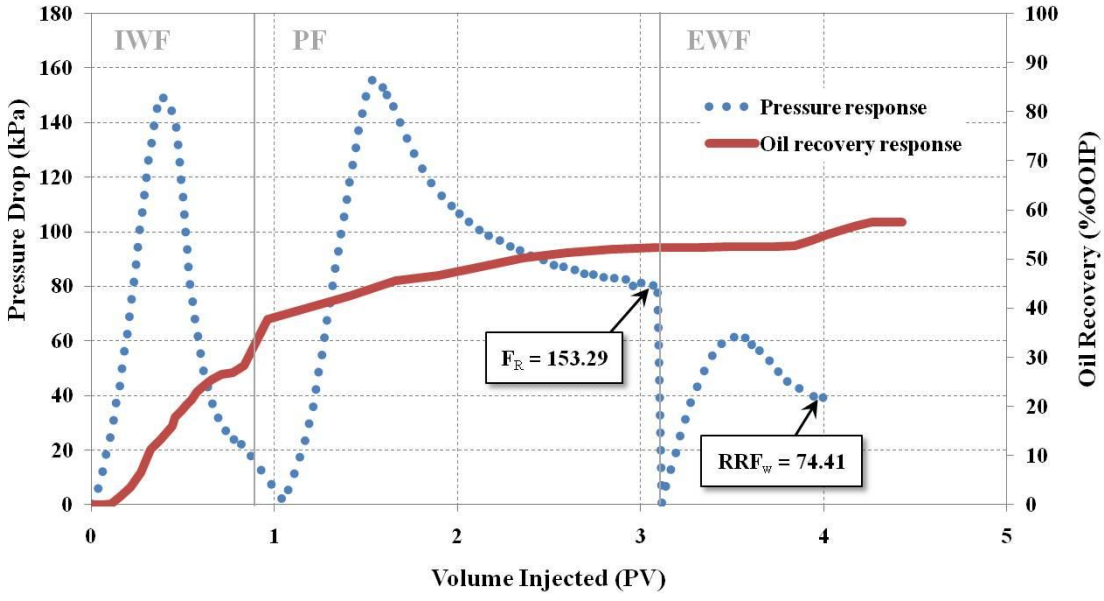

Figure 4.3.5 Oil recovery and pressure response during test #2

However, the waterflood oil recovery was approximately 10 %OOIP less with the lowest water cut of ~3 % (**Figure 4.3.6**). This discrepancy in waterflood recovery could be attributed to some instability behaviour or fines migration in the sandpack along the wall of the sandpack holder (**Figure 4.3.5**).

The viscosity of injected polymer solution as measured in the viscometer was ~24 mPa·s at a calculated theoretical shear rate of 9.66 s^{-1}. Upon switching to polymer injection, an immediate response was observed in the oil recovery followed by a much sharper increase in differential pressure across the sandpack. The stable pressure differential was indicated at 80.21 kPa (**Figure 4.3.5)**, corresponding to F_R value of 153.29. This value represents the in-situ polymer viscosity, which appeared to be 6.3 fold of increase, indicating possible shear thickening behaviour. Nearly 25 %OOIP incremental oil was recovered due to the polymer with an additional ~6 %OOIP obtained from EWF, resulting in a final S_{or} of 0.31.

The stabilized pressure drop approached 38.97 kPa for the extended waterflood, thereby giving a value of RRF_w 74.47. Therefore, the HAP-type of polymer significantly decreased core permeability to brine during subsequent brine injection.

The dynamic adsorption for this particular polymer system was found to be 73.6 µg/g. The plots of concentration and instantaneous mass of produced polymer with respect to injected volume are shown in **Figure 4.3.7**.

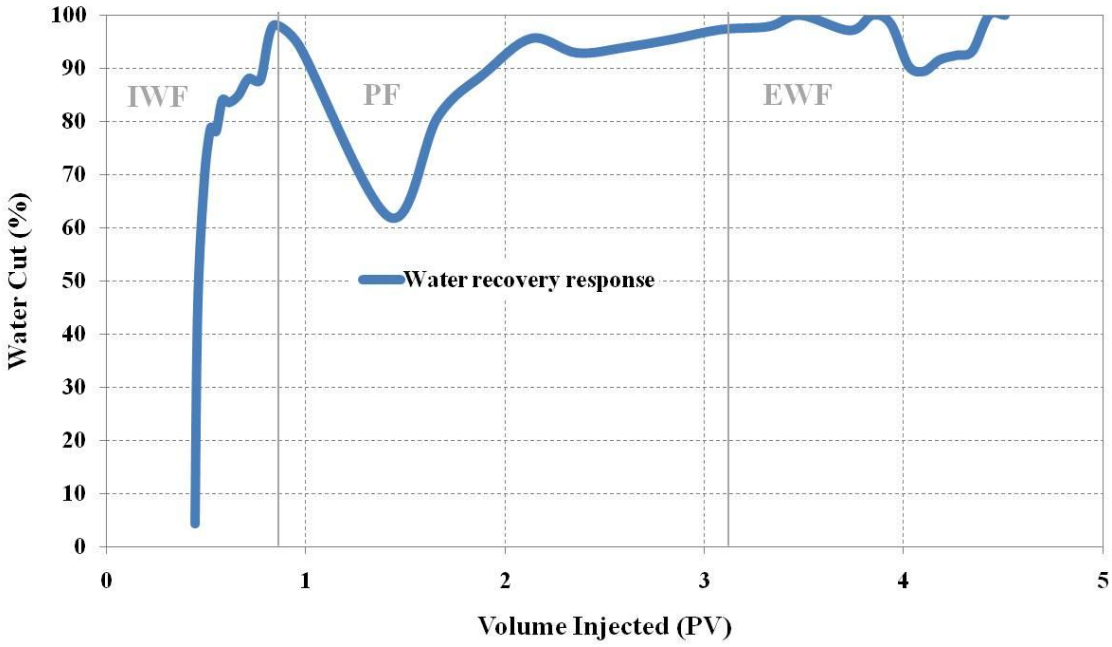

Figure 4.3.6 Water production response during test #2

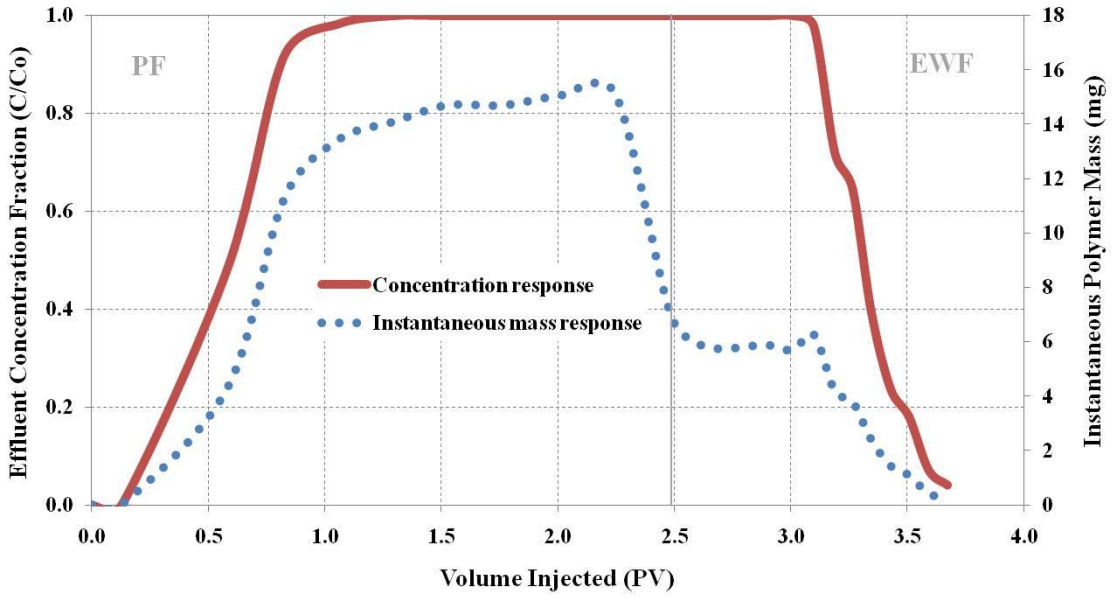

Figure 4.3.7 Concentration profile and instantaneous produced polymer mass response during test #2

4.3.3 Effect of 20:1 viscosity ratio on displacement of a heavy oil (960 mPa·s) by Flopaam 3530S HPAM

The initial waterflood of a sandpack had 0.9 PV of 1 wt% NaCl injected. The subsequent polymer injection of 2.83 PV was then commenced utilizing Flopaam 3530S HPAM in 1 wt% NaCl solution. The performance of the initial waterflooding demonstrated 25.5 %OOIP recovered with the corresponding stabilized core differential pressure of 42.96 kPa. This resulted in oil saturation decrease from 0.87 to 0.67 (**Table 4.3.2)**.

The viscosity of injected polymer solution was measured at ~56 mPa·s at a calculated theoretical shear rate of 19.17 s^{-1}. Unlike the case of HAP, HPAM showed no immediate response in oil recovery. Therefore, the incremental recovery reached only ~18 %OOIP with corresponding lowest water cut of ~81 % (**Figure 4.3.9)**. The final oil saturation after the polymer injection was determined to be 0.47. The corresponding pressure response for the polymer flood did not exceed 128 kPa, providing the F_R value of 51.11 – three times lower than for the HAP case. Therefore, the estimated in-situ viscosity from the current experiment was slightly lower.

Extended waterflood performance showed the same trend as for the previous scenario. Therefore, no additional oil was recovered (**Figure 4.3.8**). The pressure differential, on the other hand, gave an RRF_w of 5.47, which was almost 15 times lower than that for the previous case.

The oil post polymer injection gave a RRF_o of 1.42. **Figure 4.3.10** showcases an effluent analysis of 0.30 wt% (3,000 ppm) polymer solution injection in which a dynamic polymer adsorption of 178.8 μg/g was obtained.

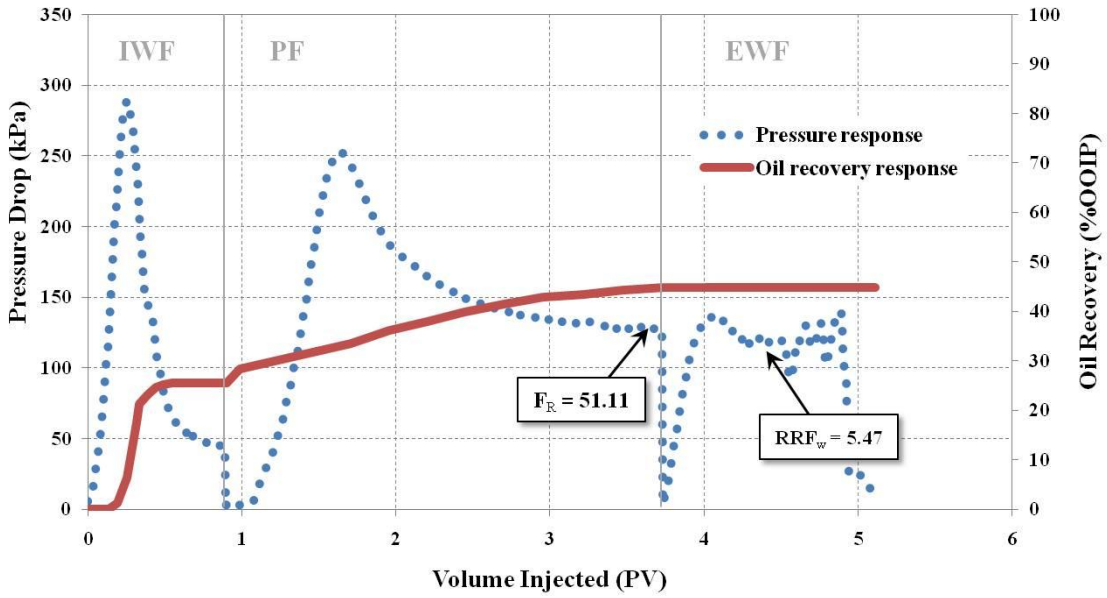

Figure 4.3.8 Oil recovery and pressure response during test #3

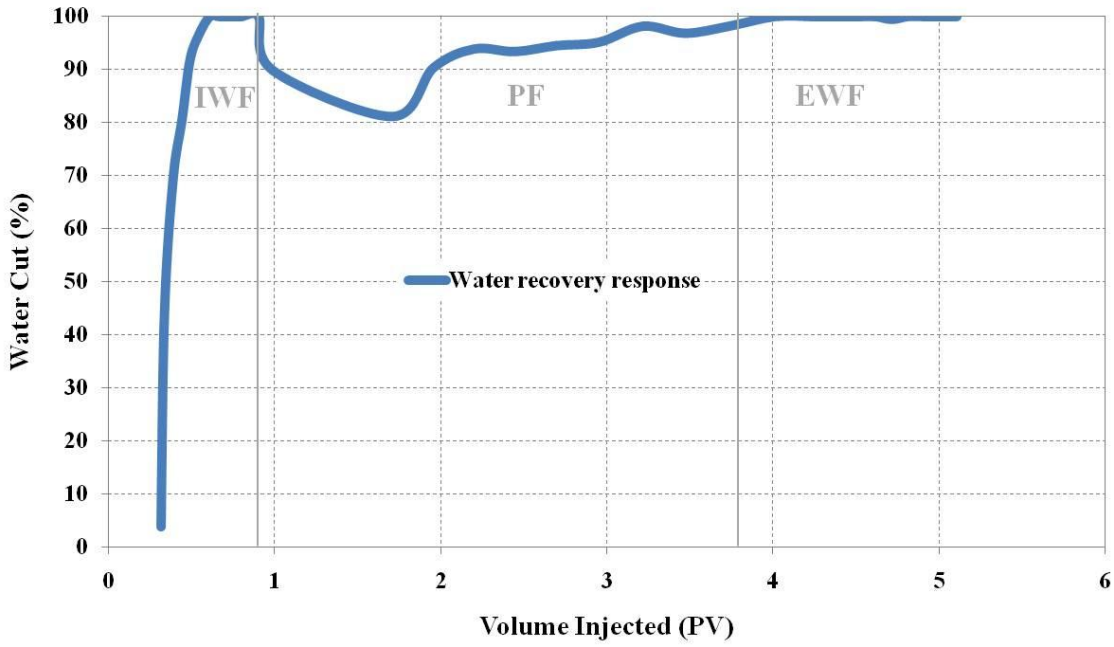

Figure 4.3.9 Water production response during test #3

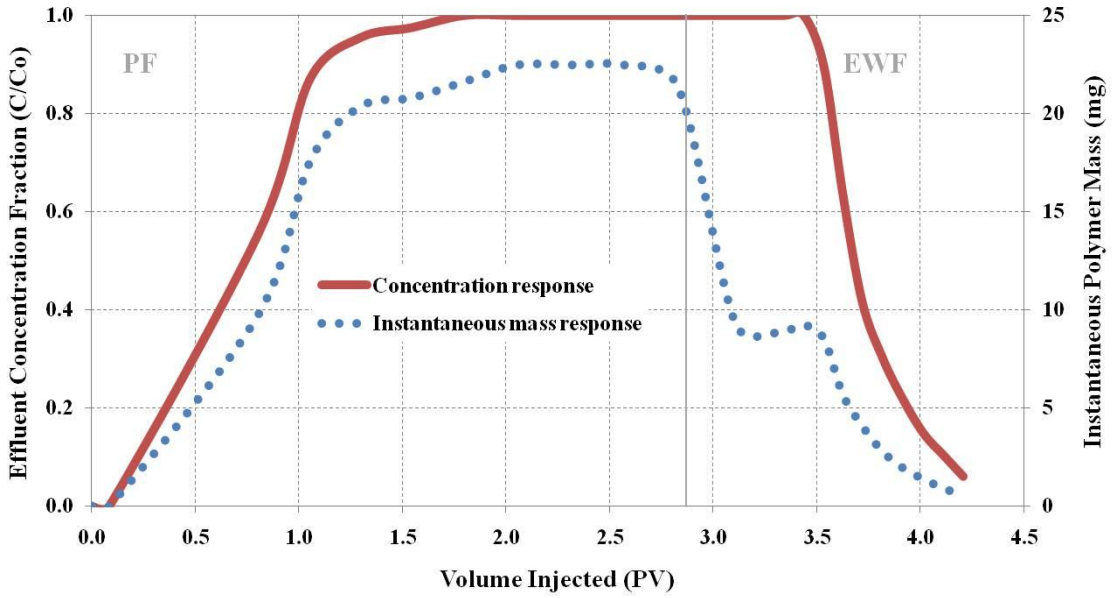

Figure 4.3.10 Concentration profile and instantaneous produced polymer mass response during test #3

4.3.4 Effect of 20:1 viscosity ratio on displacement of a heavy oil (960 mPa·s) by Superpusher C319 HAP

A waterflood was initiated to approximately 0.95 PV of injection and subsequently switched to polymer injection of Superpusher C319 HAP in 1 wt% NaCl solution. Initial waterflood performance reached 24 %OOIP and ~3.5 % of water cut (**Figure 4.3.12**), resulting in reduction of oil saturation from 0.80 to residual oil saturation of 0.58 (**Table 4.3.2)**. The corresponding pressure differential increased to approximately 50 kPa; however, a plateau of stable pressure was not ultimately reached.

The viscosity of the injected polymer solution was ~72 mPa·s at a calculated theoretical shear rate of 12.71 s^{-1}. Polymer injection, the same as in the previous HAP case, demonstrated immediate response in terms of oil recovery. This could indicate a more stable polymer slug formed with far less occurrence of fingering and channeling. However, this response appeared to be less intense than in the case of less concentrated HAP polymer solution; therefore, it contributed to comparatively lower incremental heavy oil recovery of ~20 %OOIP with ~83 % of water cut and S_{or} of 0.35. Ultimately, the stable pressure differential was indicated at 99.69 kPa, corresponding to F_R value of 152.13. This translates into the estimated viscosity from the coreflood, which appeared to be 2.1 times greater than the viscosity of injected polymer, indicating that polymer thickening took place at the calculated shear rate in the core. The viscosity of injected polymer solution tended to decrease slightly in the effluent during steady-state condition to approximately 70.91 mPa·s at theoretical shear rate.

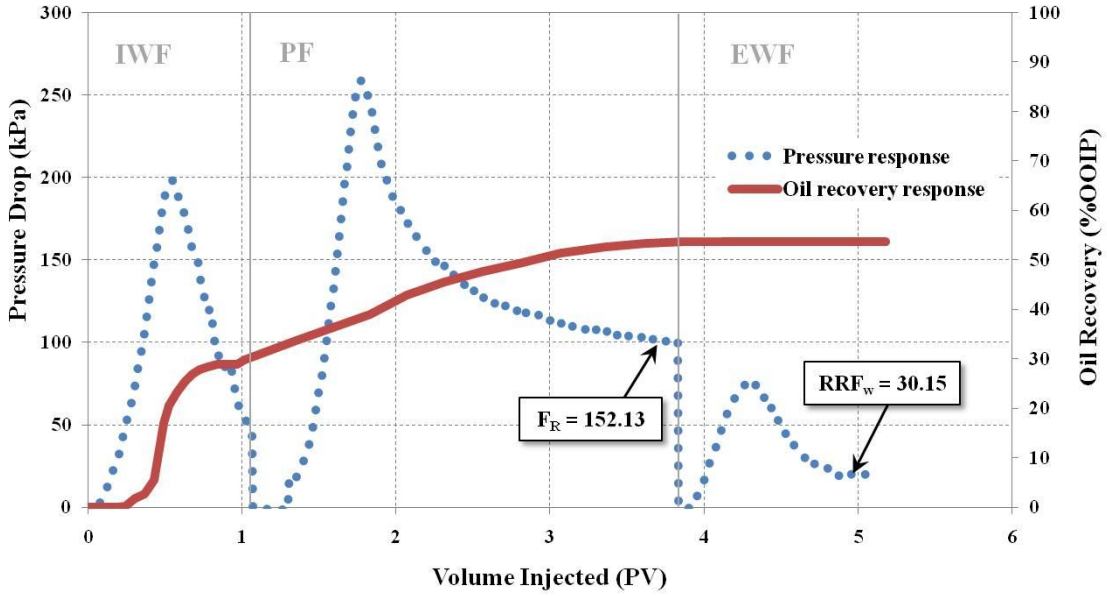

Figure 4.3.11 Oil recovery and pressure response during test #4

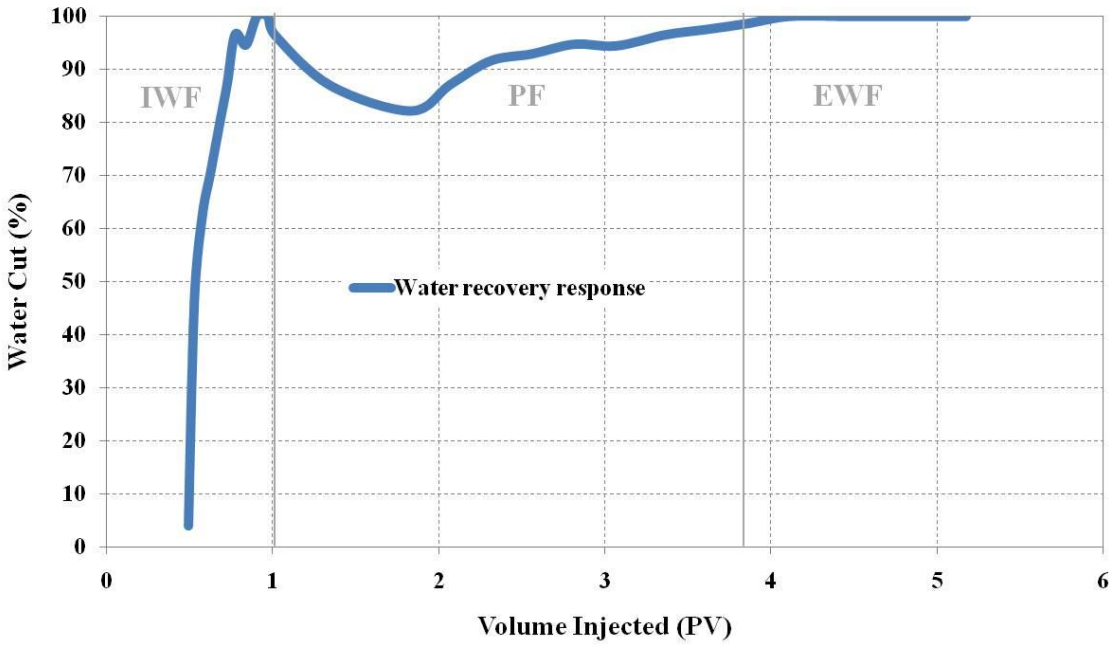

Figure 4.3.12 Water production response during test #4

The extended waterflood (EWF) demonstrated absolutely no additional oil recovery with a corresponding pressure differential of 19.75 kPa. This resulted in a residual resistance factor to water (RRF_w) of 30.15, indicating significant permeability reduction to brine.

The EWF was followed by oil post polymer injection. This resulted in a stabilized pressure drop of 362.19 kPa. As expected, the residual resistance factor to oil (RRF_o) was greater than one at 1.16. The dynamic adsorption for the tested system was calculated and appeared to be almost triple than in the previous HAP case – 220.5 µg/g for a 0.30 wt% (3,000 ppm) concentration. The plots of concentration of produced polymer and instantaneous mass versus PV throughput are depicted in **Figure 4.3.13. Figure 4.3.11** shows the plot of both oil recovery and pressure differential with respect to PV injected during Superpusher C319 HAP coreflooding at an approximate viscosity ratio of 20:1.

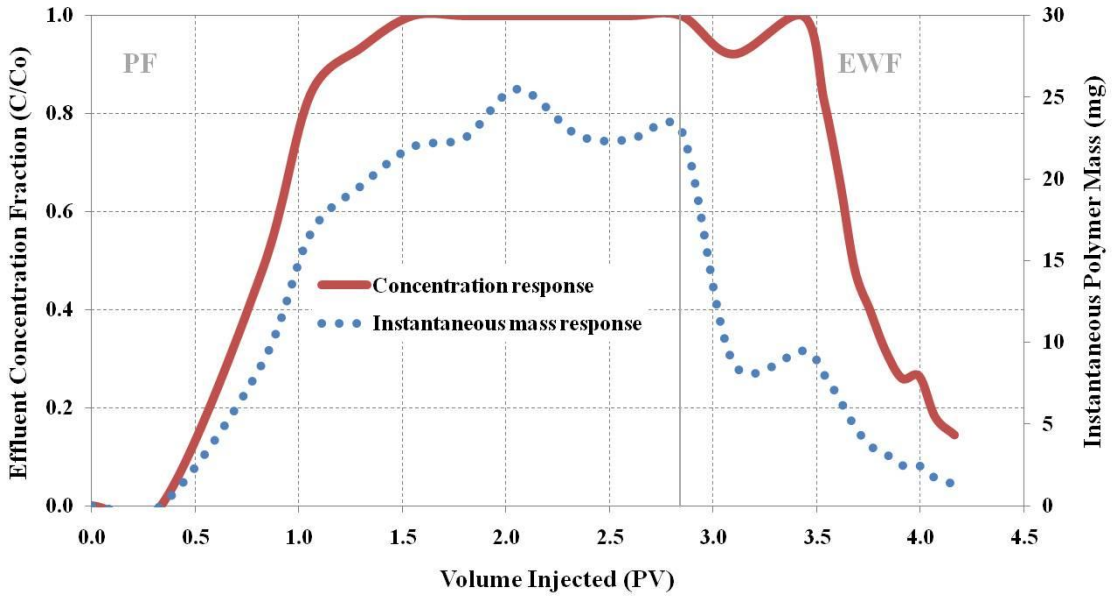

Figure 4.3.13 Concentration profile and instantaneous produced polymer mass response during test #4

Table 4.3.2 Saturation profiles for 960-mPa·s oil displacement

	Test#							
	1		2		3		4	
Parameter	S_o	S_w	S_o	S_w	S_o	S_w	S_o	S_w
Oil saturation	0.76	0.24	0.92	0.08	0.87	0.13	0.80	0.20
IWF	0.61	0.39	0.64	0.36	0.67	0.33	0.58	0.42
PF	0.38	0.62	0.37	0.63	0.47	0.53	0.35	0.65
EWF	0.38	0.62	0.31	0.69	0.47	0.53	0.35	0.65

4.3.5 Effect of 40:1 viscosity ratio on displacement of a heavy oil (2039 mPa·s) by Flopaam 3530S HPAM

Nearly 1 PV of 1 wt% NaCl was injected during the initial waterflooding sequence. The follow-up polymer flood (PF) was then carried out using Flopaam 3530S HPAM in 1 wt% NaCl solution. The initial waterflood resulted in comparatively less heavy oil recovered at 23.12 %OOIP with a higher peak of the differential pressure response. The estimated S_{or} after waterflooding appeared to be 0.66 (**Table 4.3.3**). Unfortunately, even though the oil cut in produced effluent was < 3%, a stabilized pressure plateau was not reached.

The viscosity of the injected polymer as measured was ~53.28 mPa·s at a calculated theoretical shear rate of 19.98 s^{-1}. It is critical to note that the given polymer system did not demonstrate fast recovery response, as in the case of the HAP system. The incremental oil recovery in this case slightly exceeded 20 %OOIP, with the lowest water cut of ~81 % (**Figure 4.3.15**), resulting in a residual oil saturation after polymer injection of 0.46. As expected, a comparatively higher pressure peak was found; however, the stabilized differential pressure drop was lower than in the case of 960-mPa·s heavy oil recovery of ~106.7 kPa. This resulted in a corresponding resistance factor of 21.12. Therefore, there was a slightly more than double decrease in estimated polymer solution viscosity in-situ due to shear thinning behaviour. The produced polymer viscosity was, as well, slightly decreased to 52.95 mPa·s comparing to injected solution.

An extended waterflood followed the polymer injection sequence, producing ultimately no additional oil.

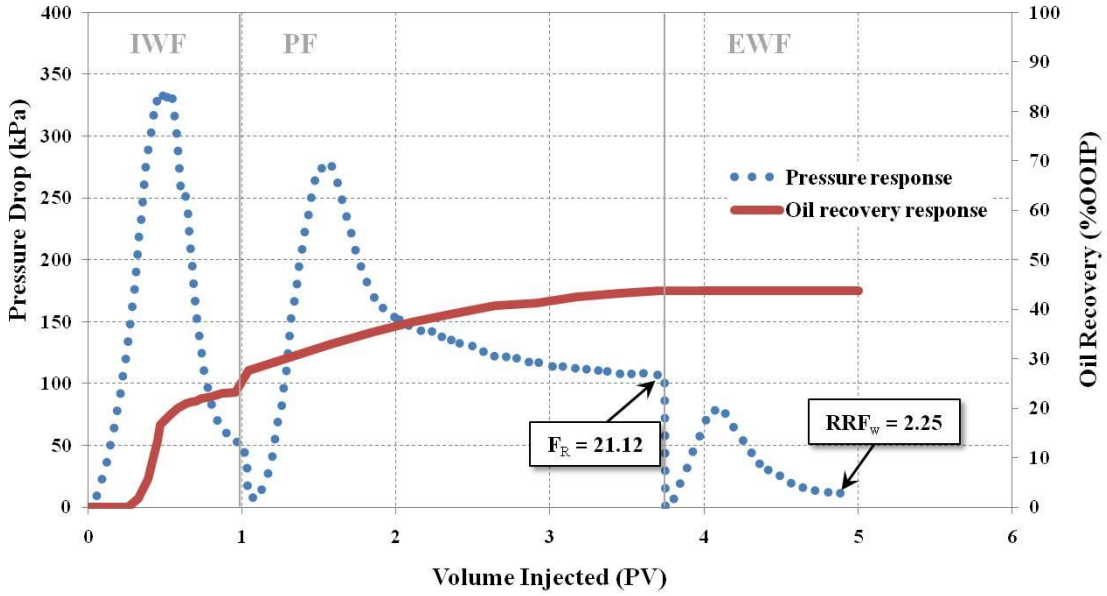

Figure 4.3.14 Oil recovery and pressure response during test #5

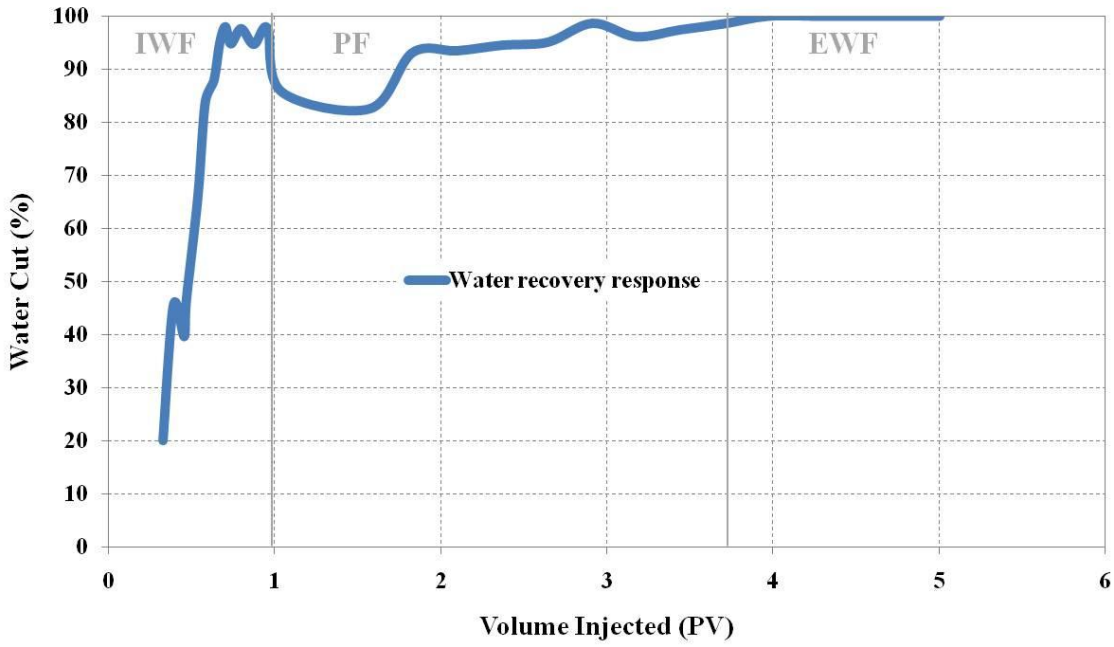

Figure 4.3.15 Water production response during test #5

The corresponding pressure response for EWF did not exceed 11.35 kPa; therefore, the residual resistance factor to water appeared to be 2.25, indicating much less permeability reduction to brine than in the case of HAP injection.

The residual resistance factor to oil after post polymer oil flood initiation represented a value of 1.24. It is unclear why dynamic polymer adsorption gave a lower value of 124.8 µg/g comparing to less viscous oil displacement (**Figure 4.3.16**). However, this could suggest that oil viscosity difference might contribute to significant change in dynamic polymer adsorption, possibly due to a stronger IPV effect (Pancharoen et al., 2010). **Figure 4.3.14** shows the plot of both oil recovery and pressure drop across the core with respect to PV injected during Flopaam 3530S HPAM coreflooding at an approximate viscosity ratio of 40:1.

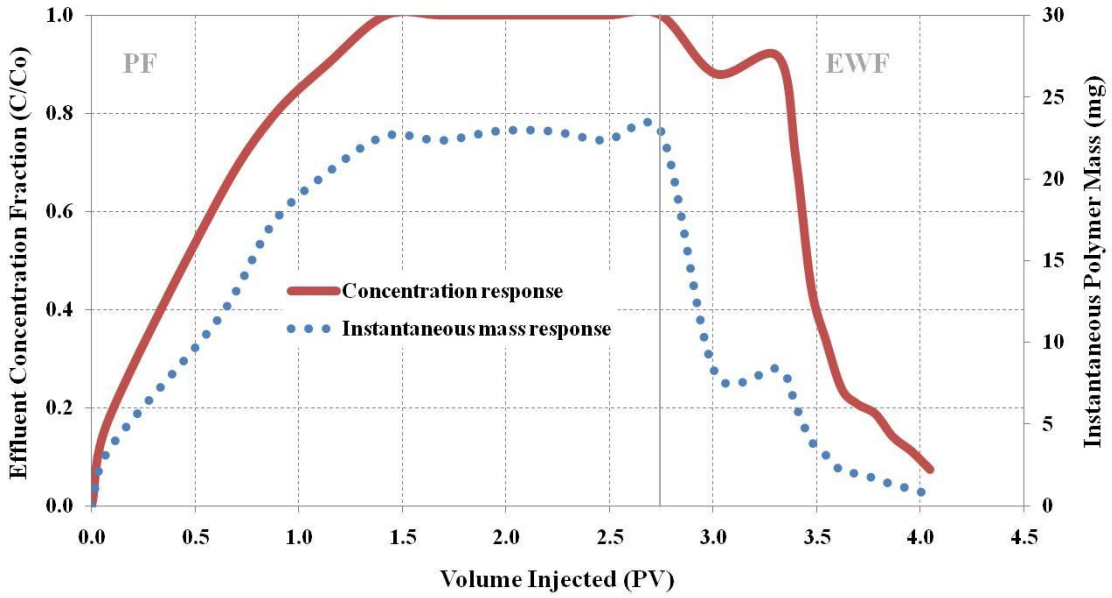

Figure 4.3.16 Concentration profile and instantaneous produced polymer mass response during test #5

4.3.6 Effect of 40:1 viscosity ratio on displacement of a heavy oil (2039 mPa·s) by Superpusher C319 HAP

An initial waterflood was carried out to approximately 0.95 PV of injection when the test was switched to injection of Superpusher C319 HAP in 1 wt% NaCl polymer solution. Recovery from IWF did not exceed 16 %OOIP (**Figure 4.3.17**), indicating much lower production compared to other tests. It is possibly due to difference in sandpack permeability, since for each new experiment freshly-packed beads were used. The estimated oil saturation profile changed from initial oil saturation of 0.81 to 0.74 of S_{or}. The corresponding stable pressure differential did not exceed 13.79 kPa.

The viscosity of the injected polymer as measured at ~66.1 mPa·s at a calculated theoretical shear rate of 11.90 s^{-1}. The tested polymer system did demonstrate comparatively the same behaviour in terms of quick recovery response as 0.30 wt% Superpusher C319 HAP at a viscosity ratio of 20:1, recovering relatively the same volume of incremental oil. This could lead to the conclusion that viscosity ratio in heavy oil systems with the same displacing phases does not contribute to substantial recovery difference. The incremental oil recovery in this case was around 20 %OOIP with a corresponding stabilized pressure differential of 81.17 kPa and the lowest water cut of ~83 % (**Figure 4.3.18**). This translated to an F_R value of 164.54, which represents a 2.5 fold increase in in-situ polymer viscosity due to a shear thickening effect. The effluent polymer viscosity slightly decreased to 61.18 mPa·s at steady-state conditions at the calculated theoretical shear rate. Residual oil saturation after polymer injection was calculated as 0.49 (**Table 4.3.3**).

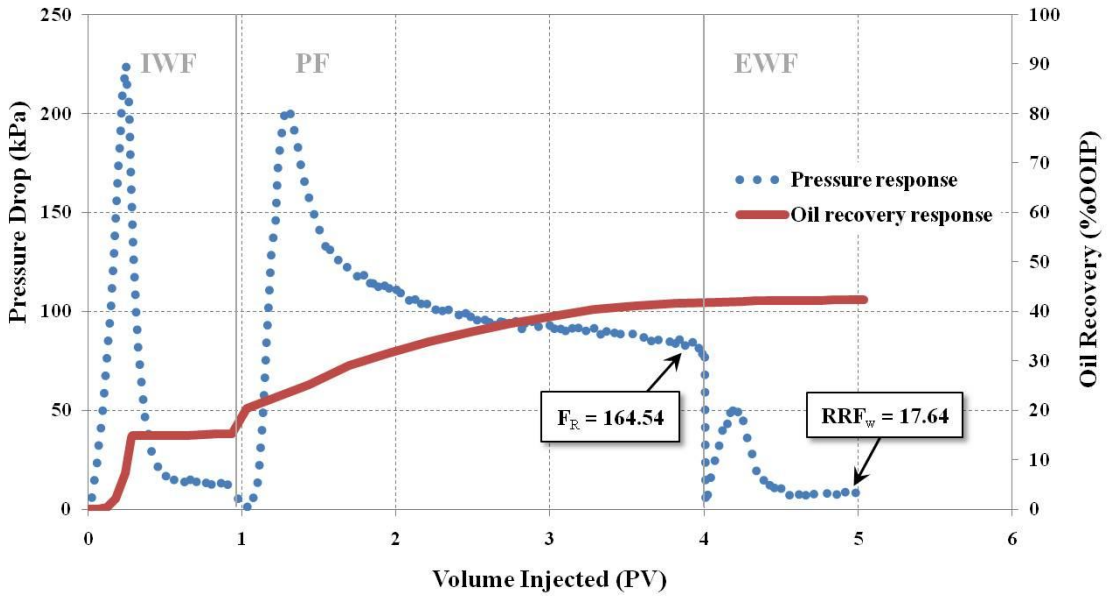

Figure 4.3.17 Oil recovery and pressure response during test #6

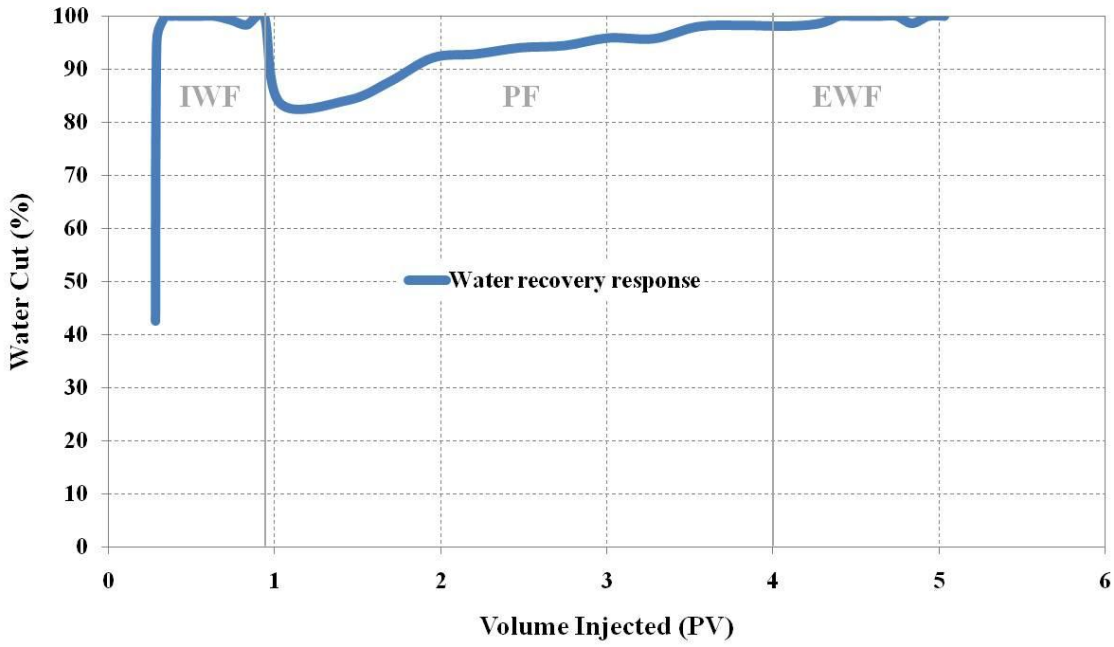

Figure 4.3.18 Water production response during test #6

Unlike the previous study on 2039-mPa·s heavy oil, the extended waterflood in the current case performed slightly better but still recovering less than one percent of additional oil in place. Interestingly, the residual resistance factor to water that was the same as in the previous HAP tests gave a higher value compared to the HPAM tests in cores with different absolute permeabilities. The corresponding stabilized dP was 8.71 kPa.

The RRF_o value (1.06) after post-polymer oil flood initiation, however, did not indicate any specific trend in terms of comparison of the two polymer types. It is unclear why dynamic adsorption of HAP 0.30 wt% (102.5 µg/g) in heavier oil systems provided a lower value than that for 960-mPa·s oil. However, it is possible that the IPV effect could have contributed to this behaviour. From the plots of concentration profile and produced polymer mass **(Figure 4.3.19)**; it is clear that the concentration response was much faster than during less viscous oil displacement. This means that polymer solution tended to follow paths previously channeled by water and not enter additional pores to sweep more oil, thereby showing a faster breakthrough response. This behaviour, therefore, negatively affected the recovery response. Nevertheless, the dynamic adsorption value was assumed to be acceptable for the given sand grain size. The plot of oil recovery with respect to PV injected during Superpusher C319 HAP coreflooding at an approximate viscosity ratio of 40:1 is depicted in **Figure 4.3.17.** The pressure differential trends of all three stages of displacement are shown on **Figure 4.3.17**, as well.

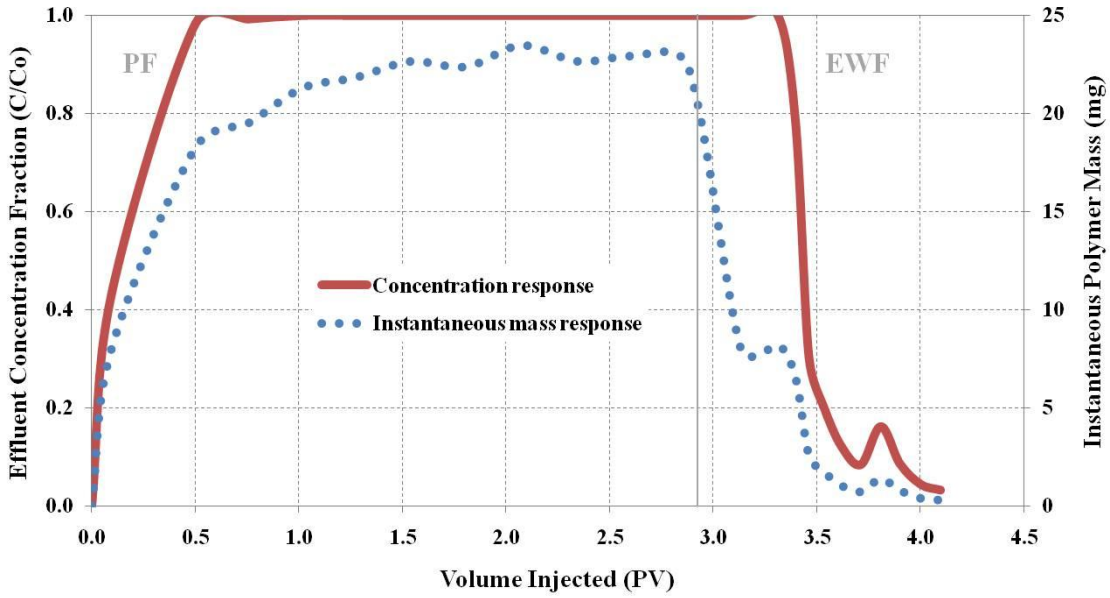

Figure 4.3.19 Concentration profile and instantaneous produced polymer mass response during test #6

4.3.7 Effect of 80:1 viscosity ratio on displacement of a heavy oil (2039 mPa·s) by Flopaam 3530S HPAM

Nearly 0.9 PV of 1 wt% NaCl was injected during the initial waterflooding sequence when the flood was changed to injection of Flopaam 3530S partially hydrolyzed polyacrylamide. Water injection resulted in low oil recovery of 13.3 %OOIP with a corresponding differential pressure of 24.2 kPa and determined oil saturation of 0.72 (**Table 4.3.3**).

The viscosity of the tested polymer solution was 30.02 mPa·s as measured in the viscometer at a calculated theoretical shear rate of 17.82 s^{-1}. The recovery from polymer injection showed a similar trend as for the previous HPAM tests, indicating a stable increase trend with no sudden response, unlike in the case with the previously tested hydrophobically-associating polymer systems. The incremental oil recovery from polymer flooding did not exceed 20 %OOIP with a corresponding final residual oil saturation of 0.52 and ~86 % of water cut (**Figure 4.3.21**). During polymer injection, a higher stabilized differential pressure of 36.91kPa was obtained, corresponding to a resistance factor of 21.62, showing a slight decrease in polymer in-situ viscosity due to shear thinning. Effluent polymer concentration slightly decreased to 29.58 mPa·s at the calculated shear rate while the system was in equilibrium.

Almost no additional oil recovery was obtained during EWF with the corresponding stabilized dP of 9.50 kPa. The conclusion that HAP provided higher residual resistance factors to water was supported by the RRF_w in this case, were it appeared to be 5.57, more than 2 times lower compared to the HAP tests.

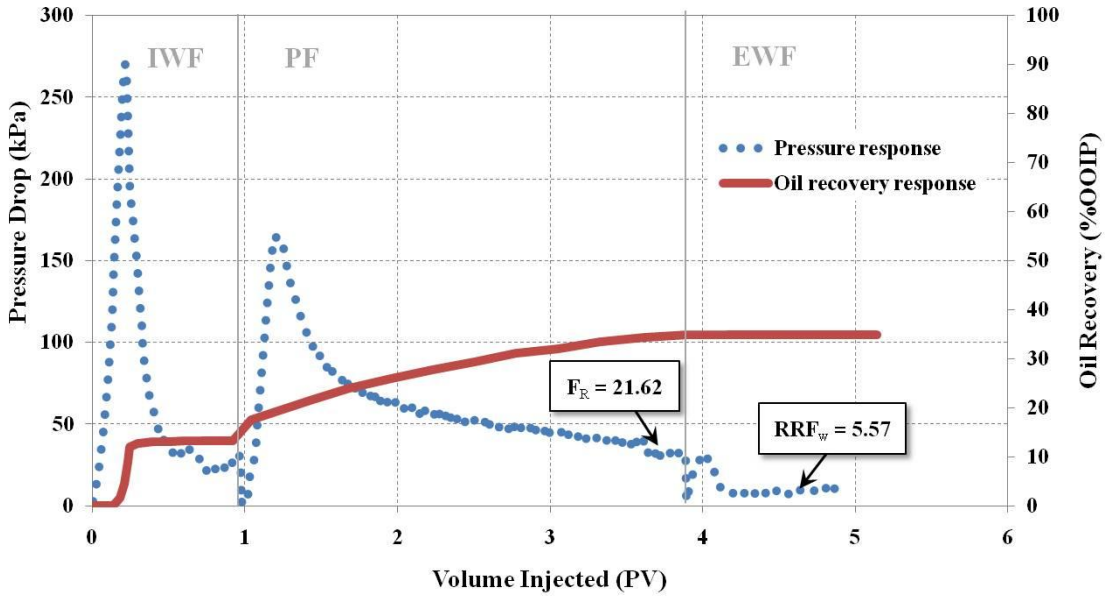

Figure 4.3.20 Oil recovery and pressure response during test #7

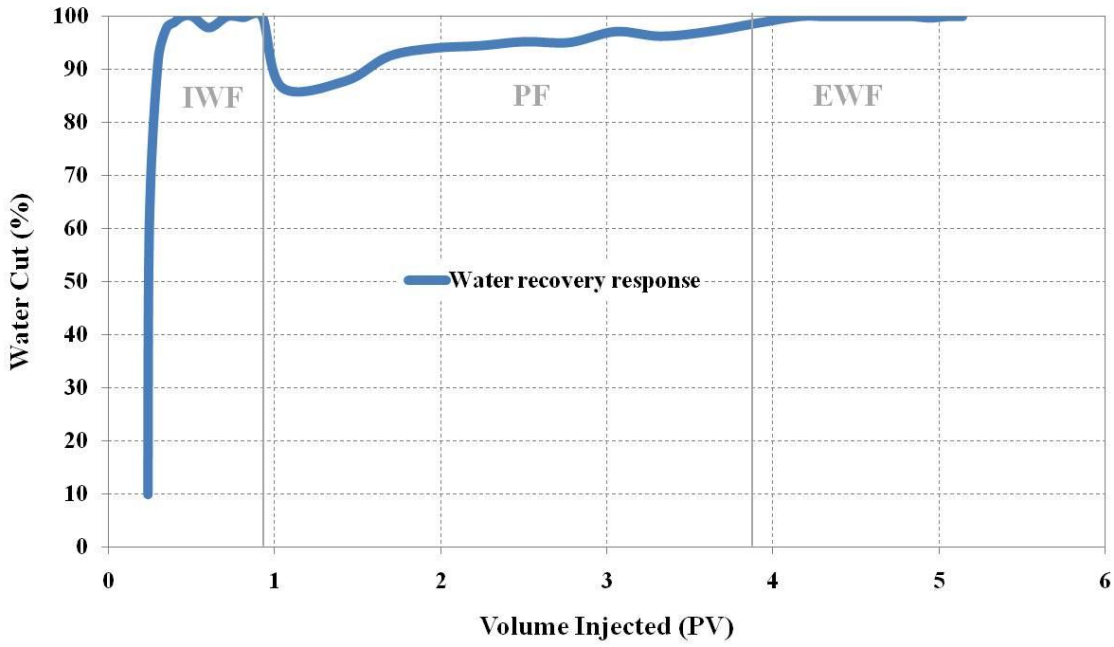

Figure 4.3.21 Water production response during test #7

RRF_o, on the other hand, demonstrated a value of 1.05, similar to the HAP test at the 40:1 ratio. Dynamic polymer adsorption demonstrated the same trend as in the previously tested polymer solutions (i.e., a 3-fold decrease compared to more concentrated polymer systems). The dynamic adsorption for this particular concentrated polymer (0.2 wt%) was found to be 36.6 µg/g (**Figure 4.3.22**). **Figure 4.3.20** shows the plots of both oil recovery and pressure differential with respect to PV injected during the Flopaam 3530S HPAM coreflood at an approximate viscosity ratio of 80:1.

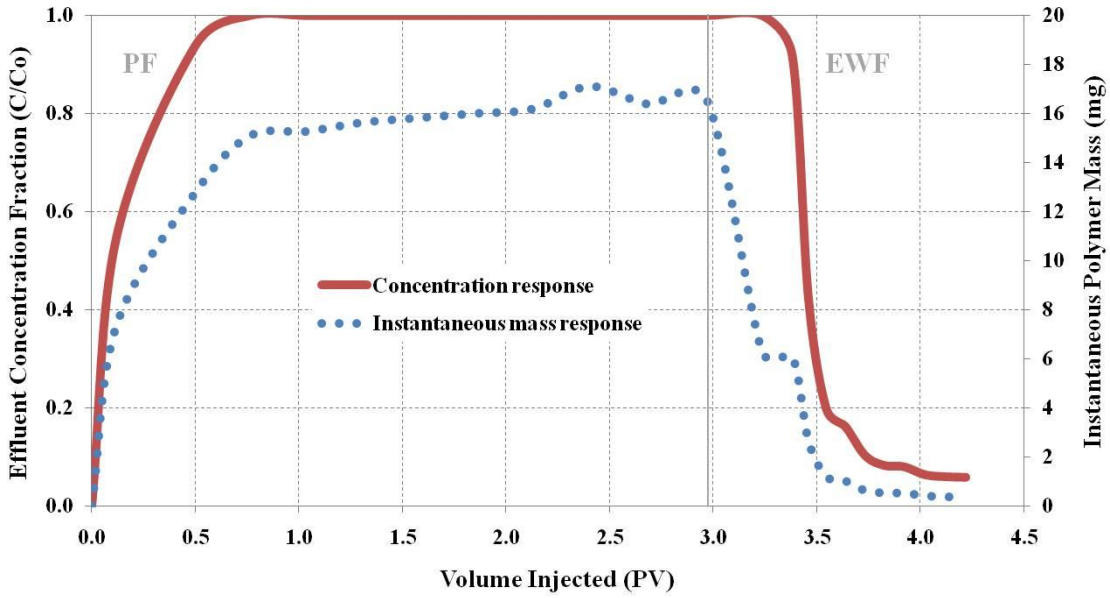

Figure 4.3.22 Concentration profile and instantaneous produced polymer mass response during test #7

4.3.8 Effect of 80:1 viscosity ratio on displacement of a heavy oil (2039 mPa·s) by Superpusher C319 HAP

Almost 0.85 PV of 1 wt% NaCl was injected during the initial waterflood (IWF) sequence. The IWF was then immediately switched to polymer injection of Superpusher C319 HAP in 1 wt% brine solution. The oil recovery from waterflooding, just as in the previous case, was low. It reached only 15 %OOIP with a corresponding stabilized pressure differential of 19.52 kPa, and the final oil saturation after waterflooding was determined to be 0.74 (**Table 4.3.3**).

As measured in the viscometer, the viscosity of polymer solution was 28.83 mPa·s at a theoretical shear rate of 18.81 s^{-1}. This is almost the same as with case of 0.18 wt% HAP at 40:1 viscosity ratio. Also, the 0.20 wt% HAP polymer solution showed a similar kind of oil recovery response. A very fast oil recovery response occurred after approximately 5-6 cm^3 of produced fluid. The initial 0.7 PV of polymer injected resulted in much faster production compared to the HPAM polymer system; however, the final incremental recovery did not exceed 20 %OOIP with ~78 % water cut (**Figure 4.3.24**). On the other hand, a lower differential pressure of 50.4 kPa was indicated, giving a resistance factor value of 29.88. This resulted in a slight increase in in-situ viscosity compared to the initial polymer solution viscosity, indicating weak polymer shear thickening behaviour. The drop in the final residual oil saturation after polymer flooding was 0.52. At the steady-state condition, the viscosity of the effluent polymer solution slightly decreased to 27.03 mPa·s.

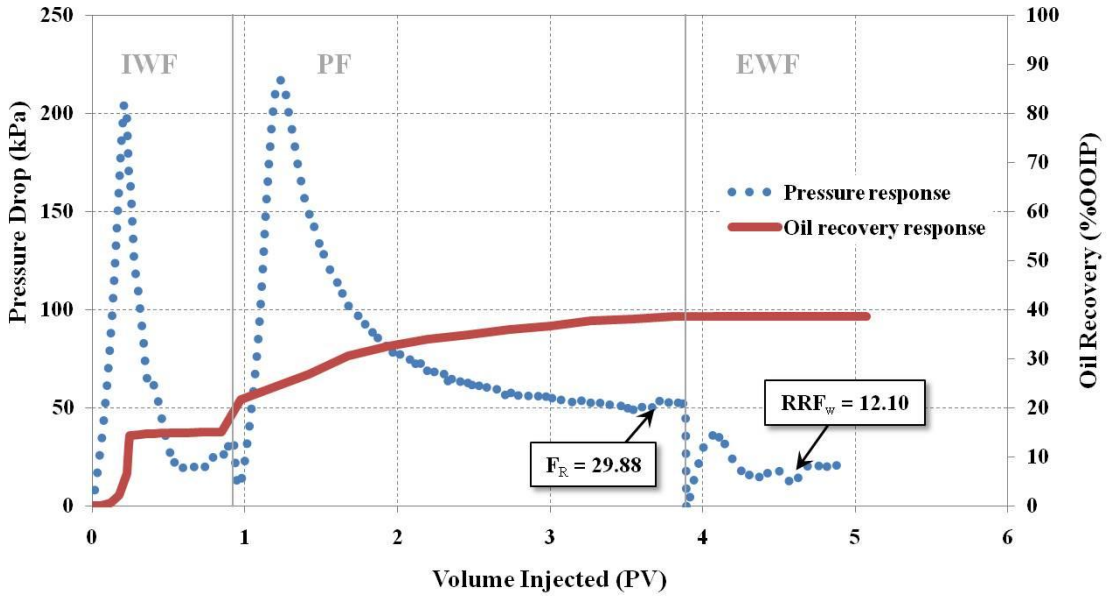

Figure 4.3.23 Oil recovery and pressure response during test #8

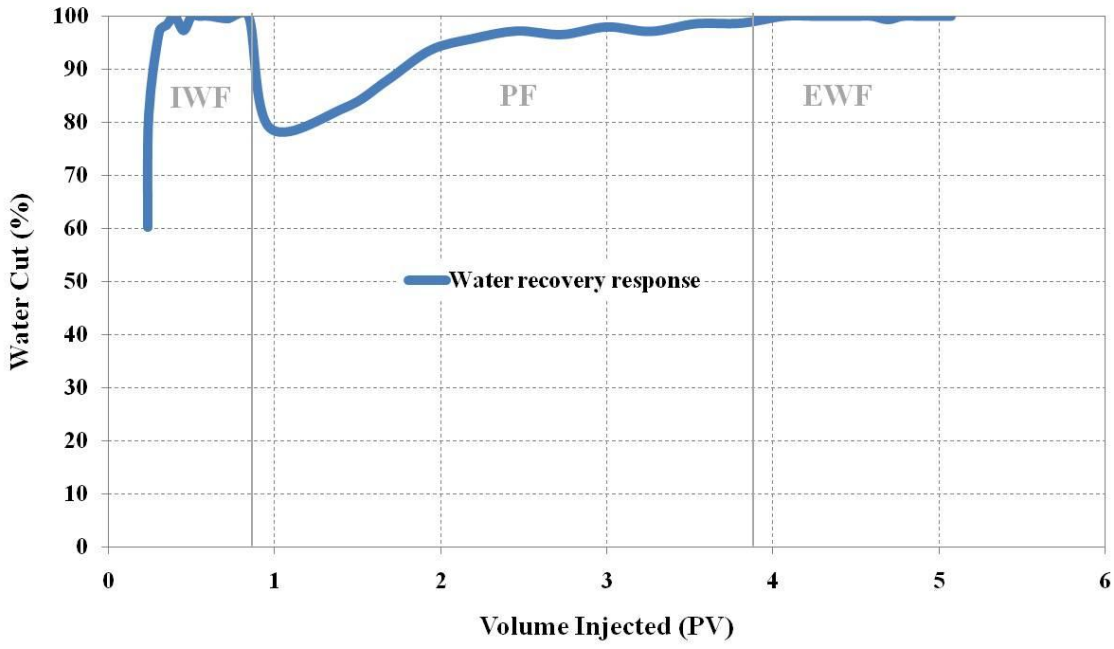

Figure 4.3.24 Water production response during test #8

The same trend in residual resistance factors to water after extended waterflood was observed in this case of HAP testing. This suggests that since the RRF_w is independent of resistance factor, it is noticeable that HAP polymers provide much higher residual resistance factors to water than conventional polyacrylamides. The result is higher permeability reduction to brine. The corresponding stabilized dP for EWF was 20.40 kPa.

The residual resistance factor to oil was calculated to be 1.1. The dynamic polymer adsorption of this particular concentrated polymer 0.2 wt% was calculated to be 33.2 µg/g of sand (**Figure 4.3.25).** The plots of both oil recovery and pressure differential with respect to PV injected during Superpusher C319 HAP coreflooding at an approximate viscosity ratio of 80:1 are depicted in **Figure 4.3.23.**

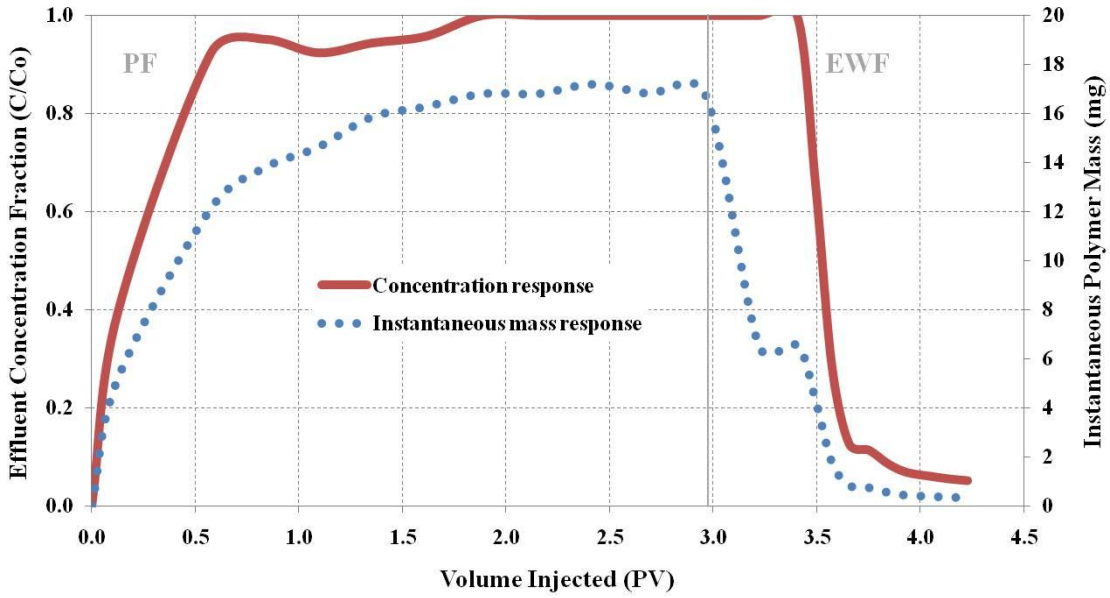

Figure 4.3.25 Concentration profile and instantaneous produced polymer mass response during test #8

Table 4.3.3 Saturation profiles for 2039-mPa·s oil displacement

	Test#							
	5		6		7		8	
Parameter	S_o	S_w	S_o	S_w	S_o	S_w	S_o	S_w
Oil saturation	0.82	0.18	0.81	0.19	0.80	0.20	0.82	0.18
IWF	0.66	0.34	0.74	0.26	0.72	0.28	0.74	0.26
PF	0.46	0.54	0.49	0.51	0.52	0.48	0.52	0.48
EWF	0.46	0.54	0.49	0.51	0.52	0.48	0.52	0.48

4.4 Summary of results

One of the main objectives of this research was to determine the relative importance of viscosity ratio in the displacement of heavy oil by employing linear coreflood tests utilizing different viscosities of displacing and displaced fluids. Also, viscous fingering sometimes plays a role of being the predominant mechanism during heavy oil waterflooding processes (Mai et al., 2008). That is why it is critical to investigate this phenomenon, especially when the addition of water-soluble polymers can reduce the susceptibility of displacement to fingering. Two different approaches to polymer flooding efficiency investigation in heavy oils were tested.

Excellent viscous fingering visual representations were obtained from 2D displacement tests utilizing both water and polymer displacement efficiencies. Different typical types of instabilities and their dynamics were similar to those obtained by Jamaloei et al., (2011), Pavone, (1992), Perkins and Johnston (1969), and Doorwar and Mohanty (2011). The results from the viscous fingering tests provided a unique look at the onset of viscous instability and the mitigation of this phenomenon through the addition of high molecular weight polymers. The results from these tests provide a baseline for what the viscous fingering phenomenon looks like for water and polymer displacing three different viscosity oils.

As initially expected, the results from 1D corefloods indicate early breakthrough of water, suggesting that viscous fingering mechanisms of displacement appear to be predominant in heavy oil waterflooding (Mai et al., 2008). As was clearly demonstrated, the viscous instabilities highly depend on the viscosity ratio of oil to water.

Table 4.4.1 Summary of obtained polymer rheological parameters from 1D corefloods

	Test#							
Parameter	1	2	3	4	5	6	7	8
Oil viscosity (mPa·s)	960	960	960	960	2039	2039	2039	2039
Polymer concentration (wt%)	0.20	0.18	0.30	0.30	0.30	0.30	0.20	0.20
Polymer type	HPAM	HAP	HPAM	HAP	HPAM	HAP	HPAM	HAP
Approximate viscosity ratio	40:1	40:1	20:1	20:1	40:1	40:1	80:1	80:1
Polymer volume injected (PV)	2.82	2.49	2.83	2.51	2.75	2.88	2.97	2.97
F_R	17.25	153.29	51.11	152.13	21.12	164.54	21.62	29.88
RRF_w	4.37	74.47	5.47	30.15	2.25	17.64	5.57	12.10
RRF_o	1.03	-	1.42	1.16	1.24	1.06	1.05	1.10
Dynamic adsorption (µg/g)	72.8	73.6	178.8	220.5	124.8	102.5	36.6	33.2
Theoretical shear rate (s^{-1})	14.72	9.66	19.17	12.71	19.99	11.90	17.82	18.81
Injected polymer viscosity at theoretical shear rate (mPa·s)	34.85	-	-	72.54	53.28	66.10	30.02	28.83
Produced polymer viscosity at theoretical shear rate (mPa·s)	31.82	24.24	56.71	70.91	52.95	61.18	29.58	27.03

From the 1D coreflood tests, it is noticeable that viscosity ratio does not play predominant role in recovery efficiency if tested in the same viscosity oil system. These results coincided with the study of Levitt et al. (2011), contradicting the Wang and Dong (2009) study. Thus, significant viscosity or concentration differences of polymer solutions did not contribute to significant changes in recoveries. The displacement of 960-mPa·s oil did not demonstrate significant changes in recovery, achieving approximately the same ultimate recovery value. The polymer solution concentration, in addition, did not alter recovery factors significantly, demonstrating a difference of 5-7 %OOIP recovered maximum between the highest and lowest polymer concentrations (**Figure 4.4.1**). At the normalized to the lowest possible recovery after initial waterflood case, the effect of possible recovery insensitivity to viscosity ratio is even more noticeable (**Figure 4.4.2**). However, complete match of ultimate recoveries was not obtained. This could lead to the effect of absolute permeability, since each time a new sandpack was used. The difference in terms of displacing performance between the two tested types of polymer systems was noticeable. Hydrophobically-associating polymer (HAP) systems provided more accelerated recovery than HPAM, especially after ~0.6 PV of injection. In addition, they exhibited higher resistance factors or higher in-situ viscosities than HPAM, as well as higher residual resistance factors to water, indicating higher permeability reduction (**Table 4.4.1**).

The same trend was observed during the 2039-mPa·s oil displacement tests with linear corefloods. However, in this case, the recoveries were much lower due to higher oil viscosity and reduced ability to displace oil by the same viscosity polymers.

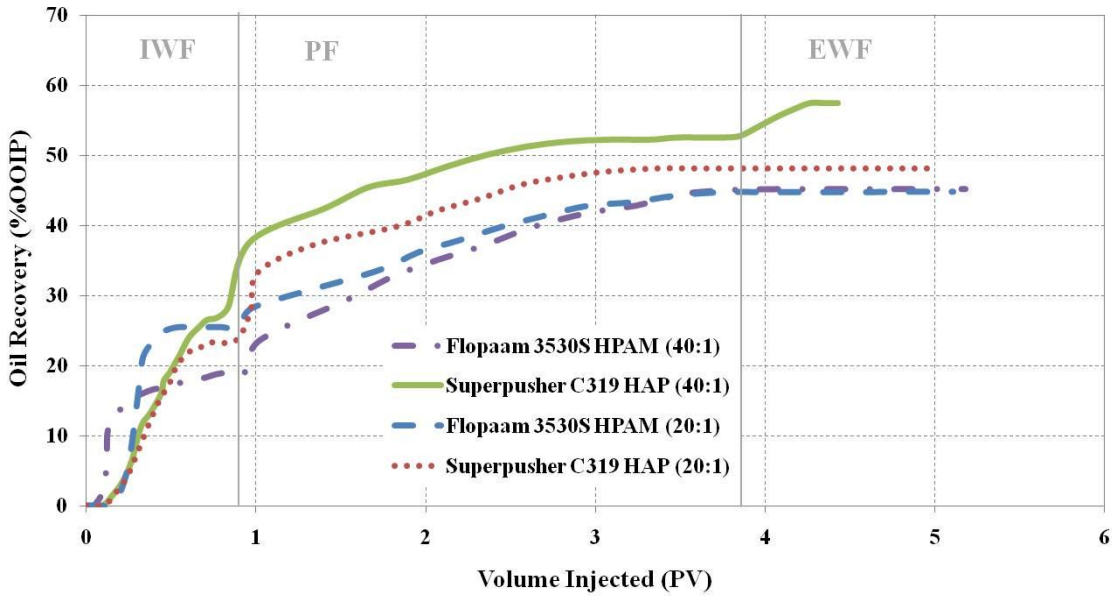

Figure 4.4.1 960-mPa·s oil recovery response at tested viscosity ratios

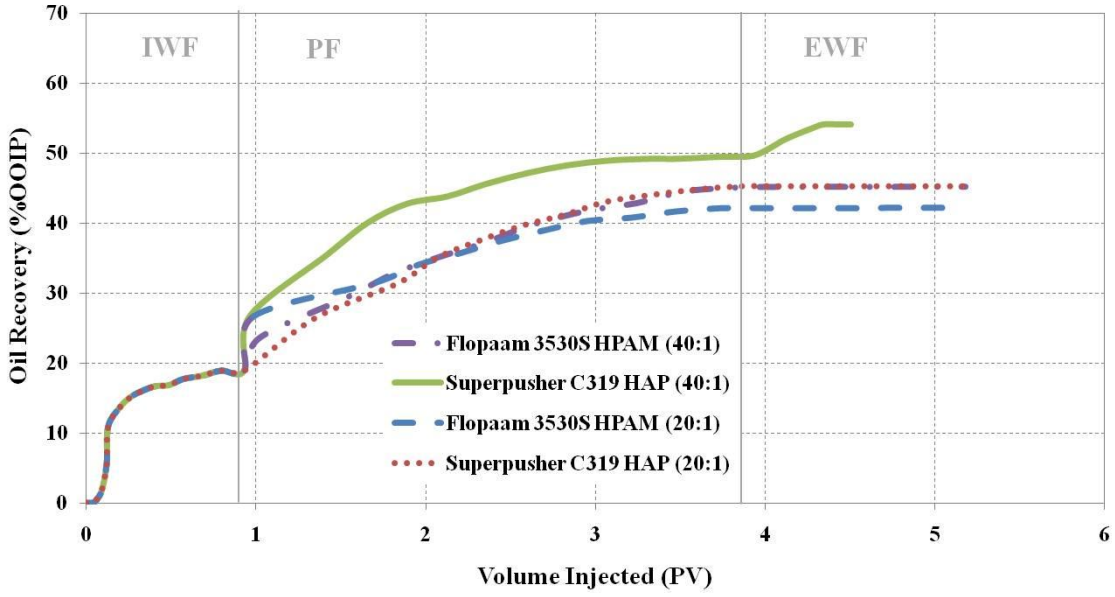

Figure 4.4.2 Normalized 960-mPa·s oil recovery response at tested viscosity ratios

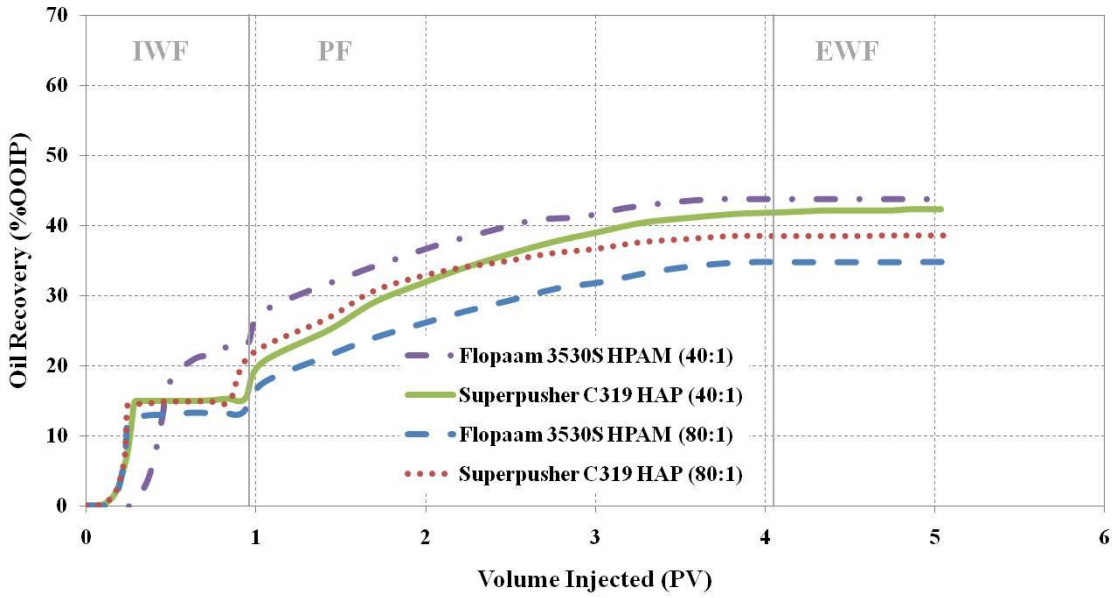

Figure 4.4.3 2039-mPa·s oil recovery response at tested viscosity ratios

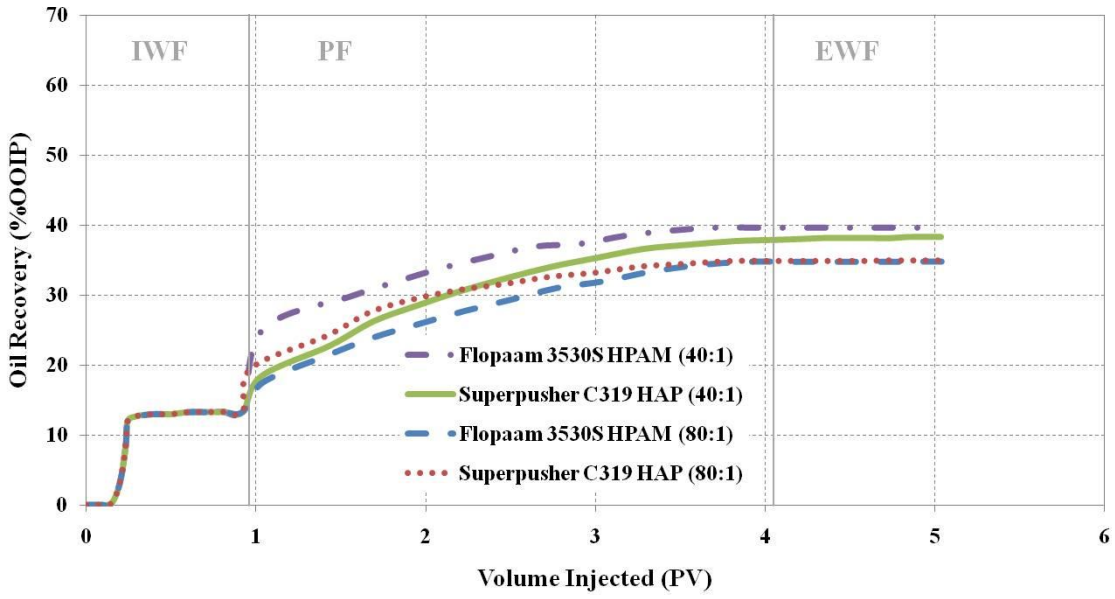

Figure 4.4.4 Normalized 2039-mPa·s oil recovery response at tested viscosity ratios

The difference in recovery between the highest and lowest concentration polymer solutions was slightly greater at with ~10 %OOIP (**Figure 4.4.3**). At the normalized recoveries the insensitivity of recovery factor to viscosity ratio was also more noticeable (**Figure 4.4.4**). Typically, the same trend of early accelerated recovery due to HAP polymer injection was found in the case of 2039-mPa·s oil displacement, as well.

5. CONCLUSIONS AND RECOMMENDATIONS

5.1 Conclusions

The following conclusions can be drawn from this research:

- Detailed visual analysis of viscous fingering patterns indicated that polymer injection provided much more stable viscous displacement with far less occurrence of complex instability behaviour. The fingering patterns also varied depending on the viscosity ratio.
- The shapes of viscous instabilities in the fingering zones were mostly "finger-like" for medium oils and "tree-like" for heavy oils. These "finger-like" instabilities were present both in front of and behind the unstable front.
- Both polymer systems (HPAM and HAP) demonstrated substantial incremental oil recovery improvement due to improved sweep efficiency during linear coreflood tests at tested viscosity ratios of 20-, 40-, and 80:1.
- Even though similar ultimate recoveries were obtained from both HPAM and HAP systems at all viscosity ratios tested, the sandpack flooded with the HAP polymer had a faster response time and accelerated recovery compared to that of the HPAM displacement.
- A quick response and accelerated recovery were more evident in lower concentration HAP polymer than in the same system with higher concentration HAP polymer.
- The results generally support Levitt et al. (2011) but contradict Wang and Dong (2009). On the other hand, the Levitt et al. (2011) tests were conducted with a significant amount of water injected until full flood out. This thesis proposed that

at the same pore volumes of injected fluids, waterflood, and polymer flood, the incremental oil recovery after polymer flooding is at similar level of 20-25 % of OOIP recovered.

- HAP polymers appeared to have much higher resistance factors than HPAM polymers. This translated into an estimated in-situ viscosity from the coreflood of ~2-3 times the viscosity of the initially injected polymer at the theoretically calculated shear rate, indicating that polymer thickening took place at the calculated shear rate in the core.
- Residual resistance factors after extended waterflooding (RRF_w) appeared to be much higher than those after post-polymer oil injection (RRF_o), which could result in the potential for a disproportionate permeability reduction (DPR) effect (Al-Sharji et al., 2001).
- The residual resistance factor to water for the HAP tests, in particular, gave higher value compared to the HPAM tests in cores with different absolute permeabilities, which can be very important from a practical and economic point of view (Jennings et al., 1971).
- Since the residual resistance factors to water are independent of overall resistance factor, it was noted that HAP polymers provided much higher permeability reduction than conventional polyacrylamides.
- Dynamic polymer adsorption was found to be triple for 20:1 compared to 40:1 during 960-mPa·s oil displacement the same as 40:1 compared to 80:1 during 2039-mPa·s displacement. Generally, no specific trend in dynamic adsorption was found when comparing HPAM with HAP in both oil systems; however, dynamic

polymer adsorption appeared to be lower for displacement of higher viscosity oil, which could indicate a larger inaccessible pore volume (IPV) (Pancharoen et al., 2010).

5.2 Recommendations

- A design of a new 2D porous media model or further adaptation of the existing one is recommended to obtain additional data such as saturation changes, precise differential pressure measurements, etc.
- It is recommended to conduct a viscous fingering analysis in the same oil system for comparison of both HPAM and HAP polymer system performance similar to Buchgraber et al. (2011) to confirm the results obtained from the 1D corefloods in this study.
- Since 1D coreflood tests were performed with early polymer flooding so no water flood-out injection was conducted, it is recommended to conduct a series of corefloods for comparison of early and late polymer injection performance (Wang and Dong, 2007).
- Internal pressure taps should be installed additionally on the existing sandpack holder in order to more accurately capture resistance and residual resistance data.
- It is recommended to study the IPV phenomenon using the methodology provided by Pancharoen et al. (2010), which is to conduct the tests in the same sand and polymer systems utilizing floods with and without the presence of oil saturation in the core.

REFERENCES

Aktas, F., Clemens, T., Castanier, L.M., & Kovscek, A.R. (2008). Viscous oil displacement with aqueous associative polymers. Paper SPE 113264 presented at the 2008 SPE/DOE Symposium of Improved Oil Recovery held in Tulsa, USA, April 19-23.

Ali, L., & Barrufet, M.A. (1994). Profile modification due to polymer adsorption in reservoir rocks. *Energy & Fuels,* **8**, 1217-1222.

Al-Sharji, H.H., Grattoni, C.A., Dawe, R.A., & Zimmerman, R.W. (2001). Disproportionate permeability reduction due to polymer adsorption entanglement. Paper SPE 68972 prepared for presentation at the SPE European Formation Damage Conference held in The Hauge, The Netherlands, 21-22 May.

Amro, M.M. (2008). Investigation of polymer adsorption on rock surface of high saline reservoirs. Paper SPE 120807 presented at the 2008 SPE Saudi Arabia Section Technical Symposium held in Alkhobar, Saudi Arabia, 10-12 May.

Asghari, K., & Nakutnyy, P. (2008). Experimental results of polymer flooding of heavy oil reservoirs. Paper SPE 2008-189 presented at the Canadian International Petroleum Conference/SPE Gas Technology Symposium 2008 Joint Conference (the Petroleum Society's 59th Annual Technical Meeting), Calgary, Alberta, 17-19 June.

Bentsen, R.G. (1985). A new approach to instability theory in porous media. *SPE Journal*, October.

Bentsen, R.G., & Saeedi, J. (1981). Liquid-liquid immiscible displacement in unconsolidated porous media. *The Journal of Canadian Petroleum Technology*, Montreal, 93-103.

Bondino, I., Nguyen, R., Hamon, G., Ormehaug, P.A., Skauge, A., & Jouenne, S. (2011). Tertiary polymer flooding in extra-heavy oil: an investigation using 1D and 2D experiments, core scale simulation and pore-scale network models. Paper SCA2011-18 presented at the International Symposium of the Society of Core Analysts held in Austin, Texas, 18-21 September.

Bonn, D., Kellay, H., Braunlich, M., Ben Amar, M., & Meunier, J. (1995). Viscous fingering in complex fluids. Elsevier Science, *Physica A*, **220**, 60-73.

Brock, D.C., & Orr Jr., F.M. (1991). Flow visualization of viscous fingering in heterogeneous porous media. Paper SPE 22614 presented at the 66th Annual Technical Conference and Exhibition of the Society of Petroleum Engineers held in Dallas, TX, October 6-9.

Brookfield (2001). Viscometers/rheometers catalog.

Broseta, D., Medjahed, F., Lecourtier, J., & Robin, M. (1995). Polymer adsorption/retention in porous media: effects of core wettability and residual oil. *SPE Advanced Technology Series*, Vol. 3, No. **1**. 103-112.

Burchgraber, M., Clemens, T., Castanier, L.M., & Kovscek, A.R. (2011). A microvisual study of the displacement of viscous oil by polymer solutions. *SPE Reservoir Evaluation & Engineering Journal*, January 5, 269-280.

Chakrabarty, C., & Bentsen, R.G. (1992). The onset of instability during immiscible displacements in cylindrical models. *The Journal of Canadian Petroleum Technology*, December, Volume **31**, No. 10.

Chuoke, R.L., van Meurs, P., van der Poel, C. (1958). The instability of slow, immiscible, viscous liquid-liquid displacement in permeable media. Paper SPE 1141-G presented at 33rd Annual Fall Meeting of Society of Petroleum Engineers in Houston, Tex., Oct. 5-8., *Trans.* AIME, Vol. **216**.

Clements, T., Tsikouris, K., Burchgraber, M., Castanier, L., & Covscek, A. (2012). Pore-scale evaluation of polymers displacing viscous oil – computational fluid dynamics simulation of micromodel experiments. Paper SPE 154169 presented at the Eighteenth SPE Improved Oil Recovery Symposium held in Tulsa, Oklahoma, USA, April 14-18.

Coskuner, G., & Bentsen, R.G. (1988). A Hele-Shaw cell study of new approach to instability theory in porous media. *The Journal of Canadian Petroleum Technology*, January-February, 87-95.

Dawson, R., & Lantz, R.B. (1972). Inaccessible pore volume in polymer flooding. *Society of Petroleum Engineers Journal*, Trans. AIME Vol. **253**, October, 448-452.

Doorwar, S., & Mohanty, K.K. (2011). Viscous fingering during non-thermal heavy oil recovery. Paper SPE 146841 presented at the SPE Annual Technical Conference and Exhibition held in Denver, Colourado, USA, 30 October-2 November.

Engelberts, W.F., Kinkenberg, L.J., (1950). Laboratory experiment on the displacement of oil by water from packs of granular material. Proc., Third World Pet. Cong., Part II, 544-54.

Gupta, S.P., Varnon, J.E., & Greenkorn, R.A. (1973). A mechanistic study of viscous finger wavelength. *Water Resour. Res*., **9**(4):1039-1046.

Hill, S. (1952). Channelling in packed columns. *Chem. Eng. Sci.* Vol. **1**, No. 6, 247- 253.

Homsy, G.M. (1987). Viscous fingering in porous media. *Ann. Rev. Fluid Mech*., **19**, 271-311.

Jamaloei, B.Y., Kharrat, R., & Torabi, F. (2010). Analysis and correlations of viscous fingering in low-tension polymer flooding in heavy oil reservoirs. Paper CSUG/SPE 137445 presented at the Canadian Unconventional Resources & International Petroleum Conference held in Calgary, Alberta, Canada, October 19-21.

Jamaloei, B.Y., Kharrat, R., & Torabi, F. (2011). A mechanistic analysis of viscous fingering in low-tension polymer flooding in heavy oil reservoirs. Elsevier. *Journal of petroleum science and engineering*, **78**, 228-232.

Jennings, R.R., Rogers, J.H., & West, T.J. (1971). Factors influencing mobility control by polymer solutions. *Journal of Petroleum Technology*, March, 391-401.

Knight, B.L., & Rhudy, J.S. (1977). Recovery of high-viscosity crudes by polymer flooding. The *Journal of Canadian Petroleum Technology*, October-December, Montreal, 46-56.

Kueper, BH., & Frid, E. (1988). An overview of immiscible fingering in porous media. *Journal of Contaminant Hydrology*, **2**, 95-110.

Levitt, D., Jouenne, S., Bondino, I., Gingras, J-P., & Bourrel, M. (2011). The interpretation of polymer coreflood results for heavy oil. Paper SPE 150566 presented at the SPE Heavy Oil Conference and Exhibition held in Kuwait City, Kuwait, 12-14 December.

Mai, A., & Kantzas, A. (2008). Improved heavy oil recovery by low rate waterflooding. Paper SPE/PS/CHOA 117648PS2008-353 presented at the 2008 SPE International Thermal Operations and Heavy Oil Symposium held in Calgary, Alberta, 20-23 October.

Mezzomo, R.F., Moczydlower, A.N., Sanmartin, A.N., & Araujo, H.V. (2002). A new approach to the determination of polymer concentration in reservoir rock adsorption tests. Paper SPE 75204 presented at the SPE/DOE Thirteenth Symposium on Improved Oil Recovery held in Tulsa, Oklahoma.

Pancharoen, M., Thiele, M.R., & Kovscek, A.R. (2010). Inaccessible pore volume of associative polymer floods. Paper SPE 129910 presented at the 2010 SPE Improved Oil Recovery Symposium held in Tulsa, Oklahoma, 24-28 April.

Pavone, D. (1992). Observations and correlations for immiscible viscous-fingering experiments. *SPE Reservoir Engineering*, May.

Perkins, T.K., & Johnson, O.C. (1969). A study of immiscible fingering in linear models. Paper SPE 2230 presented at SPE 43rd Annual Fall Meeting held in Houston, TX., Sept. 29-Oct. 2. *SPE Journal*, March, 39-46.

Peters, E.J. & Flock, D.L. (1981). The onset of instability during two-phase immiscible displacement in porous media. Paper SPE 8371 presented at the SPE 54th Annual Technical Conference and Exhibition, held in Las Vegas, Sept. 23-26. *SPE Journal*, April.

Richardson, J.G. (1957). The calculation of waterflood recovery from steady-state relative permeability data. *Trans*. AIME, **210**.

Saffman, P.G. (1959). Exact solutions for the growth of fingers from a flat interface between two fluids in a porous medium or Hele-Shaw cell. Quart, *Journ. Mech. and Applied Math*., Vol. **XXII**, Pt. 2., 146-150.

Saffman, P.G., Taylor, G. (1958). The penetration of a fluid into a porous medium or Hele-Shaw cell containing a more viscous liquid. The Royal Society. Proceedings of the Royal Society of London. Series A, *Mathematical and Physical Sciences*, Vol. **245**, No. 1242, Jun. 24. 312-329.

Sarma, H.K. (1986). Viscous fingering: one of the main factors behind poor flood efficiencies in petroleum reservoirs. *Powder Technology*, **48**. 39-49. January 2.

Sarma, H.K., & Bensen, R.G. (1987). An experimental verification of a modified instability theory for immiscible displacements in porous media. *The Journal of Canadian Petroleum Technology*, July-August, Montreal.

Sarma, H.K., Maini, B.B., Purves, K.N. (1994). A laboratory investigation of the pseudo relative permeability characteristics of unstable immiscible displacements. *The Journal of Canadian Petroleum Technology*. January, Volume **33**, No. 1.

Sheng, J. J. (2011). Modern Chemical Enhanced Oil Recovery: Theory and Practice. Gulf Professional Publishing.

Shriwal, P. & Lane, R.H. (2012). Impact of timing of crosslinker addition on water shutoff polymer gel properties. Paper SPE 153241 presented at the eighteenth SPE Improved Oil Recovery Symposium held in Tulsa, Oklahoma, USA, 14-18 April.

Skauge, A, Horgen, T., Noremark, B., & Vik, B. (2012). Experimental studies of unstable displacement in carbonate and sandstone material. Paper SPE 9880 presented at the EAGE IOR Symposium 12-14 April, Cambridge, UK.

Skauge, A., Ormehaug, P.A., Gurholt, T., Vik, B., Bondino, I., & Hamon, G. (2012). 2-D visualization of unstable waterflood and polymer flood for displacement of heavy oil. Paper SPE 154292 presented at the Eighteenth SPE Improved Oil Recovery Symposium held in Tulsa, Oklahoma, USA, April 14-18.

SNF FLOERGER®, http://www.snf-oil.com/

SNF FLOPAAM™ (2004). Flopaam for enhanced oil recovery brochure.

Sorbie, K.S., Parker, A., & Clifford, P.J. (1987). Experimental and theoretical study of polymer flow in porous media. *SPE Reservoir Engineering*, August, 281-304.

Torabi, F. & Wilton, R.R. (2012). Mechanistic evaluation of polymer flooding for enhanced heavy oil recovery – year 2. *Final Report: Petroleum Technology Research Centre*, PTRC No. HO-UOR-00182-2012.

van Meurs, P. (1956). The use of transparent three-dimensional models for studying the mechanism of flow processes in oil reservoirs. SPE paper 678-G presented at Petroleum Branch Fall Meeting in Los Angeles, Oct. 14-17. *Trans*. AIME, Vol. **210**.

van Meurs, P., van der Poel, C. (1958). A theoretical description of water-drive processes involving viscous fingering. Paper SPE 931-G presented at 32nd Annual Fall Meeting of Society of Petroleum Engineers in Dallas, Tex., Oct. 6-9, *Trans*. AIME, Vol. **213**.

Varnon, J.E. & Greenkorn, R.A. (1968). Unstable two-fluid flow in porous medium. Paper SPE 2182 presented at 43rd Annual Fall Meeting held in Houston, Sep. 29-Oct. 2. *SPE Journal*.

Wang, D., & Wang, G. (2012). New insights on the mechanism of displacement efficiency of natural cores by chemical flooding and its influence on the development and selection of chemicals for EOR. Paper SPE 153070 presented at the Eighteenth SPE Improved Oil Recovery Symposium held in Tulsa, Oklahoma, 14-18 April.

Wang, D., Cheng, J., Yang, Q., Gong, W., Li, Q., & Chen, F. (2000). Viscous-elastic polymer can increase microscale displacement efficiency in cores. Paper SPE 63227 presented at the 2000 SPE Annual Conference and Exhibition held in Dallas, Texas, 1-4 October.

Wang, D., Wang, G., Wu, W., Xia, H., & Yin H. (2007). The influence of viscoelasticity on the displacement efficiency – from micro- to macroscale. Paper SPE 109016 presented at the 2007 SPE Annual Technical Conference and Exhibition held in Anaheim, California, 11-14 November.

Wang, J., & Dong, M. (2009). Optimum effective viscosity of polymer solution for improving heavy oil recovery. *Journal of Petroleum Science and Engineering*, 67, 155-158.

Wang, J., Dong, M. & Asghari, K. (2006). Effect of oil viscosity on heavy-oil/water relative permeability curves. Paper SPE 99763 presented at the 2006 SPE/DOE Symposium on Improved Oil Recovery held in Tulsa, Oklahoma, 22-26 April.

Wang, J., Dong, M. (2007). A laboratory study of polymer flooding for improving heavy oil recovery. Paper SPE 2007-178 presented at the Petroleum Society's 8th Canadian International Petroleum Conference (58th Annual Technical Meeting), Calgary, Alberta, June 12-14.

Wassmuth, F.R., Green, K., Hodgins, L., & Turta, A.T. (2007). Polymer flood technology for heavy oil recovery. Paper SPE 2007-182 presented at the Petroleum Society's 8th Canadian International Petroleum Conference (58th Annual Technical Meeting), Calgary, Alberta, June 12-14.

Wilton, R.R. (2010). Improving conformance control technologies – Application to heavy oil reservoirs – year 2. *Final Report: Petroleum Technology Research Centre*, SRC Publication No. 12418-3C09.

Zaitoun, A., & Kohler, N. (1988). Two-phase flow through porous media: effect of an adsorbed polymer layer. Paper SPE 18085 presented at the 63rd Annual Technical Conference and Exhibition of the Society of Petroleum Engineers held in Houston, TX, October 2-5.

Zaitoun, A., Bertin, B., & Lasseux, D. (1998). Two-phase flow property modifications by polymer adsorption. Paper SPE 39631 presented at the 1998 SPE/DOE Improved Oil Recovery Symposium held in Tulsa, Oklahoma, 19-22 April.

APPENDICES

APPENDIX A

A.1 List of suppliers

A.1.1 Chemicals

Flopaam 3630S (HPAM)	SNF FLOERGER®
Flopaam 3530S (HPAM)	SNF FLOERGER®
Superpusher C319 (HAP)	SNF FLOERGER®
Sodium Chloride SX0420-3	EMD chemicals Inc.
Green food colouring	Loretta Foods™

A.1.2 Hydrocarbons

MX 1560/2 mineral oil	EM® Science
MX 1561/2 mineral oil	EM® Science
Spartan 680 industrial gear oil	ESSO
Kerosene (clear)	ESCORT®

A.1.3 Apparatus and process materials

1D Sandpack holder	Swagelok®
2D Acrylic Fracture visual cell	University of Regina, Engineering workshop
HDR-CX350V high definition camcorder	Sony
B10, mixed mesh size synthetic glass beads	Opta Minerals Inc.

Syringe Pump Model 250D	Teledyne Isco Inc.
Digi Sense® Temperature Controller	Cole-Parmer®
Pressure Transducer	Validyne Diaphragm: 85.5, 344, 861.8, 1378.95 kPa
Pressure Data Gathering System	Validyne UPC Easy Sense 2100
Maxima C PLUS Vacuum pump	Fisher Scientific
5.0 µm Cellulose nitrate membrane filter	Whatman®
1500W Heater	Nordik
5000 psi Transfer cylinder	Core Lab Instruments

A.1.4 Analytical equipment

AG204 Weigh Balance	Metter Toledo
ED2000 Weigh Balance	Symmetry™ Cole-Parmer®
Centrifuge Centrific™	Fisher Scientific
Isotemp Magnetic Stirrer	Fisher Scientific
ARROW 6000 Mechanical Stirrer	ARROW Engineering Co., Inc.
Viscometer Model LV-DV II+	Brookfield

APPENDIX B

B.1 Formulations for chemical solutions

B.1.1 Preparation of 5.25 wt% kerosene in Spartan 680 industrial gear oil (~200 cm^3)

10.5 g kerosene

200 g Spartan 680 industrial gear oil

Stirred for 24 hr

B.1.1 Preparation of 1 wt% NaCl solution (~2000 cm^3)

21 g NaCl

1990 g de-ionized H_2O

Stirred for 1 hr

B.1.2 Preparation of 0.10 wt% HPAM polymer solution in green food colouring (~300 cm^3)

3 g Flopaam 3630S powder

289 g green food colouring

Stirred for 24 hr

B.1.3 Preparation of 0.33 wt% HPAM polymer solution in green food colouring (~300 cm^3)

10 g Flopaam 3630S powder

289 g Green food colouring

Stirred for 24 hr

B.1.4 Preparation of 0.30 wt% HPAM or HAP polymer solution in 1 wt% NaCl (~1000 cm^3)

3 g Flopaam 3530S or Superpusher C319 powder

997 g 1 wt% degassed NaCl

Stirred for 24 hr

B.1.5 Preparation of 0.20 wt% HPAM or HAP polymer solution 1 wt% NaCl (~1000 cm^3)

2 g Flopaam 3530S or Superpusher C319 powder

998 g 1 wt% degassed NaCl

Stirred for 24 hr

B.1.6 Preparation of 0.18 wt% HPAM or HAP polymer solution 1 wt% NaCl (~1000 cm^3)

1.8 g Flopaam 3530S or Superpusher C319 powder

998.2 g 1 wt% degassed NaCl

Stirred for 24 hr